PhD Thesis in System Engineering

XXIV Ciclo

Modeling and Control of Robots with Compliant Actuation

Fabrizio Flacco

Advisor Prof. Alessandro De Luca

April 2012

Dipartimento di Ingegneria Informatica, Automatica e Gestionale
SAPIENZA Universitá di Roma

To my wife, Floriana,
and to my child who will be born in May.

Abstract

Robotics has always contemplated the most perfect existing machine, *Human being*, dreaming to realize robots able to catch a small spark of this shining light. Robots that are able to emulate human reasoning, but also human motion capabilities, robots that are qualified to coexist and cooperate safely with humans, helping us in our everyday life.

Compliance is one of the most fascinating characteristic of human joints, it gives the possibility to crash an aluminum can but in the same way to grab gently a little flower. Thanks to compliant joints human beings are able to do very stiff and accurate motions or moving softly reducing possible injuries in case of unforeseen collisions. Moreover it permits to store energy and release it quickly, for example for trowing objects or for jumping.

Inspired by human joints, robotics research groups started to investigate deeply this characteristic, trying either to emulate or reproduce compliant behaviors with robot joints. These researches result in different views for obtaining compliant robot, they can be categorized in: *passive* compliance, where passive elements, i.e., springs, are arranged into the joint. In this way safety is improved, but the price is in term of performance; *active* compliance obtained by controlling rigid joints such as to emulate compliant behaviors. The principal disadvantage of this approach is that energy cannot be stored, and some safety issue cannot be completely solved; *actively controlled* passive compliance, where the characteristic of passive elements inside the device can be controlled in order to vary the joint compliance. The third approach seams to be the best thread-off between safety, capabilities and performance, and as a results of this research field new devices, which permit to control the compliance of the joint, called Variable Stiffness/Impedance Actuator (VSA / VIA), have been developed.

These new actuators have been realized with different arrangement of motors and mechanisms with passive elements. In the first part of this dissertation an overview of compliant actuators developed by research centers and universities

around the world is shown, then a categorization, which groups all existing compliant actuators in three different typologies, is presented. We characterize each compliant actuator typology , single actuated flexible transmission, antagonistic variable stiffness actuator and serial variable stiffness actuator, by an equivalent arrangement of motors and flexible transmissions and we present the dynamic model associated to it.

From a control point of view these new devices give the possibility to control simultaneously the link motion and the joint stiffness behavior. To take advantage of these capabilities new control methodology ere needed. In the second part of the Thesis we present the control algorithms for compliant joints we developed:

1. A feedback linearization controller which permits to control the link position and the stiffness in a decoupled way.
2. A gravity cancellation methodology which solve problematic due to the presence of gravity allowing a simpler and more stable control of compliant joints.
3. A collision detector which estimates external forces using a residual-based methodology.
4. An online stiffness estimator needed to control compliant joints.

All methods proposed are developed for each of the three typologies of compliant actuators, and their effectiveness is proved by simulations and experiments.

Keywords: *Robotics, Physical Human-Robot Interaction, Compliant Actuators, Modeling, Nonlinear Control, Collision Detection, Nonlinear Estimation.*

Acknowledgements

At the end of this journey I need to express my gratitude to all those who have helped me during this three years. It is my pleasure to thank my supervisor, Prof. Alessandro De Luca, for being my guide and my teacher. Thanks!

In addition, I would like to thank Prof. Giuseppe Oriolo and Dr. Marilena Vendittelli for many inspiring conversation. Prof. Antonio Bicchi who instilled in me the idea to do research. Prof. Oussama Khatib and the AI group at Stanford University who gave me the possibility to consider my researches from a different point of view

Hearty thanks also go to all my colleagues from the Robotics Lab who shared with me this adventure: Paolo Stegagno, Antonio Franchi, Pietro Peliti, Lorenzo Rosa and Antonio Paolillo; and to all those people who are used to stay in the lab for working or for "pleasure"!
Many thanks to "the guys from higher floors" for letting me take some rest during the day.

Last, but not least, a big thanks to my parents for all they did!

Finally, I would like to thank for the generous funding of my work, provided by the European Commission Sixth Framework Programme as part of the project PHRIENDS under grant no. 045359 and the FP7 ICT-287513 SAPHARI project.

Contents

Notations

General rules

Throughout the text, the following conventions hold

- scalar quantities are denoted by plain lower-case symbols (e.g., m, n, t)
- vector quantities, intended as column vectors unless otherwise stated, are denoted by bold lower-case symbols (e.g., $\boldsymbol{g}$, $\boldsymbol{b}$, $\boldsymbol{a}$)
- matrix quantities are denoted by bold upper-case symbols (e.g., $\boldsymbol{M}$, $\boldsymbol{A}$, $\boldsymbol{J}$)
- for the sake of legibility in many equations the arguments of a function is omitted. e.g., $\sigma(\theta_c, \phi) \longmapsto \sigma$

Acronyms

w.r.t.	$\longmapsto$	with respect to
d.o.f.	$\longmapsto$	degree of freedom
SAFT	$\longmapsto$	Single Actuated Flexible Transmission
VSA	$\longmapsto$	Variable Stiffness Actuator
AwAS	$\longmapsto$	Actuator with Variable Stiffness
pHRI	$\longmapsto$	physical Human Robot Interaction
AMASC	$\longmapsto$	Actuator with Mechanically Adjustable Series Compliance
VS-Joint	$\longmapsto$	Variable Stiffness Joint
QA-Joint	$\longmapsto$	Quasi Antagonistic Joint
SJM	$\longmapsto$	Safe Joint Mechanism
SDAU	$\longmapsto$	Serial Dual Actuation Unit
PDAU	$\longmapsto$	Parallel Dual Actuation Unit
HDAU	$\longmapsto$	Hybrid Dual Action Unit
SEA	$\longmapsto$	Serial Elastic Actuator
DM^2	$\longmapsto$	Distributed Macro Mini
S2ρ	$\longmapsto$	Stanford Safety Robot
PPAM	$\longmapsto$	Pleated Pneumatic Artificial Muscle
MACCEPA	$\longmapsto$	Mechanically Adjustable Compliance and Controllable Equilibrium Position Actuator
MIA	$\longmapsto$	Mechanical Impedance Adjuster

Introduction

A successful paradigm in physical Human-Robot Interaction (pHRI) is to design robots for safety and to control them for performance [Bicchi et al., 2001, Bicchi and Tonietti, 2004]. In the recent years, this co-design has led to the development of several manipulators and actuation systems that integrate in different ways the common concepts of lightweight link structure [Hirzinger et al., 2001], compliant transmissions and arm coverage [Ikuta et al., 2003, Wyrobek et al., 2008], hybrid actuation with remote displacement of the main motors [Zinn et al., 2005], and variable stiffness/impedance actuators (VSA/VIA). In particular, VSA devices may either have a passive variation of joint stiffness [Park et al., 2008], or actively modify it, with an antagonistic arrangement of two motors [Migliore et al., 2005, Tonietti et al., 2005, Schiavi et al., 2008] or with separate actuation for motion and stiffness [Choi et al., 2008, Wolf and Hirzinger, 2008]. All the above mechanical/actuation choices allow to reduce intrinsically the risk of user injuries resulting from possible unexpected collisions of a robot that closely cooperates with humans [Boccadamo et al., 2006, Haddadin et al., 2008].

Flexibility in the robot transmissions has been considered in the past as an undesired behavior, being a source of static and dynamic inaccuracy at the robot end-effector level and potentially leading to control instability problems De Luca and Book [2008]. Recent research in physical Human-Robot Interaction (pHRI) has shown that a generalized use of compliance in the robot structure helps in reducing the danger of injuries due to accidental human-robot collisions Haddadin et al. [2007], Bicchi et al. [2008b], since compliant elements absorb part of the energy of a collision Ikuta et al. [2003].

A compliant robot behavior may be achieved through flexible mechanical components, via feedback control, or by combining the two De Santis et al. [2008]. In view of the intrinsic limited bandwidth of control algorithms, a convenient way to introduce mechanical compliance in a robot arm is to design on purpose flexible joints/transmissions. In this way, an inertial decoupling is obtained between the heavier motors and the typically lightweight links, limiting

the energy transfer from the former to a human at the impact. This is a relevant feature of manipulators such as the Barrett WAM Salisbury et al. [1988] or the DRL/KUKA LWR series Hirzinger et al. [2001]. The transmission flexibility in these robots is due to the use of Harmonic Drives or cables, and can be reasonably considered as a linear effect (joint elasticity). The same is often true also in robotic structures based on Series Elastic Actuation (SEA) Pratt and Williamson [1995]. From the control point of view, robots with joint elasticity can perform very accurate free motion as well as compliant interaction tasks thanks to nonlinear control design, see, e.g., Spong [1987], De Luca and Lucibello [1998], De Luca et al. [2005], Kugi et al. [2008], once a reliable dynamic model (including joint stiffness) is available. Since the joint stiffness is assumed to be constant in this case, its identification by off-line static calibration procedures is feasible.

It should be noted that a fixed stiffness of the joints allows only a limited range of Cartesian compliance at the robot end-effector, both in size and direction, and requires thus to be complemented by a feedback control action Petit and Albu-Schäffer [2011]. In addition, a safer pHRI asks for very compliant joints while high motion performance with fast acceleration transients requires the transmissions to be stiffer, so as to transfer efficiently the kinetic energy from the motors to the links. These considerations have led in the recent years to the development of Variable Stiffness Actuation (VSA) for robot arms (and legs), where the joint stiffness can be varied on the fly during the commanded motion by using two motors and flexible transmissions that have nonlinear deformation/torque characteristics. Several different realization of the VSA principle have been investigated, but most designs can be grouped in two main categories. The first arranges the two motors and nonlinear transmissions in an *agonistic-antagonist configuration* Migliore et al. [2005], Tonietti et al. [2005], Schiavi et al. [2008]. In this bio-inspired design, motion and stiffness actuation are strongly dynamically coupled. The second category of VSA in the so-called *serial configuration* is conceptually different: there is a single flexible transmission driven by a principal motor for controlling the link motion, while a a secondary, typically a smaller motor controls separately the actual stiffness of the transmission Ham et al. [2007], Choi et al. [2008], Wolf and Hirzinger [2008], Ikegami et al. [2009], Jafari et al. [2010].

In parallel to the development of VSA devices, control laws that are able to assign a desired behavior to both the joint stiffness and link motion have been investigated. Classical PD with feedforward compensation or PID laws have been designed for regulating both the position and the stiffness to constant values, in the absence Tonietti et al. [2005] or presence De Luca and Flacco [2010a] of gravity. The interplay between VSA design and the possibility of regulating the output stiffness of the device without changing the stored potential energy in the system has been studied in Visser et al. [2011] by following a port-Hamiltonian approach. For the simultaneous tracking of smooth stiffness/motion trajectories, a nonlinear decoupling and exact linearizing state feedback law has been proposed in De Luca et al. [2009] for the VSA-II device developed by the University of Pisa, and then generalized to any multi-dof robot driven by antagonistic VSAs in Palli et al. [2008]. This control law has the best possible nominal performance, but requires also the evaluation of the first and second derivatives of the stiffness w.r.t. the deformation variables.

Organization of the Thesis

This Thesis is composed of two main parts: Modeling and Control. Within each part, Chapters represent self-consistent modules with their own introductive sections and overviews. Any dependency among units is explicitly reported throughout the text to the best of the author's possibilities.

Outline of Part I

In the first part of this Thesis an overview of compliant actuators and their mathematical model is proposed.

Chapter 1 Introduces the modeling of compliant joints.

Chapter 2 presents an overview of developed compliant actuators, organized into research centers and universities. A short description of the mechanical solution and the principal characteristics of each device is proposed

Chapter 3 introduces the mathematical models for compliant actuators, grouping them in three typologies :

- Single Actuated Flexible Transmission (SAFT);
- Antagonistic Variable Stiffness Actuator (aVSA);
- Serial Variable Stiffness Actuator (sVSA);

For each typology the dynamic model is described, how to compute the internal stiffness of the device from the model is explained, and the extension to multi d.o.f. robots is proposed.

Chapter 4 contains a more accurate description of the VSA-II (Variable Stiffness Actuator II) developed by the University of Pisa and the AwAS (Actuator with Adjustable Stiffness) developed by the Italian Institute of Technology. This two devices will be used throughout the Thesis for simulation and experiments.

Outline of Part II

In the second part is proposed a series of control technique specially designed for compliant actuators.

Chapter 5 introduces the control theory of compliant joints.

Chapter 6 presents the feedback linearization control law applied to compliant actuators. Using the feedback linearization is possible to control in a decoupled way the link position of a SAFT, and, position and stiffness for antagonistic and serial VSA. This characteristic is very important especially in antagonistic VSA, where position and stiffness are highly coupled. The Chapter includes a simple motion control which permits to track a desired position-stiffness behavior. Part of this material has been published as author's original work in De Luca et al. [2009].

Chapter 7 describes a control law which permits to remove, by using the feedback equivalence between compliant joints with and without gravity, any effect of the gravity to some outputs of compliant joints, resulting in a system simpler to analyze and control. The ideas and methods presented in these Chapters have been published as author's original work in De Luca and Flacco [2010a],De Luca and Flacco [2010b] and De Luca and Flacco [2011].

Chapter 8 contains a collision detection methodology which considers only encoders informations to estimate external forces. The collision detector uses a residual signal based on the generalized momentum of the system. This method is completed by a reaction strategy, based on the feedback linearization, which push away the robot to a safer configuration. Part of this material has been published as author's original work in De Luca et al. [2009].

Chapter 9 presents an estimator of the internal stiffness of a compliant device. The stiffness is very important in the control of compliant actuator, but there not exist sensors which permit to measure it. Evaluation of the stiffness obtained with a parametrized model are not enough accurate, due to the difficulty to tune the parameters. The methodology presented uses a residual signal based on the generalized momentum of the motors, and it is able to estimate the internal stiffness of the device by using only the sensors which are normally used to control the joint. The ideas and methods presented in these Chapters have been published as author's original work in Flacco and De Luca [2011a],Flacco and De Luca [2011b] and Flacco et al. [2011].

Part I

Modeling

1 Introduction

Modeling a compliant actuator means to find the relation between the motors torque, the inertia energy due to the motion of the components and the potential energy, which is composed of two part, an external potential energy due to the gravity, and an internal potential energy given by the energy stored in the passive elements of the actuator. The presence of passive elements which compose a flexible transmission in the actuator is the principal difference w.r.t. a rigid joint. The flexibility in the transmission produces a non collocation in the input output relation, in other words, the motor torque do not control directly the link shaft, but it exchanges energy with the transmission generating a flexibility torque. From the other side, the link motion is actuated by this flexibility torque.

The flexibility torque plays a key role in compliant actuators, for this reason different mechanical solutions have been developed for generating and even controlling the flexibility of the transmission. Chapter 2 presents an overview of compliant devices developed in universities and research centers. A compliant devices is characterized by the arrangement of motors, flexible elements and rigid elements, and, despite the infinite possibilities is possible to group all compliant joints[1] in three categories:

- Single Actuated Flexible Transmission (SAFT);
- Antagonistic Variable Stiffness Actuator (aVSA);
- Serial Variable Stiffness Actuator (sVSA);

All devices in the same category share the same mathematical model, which will be described in Chapter 3.

When multiple compliant joints compose a robot the modeling is more complex, and usually a reduced model (see Spong [1987]) is used. The reduced model is based on the following assumption

1. Joint deflections are small, so that flexibility effects are limited to the domain of linear elasticity;

[1] In this Thesis we focused on compliant joints actuated by motors.

2. The actuators rotors are modeled as uniform bodies having their center of mass on the rotation axis;

3. Each motor is located on the robot arm in a position preceding the driven link. (This can be generalized to the case of multiple motors simultaneously driving multiple distal links);

4. The angular velocity of the rotors is due only to their own spinning;

The first assumption can be extended to nonlinearity, provided that the map from deflection to force is smooth and invertible.

2 Compliant Devices

Under the propulsion of new safety concepts many research centers have worked on the development of new generation of joints based on compliant actuators. The starting point has been the use of elastic transmissions in order to have joints with passive compliance. Then, new arrangements of flexible elements have been evaluated to obtain joints where the compliance can be actively controlled. In this chapter an overview of the research centers and universities which are involved in the development of compliant joints, with a brief description of the results obtained, will be presented. Part of this overview is based on Ham et al. [2009].

2.1 Carnegie Mellon University

A no longer active project of Carnegie Mellon University, headed by Professor Alfred Rizzi, was the development of robots that are capable of running, jumping, and stumble recovery, while being energetically efficient. The Actuator with Mechanically Adjustable Series Compliance (AMASC) is an actuation method that utilizes a large physical spring capacity and variable compliance, to enable such highly dynamic gaits.

AMASC

A design based on the principle of mechanically adjustable series compliance (AMASC) developed by Hurst et al. [2004]. As shown in Figure 2.1, the AMASC is a rather complex mechanism with a great number of pulleys and cables. Nevertheless, the advantage is that only one actuator is used to control compliance or equilibrium position. The working principle is based on the antagonistic setup of two nonlinear springs. In Figure 2.2, a schematic overview of the AMASC is given.

In the case of the AMASC, the nonlinear spring is formed by a set of spiral pulleys, which deform the two fiberglass leaf springs F_y, which are placed on both sides of the prototype (Figure 2.1). The pulleys are also used to uncouple the control of compliance and equilibrium position. The AMASC is an actuator where the compliance and the equilibrium position can be controlled independently, each by a dedicated motor. This independence makes the control easier and allows one to design the two motors separately to meet the demands of a specific application, e.g., compliance varies slowly while the equilibrium position has to be set faster. The main disadvantage of the AMASC is its complexity. Based on this concept, the biped robot BiMASC is designed. Here, the stiffness of the whole leg can changed instead of the stiffness of the joints.

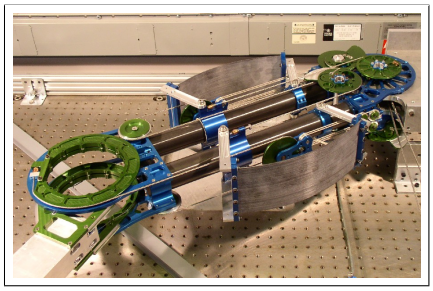

Figure 2.1: *The Actuator with Mechanically Adjustable Series Compliance (AMASC), developed by Carneige Mellon University. (figure from Hurst et al. [2004])*

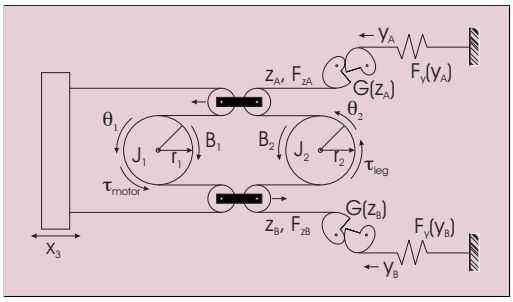

Figure 2.2: *Schematic overview of the AMASC (figure from Hurst et al. [2004])*

2.2 DLR

The departments of the institute of robotics and mechatronics at DLR, the German Aerospace Center in Germany, directed by Dr. Gerd Hirzinger, has been one of the most productive and advanced laboratory for the development and control of compliant devices. A particular mention has to be made to Dr. Alin Albu-Schäffer, director of the Mechatronic Component and System department, and his group.

VS-Joint

The core of the Variable Stiffness Joint (VS-Joint) presented by Wolf and Hirzinger [2008] is shown if Figure 2.3. The vertical position of the spring base slider is defined by the spindle that is actuated by the small motor for the stiffness operating point. This upper plate compresses the springs. The angular position of the upper plate is controlled by the position motor.

The cam disk (lower part) is connected to the joint. Figure 2.4 shows the unwinded schematic of the VS-Joint. The shaded part is one of the three cam disks, which are connected to the joint, whereas the linear bearing in the figure is connected to the upper plate and position motor. A roller is pushed by a spring to the lowest position in the cam disk. When a torque is applied on the joint, there will be a joint deflection of the roller, e.g., to the right, as shown in Figure 2.4(b), and pushing the roller upward causing a translational deflection of the springs. The spring pushes the roller downwards, which will generate a force in the direction of the lowest point of the cam disk. This lowest point is the equilibrium position of the joint. By changing the position motor, the angle of the stiffness mechanism is adjusted, and thus also the position where no torque is generated.

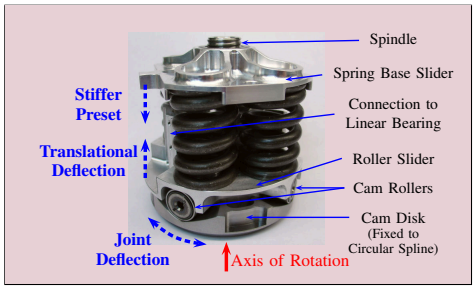

Figure 2.3: *The DLR Variable Stiffness Joint (VS-Joint). (figure from Wolf and Hirzinger [2008])*

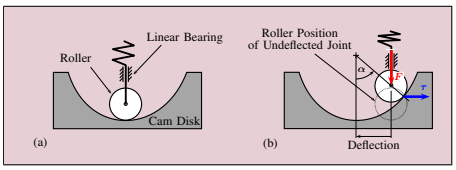

Figure 2.4: *Schematic of the cam disk principle of the VS-Joint: (a) in equilibrium position and (b) deflected position. (figure from Wolf and Hirzinger [2008])*

The advantage of this design is that can easily be integrated into a robotic arm. The shape of the cam disk can be adjusted to obtain a progressive, degressive, or linear system behavior. Although one spring is enough, the VS joint uses three springs for symmetry. It is also a design where two motors of different sizes can be used: a small one for the stiffness preset and a more powerful motor for the link position.

QA-Joint

In Eiberger et al. [2010] is presented the DLR Quasi-Antagonistic Joint (QA-Joint). The QA-Joint consists of a link positioning drive with HarmonicDrive gears and the elastic mechanism with the stiffness actuation drive. The main difference to a classical antagonistic joint is that the two motors are not used in a symmetric configuration as agonist and antagonist, c.f. Fig. 2.5(a). Instead, one motor (the link drive) adjusts the link side position, while the second motor (the stiffness drive) operates stiffness adjustment, c.f. Fig. 2.5(b). With this arrangement the adjustment of position and stiffness are already decoupled to a high extend in hardware design. This special form of antagonistic actuation is very advantageous for configurations with pronounced agonist actuation. The compliance consists of two progressive elastic elements opposing each other with a variable offset that supports the link with variable range of elastic motion, c.f. Fig. 2.6. The ordinary fixed Circular Spline of the Harmonic Drive gear for link positioning is held in a bearing and has a cam bar attached to it. Two pairs of rocker arms with cam rollers, each pair linked by a linear spring, act on different faces of this cam bar. External loads result in rotational displace-

ment of the entire gear and force the rocker arms of the supporting direction to spread against the linear spring. This causes a progressive centering torque. The agonist rocker arms are fixed w.r.t. the housing. The opposing antagonist part is positioned with at a rotational offset w.r.t. the stiffness actuator. In the QA-Joint the link position can be changed without moving the elasticity mechanism. This significantly reduces the inertia of the moving part of the join. The use of a cam-roller mechanism offers another advantage: The shape of the cam faces can be adapted to provide any desired torque characteristic that fits the maximum potential energy storable in the linear spring. Thus, the design is well suited to realize different torque/displacement characteristics with little overhead.

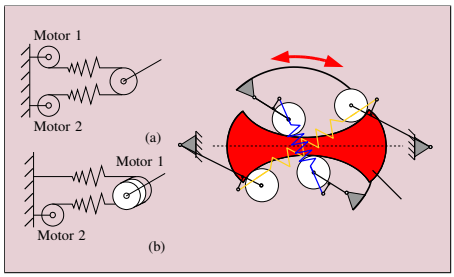

Figure 2.5: *Variable Stiffness Actuator with nonlinear progressive springs in antagonistic (a) and quasi antagonistic (b) realization. Principle of the elastic mechanism (right). (figure from Eiberger et al. [2010])*

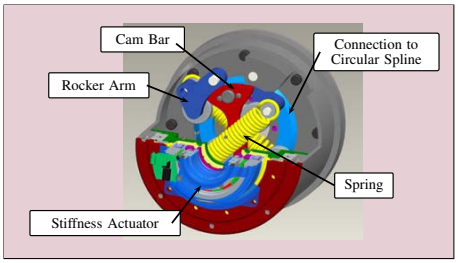

Figure 2.6: *Cross section of the Quasi Antagonistic Joint design. (figure from Eiberger et al. [2010])*

2.3 Italian Institute of Technology

The Italian Institute of Technology is a relatively new research center, very active in the development of compliant actuators. The Advanced Robotics department is directed by Darwin G. Caldwell.

AwAS

Figure 2.7 shows the conceptual schematic of the Actuator with Adjustable Stiffness (AwAs), where two antagonistic springs are connected on one side to the intermediate link and on the other side to the output link. The intermediate link is rigidly attached to the main joint motor. The lever arm is defined as the vertical distance between center of rotation of the link and the point at which springs are attached. A guiding mechanism driven by another motor allows the control of the length of the arm by moving the two springs toward to (to reduce stiffness) and away from (to increase stiffness) the center of rotation. When the output link is in its equilibrium position (the angular position where zero torque is generated, so when the extension of both springs is equal), then the force generated by the springs is perpendicular to the displacement needed to

change the stiffness. This has the important consequence that in principle no energy is needed to change the stiffness. In different designs the force is always parallel to the displacement requiring a strong motor and sufficient amount of energy to change the stiffness. In reality, the presence of friction has to be overcome. In addition if the joint is not in the equilibrium position the force generated by the spring has a small component parallel to the displacement and a small amount of energy is needed. However due to this property the motor controlling the stiffness can be significantly smaller than that in other designs of variable stiffness actuators. An additional advantage of this design is that it does not require the use of non-linear springs or mechanisms to provide the nonlinear force/displacement profile which is necessary for the stiffness regulation.

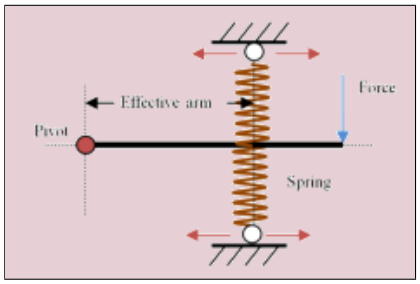

Figure 2.7: *Conceptual schematic of the Actuator with Adjustable Stiffness (AwAS). (figure from Jafari et al. [2011])*

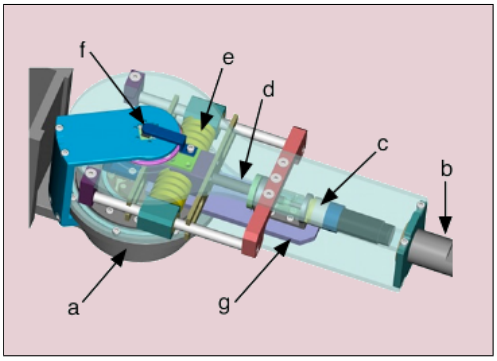

Figure 2.8: *CAD model of the Actuator with Adjustable Stiffness (AwAS). The principal motor (a) adjusts the link (b) positioning; the secondary motor (c) drives a ball screw mechanism (d), which moves the relative position of a pair of antagonistic springs (e) with respect to the center of rotation of the joint (f); the springs connect both the output link (b) and the intermediate link (g), which in turn is connected with the principal motor. (figure from Jafari et al. [2010])*

The AwAS has been used in this Thesis for simulations and experiments, for this reason the AwAS model is presented more in detail in section 4.2.

AwAS-II

The concept of AwAS-II is based on the variable ratio lever mechanism. In this case as it is shown in Figure 2.9 to tune the stiffness the location of the force and springs are kept fixed but instead the position of the pivot is changing. In the mechanical realization of AwAS-II as it can be seen in Figure 2.10 two antagonistic torsion springs are connected with a pre-deflection on one side to the output link and on the other side to one end of the lever. The other end of the lever is connected to the output link through a rotational joint. The intermediate link is rigidly attached to the main motor of the joint (M1). The pivot is a cam follower placed within the lever and connected to the slider which is actuated by a ball screw mechanism driven by another motor (M2). A linear guide passing through

the slider prevents the rotation of slider around the ball screw and supports the later forces when the output link is deflected from its equilibrium position.

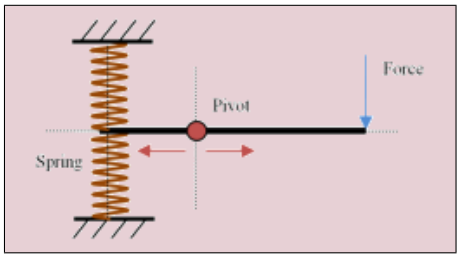

Figure 2.9: *Conceptual schematic of the AwAS-II. (figure from Jafari et al. [2011])*

The stiffness depends on the ratio which is defined as L1 the distance between the pivot and the end of the lever which is connected to the springs over L2 the distance between the pivot and another end of the lever which is connected to the output link. The lever can rotate around this latter end with respect to the output link. The lever can also rotates around the pivot, therefore if the link deviates from its equilibrium position springs become deflected depending on the position of the pivot. When the pivot is aligned with the center of rotation of M1, the ratio becomes zero (L1 =0) and the link exhibits zero stiffness. Moving the pivot away from this end, increase the stiffness until pivot reaches the other end and is aligned with the axis of the joint between the output link and the lever. In this position the ratio goes to infinitive (L2 =0) and the link becomes rigid. When the link deviates from its equilibrium position, the end of the lever

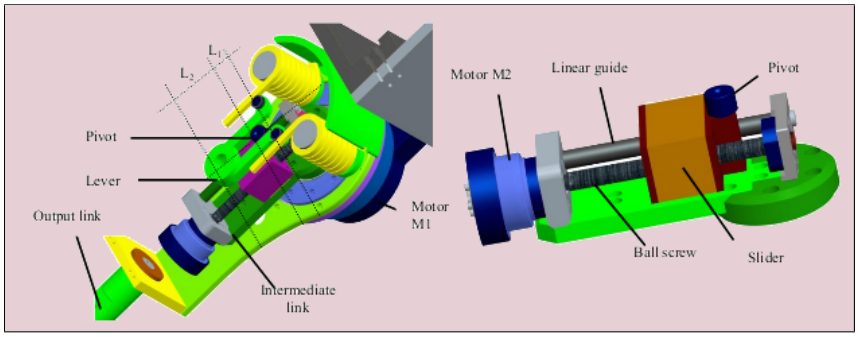

Figure 2.10: *CAD model of the AwAS-II. (figure from Jafari et al. [2011])*

which is connected to the springs slides along the springs legs, therefore to have a frictionless sliding motion, two rollers are placed between the lever and the each springs.

CompAct

The functional principle implemented for the CompAct-VSA is based on the same concept of lever with moving pivot of the AwAS-II shown in Figure 2.9. For the mechanical realization of CompAct-VSA unit particular attention was paid in Tsagarakis et al. [2011] to optimize the size, weight and modularity of the mechanical assembly in order to allow the future integration of the actuation unit into multi-dof VSA robotic systems. The high density of the integration is due to the novel mechanical implementation of the variable stiffness module. To minimize dimensions while achieving wide stiffness range, high torque capacity and fast stiffness regulation a mechanical arrangement involving a cam based profile lever arm mechanism with a variable pivot point was implemented. The

stiffness module of the CompAct-VSA is showed in Figure 2.11. Here, the cam lever arm (C) is connected with and transmits the torque to the output link through a rotational joint (A). In addition, two antagonistically arranged springs (H) are in contact with the cam lever arm through two cam rollers (E), to minimize friction. When a load is applied at the output link, the cam lever arm rotates around the pivot axis (P) and the two linear springs are displaced. To adjusts the stiffness, the position of the pivot point (a cam roller) of the lever arm, is regulated by a rack (F) and pinion transmission powered by the stiffness actuator (G), hereafter mentioned as M2.

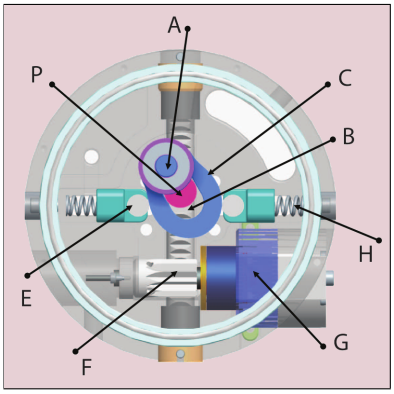

Figure 2.11: *CAD model of the CompAct-VSA. (figure from Tsagarakis et al. [2011])*

2.4 Korea University

The Intelligent Robotics Laboratory was established in 1993 when Dr. Jae-Bok Song joined the Department of Mechanical Engineering, College of Engineering, Korea University. In recent years they explored the use of compliant actuator for safe pHRI, developing their own mechanical solution.

SJM

The Safe Joint Mechanism (SJM), presented in Park et al. [2008], is composed of the passive mechanical elements such as linear springs and a modified slider-crank mechanism. The springs are used to absorb the large collision force for safety, while the slider-crank mechanism shown in Figure 2.15 determines whether the safety feature is activated or not so that the SJM operates only in case of an emergency. The main contribution of this device is the variable stiffness capability implemented only by use of simple passive mechanical elements. Without sacrificing positioning accuracy for safety, both features can be achieved simultaneously with the SJM.

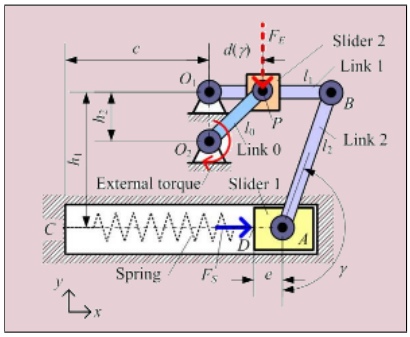

Figure 2.12: *Slider-crank mechanism combined with spring of the Safe Joint Mechanism (SJM). (figure from Park et al. [2008])*

SDAU

The Serial-type Dual Actuation Unit (SDAU) Kim et al. [2010] is composed of two actuators and a planetary gear train. Two actuators are connected in series via a planetary gear train, and each actuator is responsible for positioning and variable stiffness independently. Since one actuator [called a positioning actuator (PA)] controls position and the other actuator [called a stiffness modulator (SM)] modulates stiffness, the DAU can control position and stiffness simultaneously at the same joint. By using a planetary gear train, it is possible to adjust its gear ratio depending on the applications, thereby optimizing the system size.

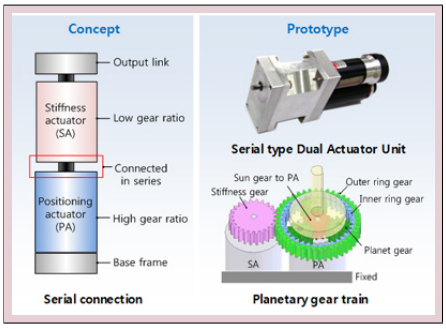

Figure 2.13: *Conceptual schematic and prototype of the Serial-type Dual Actuator Unit (SDAU). (figure from IRL website)*

PDAU

Though the SDAU can control the joint stiffness directly at any time, there is some limitation to obtain a high stiffness due to the serial connection of two actuators. Unlike the SDAU, the parallel-type dual actuator unit (PDAU) adopts the antagonistic mechanism of the muscular skeletal system of human articulation. The PDAU consists of a dual-cam follower mechanism, which acts like a human muscle, and a drive module with two motors. Each cam placed inside the dual cam-follower mechanism has two types of cam profile to provide a wide range of stiffness variation and collision safety. The use of the PDAU enables simultaneous position and stiffness control. Moreover, the PDAU can immediately change a joint stiffness to a very low value when an external force greater than a predetermined threshold occurs, so that it offers collision safety without an expensive joint torque sensor.

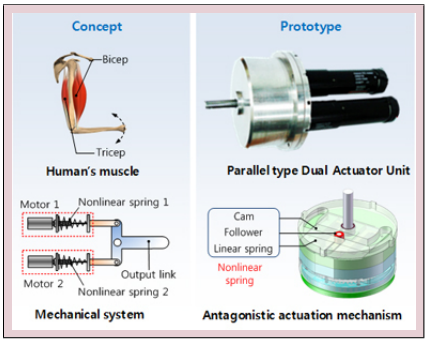

Figure 2.14: *Conceptual schematic and prototype of the Parallel-type Dual Actuator Unit (PDAU). (figure from IRL website)*

HDAU

Variable impedance actuators require a wide range and a fast response time of stiffness variation as well as a large passive deflection angle. Furthermore, constant joint stiffness, which is independent of the passive deflection angle, is advantageous to control the contact force. To satisfy these requirements, the

Hibrid-type Dual Actuator Unit (HDAU) Kim and Song [2010] adopts a hybrid control mechanism. The HDAU is composed of a hybrid control module based on an adjustable moment arm mechanism and a drive module with two motors. We can control position and stiffness simultaneously for the same joint by controlling the relative motion of gears in the hybrid control module. The HDAU provides a wide range of joint stiffness due to nonlinearity obtained from the adjustable moment arm. Joint stiffness can be kept constant independent of the passive deflection angle of the output shaft. Furthermore, stable interaction can also be achieved because the joint stiffness is indirectly adjusted by position control of the hybrid control module.

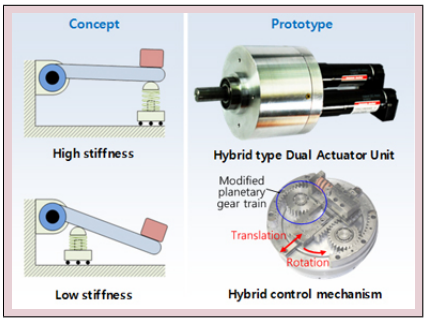

Figure 2.15: *Conceptual schematic and prototype of the Hibrid-type Dual Actuator Unit (HDAU). (figure from IRL website)*

2.5 MIT

The Leg Laboratory at Massachuset Institute of Technology (MIT), founded by Marc Raibert , was one of the first research group who started to study the benefits of compliant actuation. Their research was focused on mimic the elastic behavior of human legs.

SEA

The Serial Elastic Actuator (SEA) Pratt and Williamson [1995] is essentially a spring in series with a stiff actuator. The compliance is determined by the spring constant and is therefore not adjustable during operation. The SEA is a compliant actuator allowing force to be controlled in an easy manner. Figure 2.16 shows a typical setup of a SEA for force control. The elongation of the spring is used as force measurement and fed back in the control loop.

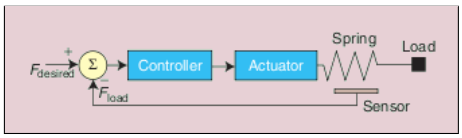

Figure 2.16: *Force control of a Serial Elastic Actuator (SEA) (figure from Ham et al. [2009])*

2.6 Stanford University

The Artificial Intelligence Laboratory at Stanford University, directed by Professor Oussama Khatib, is involved on the development of human-friendly robots.

DM^2

The distributed macro-mini actuation approach (DM^2) Zinn et al. [2005], has been developed to overcome the safety limitations of joint torque control and the performance limitations of series elastic actuation. As the name implies, the DM^2 approach employs a pair of actuators, connected in parallel and distributed to different locations on the manipulator. The effective inertia of the overall manipulator is substantially reduced by isolating the reflected inertia of the actuator while greatly reducing the overall weight of the manipulator. Performance is maintained with small actuators collocated with the joints. Their approach partitions the torque generation into low and high frequency components and distributes these components to the arm location where they are most effective. The overall approach is shown in Figure 2.17.

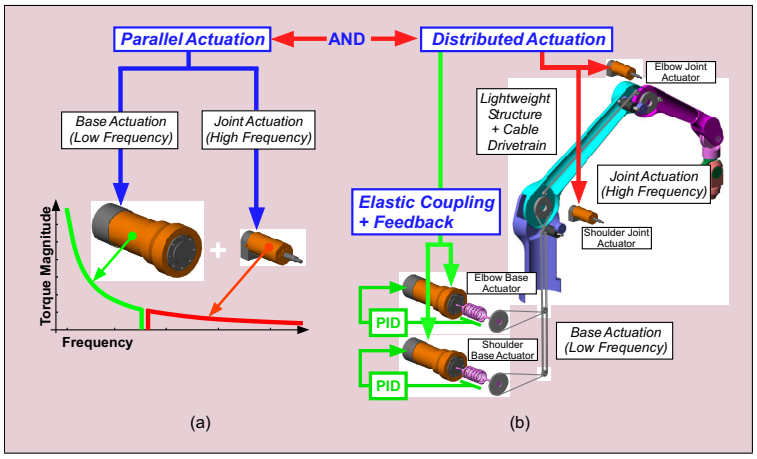

Figure 2.17: *Distributed Macro-Mini (DM^2) actuation approach (a)Partition of torque into low and high frequency (parallel) components (b) Distributed actuation: Large, low frequency actuators are located at base. Small, high frequency actuators are located at the joints. (figure from Zinn et al. [2005])*

$S2\rho$

The Stanford Safety Robot (S2ρ),Shin et al. [2010], shown in Figure 2.18, is an evolution of the DM^2 approach in which compliant pneumatic muscles replace the macro actuators at the base. The S2ρ robotic arm uses two McKibben muscles in parallel on each side of the pulley as macro actuator. Pairs of muscles were used in an antagonistic configuration, pulling on a cable that wraps around a pulley at the joint. The S2ρ robotic arm is controlled employing macro and mini actuators in parallel. The controller partitions the Note that due to the redundancy in the actuation, given a joint torque, there is an infinite set reference input torque between the low frequency macro actuator and the high frequency mini actuator. Because of slow dynamics of the low frequency actuator, the high frequency components of the reference input are directly commanded into the high frequency actuator as the error. For low frequency actuation, low impedance output is achieved by using the light and compliant

pneumatic muscles connected directly to the joint. For high frequency actuation, low impedance is achieved by using a small, low-inertia motor connected through a low-ratio transmission. This combination reduces the effective inertia of the arm and increases the bandwidth for closed-loop control.

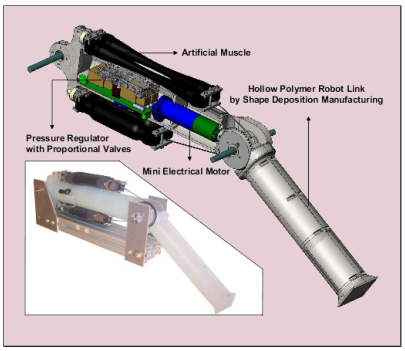

Figure 2.18: *The Stanford Safety Robot (S2ρ) prototype (figure from Shin et al. [2010])*

2.7 University of Pisa

The interdepartmental research center "E. Piaggio" at the University of Pisa, directed by Professor Antonio Bicchi, has been one of the precursor of variable stiffness actuators, using antagonistic arrangement of nonlinear transmission.

VSA

The Variable-Stiffness Actuator (VSA) Tonietti et al. [2005] is composed of a timing transmission belt (Figure 2.19(1)), tensioned by linear springs (Figure 2.19(5-6-7)). The transmission belt connects nonlinearly the main shaft (Figure 2.19(4)) to the antagonistic pair of actuators pulleys (Figure 2.19(2-3)) rigidly connected to position-controlled back-drivable DC motors. The conceptual design of the VSA prototype is described in Figure 2.19.

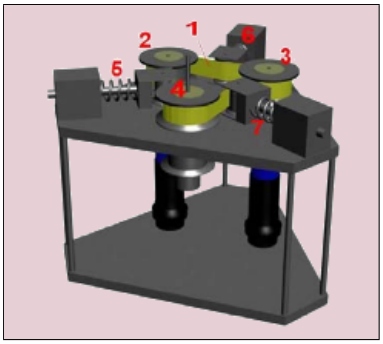

Figure 2.19: *Transmission belt 1 connects the DC Motors pulleys 2-3 to the joint shaft 4, and it is tensioned by passive elastic elements 5-6-7. Perspective view of the Variable Stiffness Actuator. The (figure from Tonietti et al. [2005])*

VSA-II

The VSA-II Schiavi et al. [2008] actuator is based on a bi-directional antagonistic arrangement of two motors driving a single joint through a flexible transmission system. The basic element of the transmission is a 4-bar mechanism. a so-called Grashof neutral linkage, with a linear spring (see Fig. 2.20), which introduces a nonlinear torque-displacement characteristic between the input torque applied by the motor and the angular deflection of the joint shaft. We note that the nonlinearity is due to the geometry, not to the spring itself which behaves in the elastic domain. The design is more robust than the original VSA-I prototype Tonietti et al. [2005].

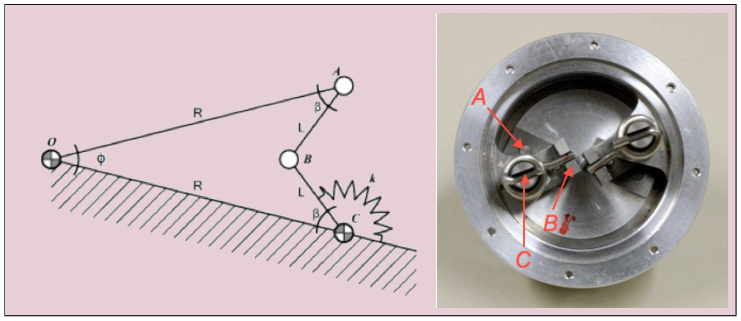

Figure 2.20: *Left: A single four-bar linkage of the VSA-II (modified from Schiavi et al. [2008]). Right: The assembly of two such linkages for one of the two motors (A, B, and C are corresponding points in the two pictures)*

The VSA-II has been used in this Thesis to test the control algorithms in simulations. For this reason the VSA-II model is presented more in detail in section 4.1.

VSA-HD

The four-bar mechanism of the VSA-II presents an intrinsic limitation due to a singularity. In the VSA-HD Catalano et al. [2010a], a cam profile is adopted to overcome the singularity. Fig. 4.3 shows an isometric view of the lower part of the actuator with detail of the cam component: a sequence of screenshots is reported to illustrate the singularity trespassing. The cam profile (red), centered in O, and its conjugate profile on link L1 (green) are designed so as to guide L1 when in proximity of its singular position. This solution preserves the PE allowing smaller value of minimum stiffness and giving the actuator pure symmetric bidirectional behavior.

2.8 University of Twente

The Control Engineering group at the University of Twente, directed by Professor Stefano Stramigioli, started few years ago to develop new compliant devices.

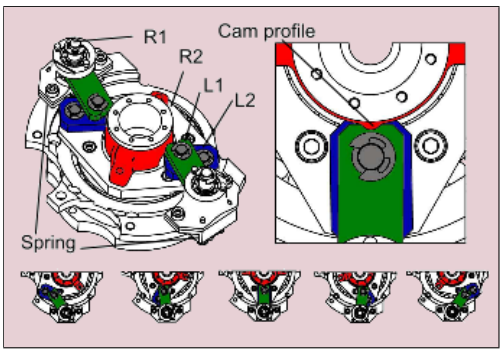

Figure 2.21: *Isometric view of the actuator lower side (left) with a couple of four bar linkages; detail of cam system (left) and screenshots sequence of linkages movements. (image from Catalano et al. [2010a])*

vsaUT

The variable stiffness actuator of the University of Twente (vsaUT) Groothuis et al. uses the same lever with moving pivot used in the AwAs-II and the CompAct (Figure 2.9). Fig. 2.22(left) shows a clear CAD drawing of the actuator. The actuator frame is rotated by a motor via a timing belt. The other motor is used to vary the pivot point position. The output can be recognized as a solid bar sticking out of the actuator frame. The lever arm is connected to the frame by means of linear springs. The spring setting is shown in Fig. 2.22(right), in an unloaded (no load on the output), but pretensioned, and loaded (a force on the output) configuration. While the springs are connected to one end of the lever arm, the output (not shown here) is connected to the other end. As a result of the pivot position in the lever arm, the stiffness perceived at the output, due to the tension in the springs, is varied.

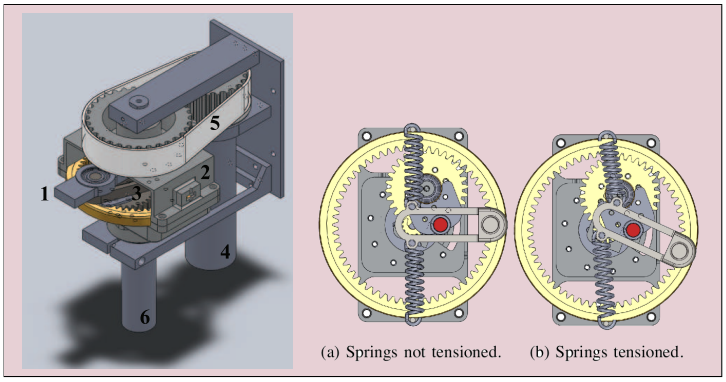

Figure 2.22: *The vsaUT-II variable stiffness actuator CAD (left) The labels indicate 1) the output, 2) the actuator frame, 3) the lever arm and gears mechanism, 4) motor for changing output position, 5) timing belt transmission and 6) motor for varying output stiffness. View of the lever arm mechanism connected to the springs (right). (figure from Groothuis et al.)*

2.9 Vrije Universiteit Brussel

The Robotics and Multibody Mechanics at Vrije Universiteit Brussel, directed by Professor Dirk Lefeber, developed two compliant actuators using different actuation methodologies.

PPAM

Instead of using a SEA, pneumatic artificial muscles (PAMs) are often used. When pressurized, the muscle contracts axially while expanding radially. The compressibility of air makes them inherently compliant, behaving in a spring-like fashion. One of the drawbacks is the hysteresis introduced by friction, which makes it difficult to control, and it has a substantial threshold of pressure, before any force is generated. The pleated PAM (PPAM) Verrelst et al. [2005] drastically reduces hysteresis and overcomes the threshold of pressure. Figure 2.23 shows an implementation of the PPAM in the biped Lucy Verrelst et al. [2005]. Pneumatic muscles are actuators with a high power-to-weight ratio and can be directly coupled to the joint without a heavy and complex gearing mechanism. The drawbacks of a joint actuated by two pneumatic muscles are the nonlinear characteristic of the joint, slow dynamics (especially depressurizing the muscle is slow), presence of hysteresis, and need for pressurized air.

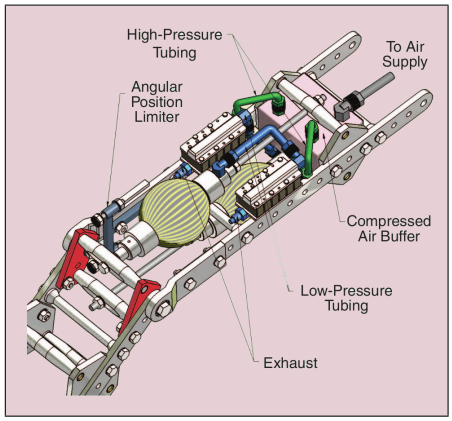

Figure 2.23: *Antagonistic setup of two pleated PAM (PPAM). (figure from Ham et al. [2009])*

MACCEPA

Besides the development and implementation of the PPAM, they developed a second actuator with adaptable compliance. The Mechanically Adjustable Compliance and Controllable Equilibrium Position Actuator (MACCEPA) Ham et al. [2007] is a straightforward and easy to construct rotational actuator, of which the compliance can be controlled separately from the equilibrium position. Each of these parameters is set by a position controlled servo motor. Moreover, the torque is a linear function of the compliance and of the angle between equilibrium position and actual position. Thus this actuator can be

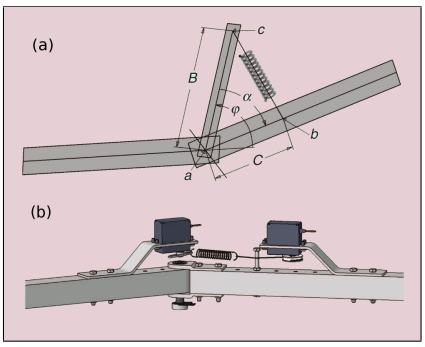

Figure 2.24: *Working principe (a) and CAD (b) of the MACCEPA. (figure from Ham et al. [2009])*

seen as a fully adaptable torsion spring, where one motor sets the stiffness of the torsion spring, and another set the equilibrium position. Since this actuator has a spring it can store and release energy. This makes this actuator perfectly suitable for dynamic walking and human-robotic interfaces.

2.10 Waseda University

In the Sugano Laboratory at Waseda University, directed by Shigeki SUGANO, was developed the first prototype of compliant actuator which uses two separate actuators. The first actuator control the joint position, while the second motor change the stiffness of the joint. In this Thesis we will refer to this actuation approach as serial VSA.

MIA

The Mechanical Impedance Adjuster (MIA) Morita and Sugano [1995] consists of three components, a Compliance Adjuster, a Pseudo Damper and a Joint Driver. A configuration and fundamental motions of the MIA is shown in Figure 2.25. The MIA can realize an extremely high level compliance to adapt to the environments and follow external forces by using the Compliance Adjuster. The Compliance Adjuster employs a mechanically compliant leaf spring which is directly mounted in it, to ensure ideal joint compliance without being affected by the servo response. So, the MIA can always provide passive compliance against any disturbance forces. By changing it to a stiff state using a slider mechanism, the MIA can perform high-power work and realize stable manipulation (Figure 2.25 (a), (b)). In the MIA, a joint angle is positioned as the Joint Driver moves in reference to the main shaft which is connected to the leaf spring. When the leaf spring is set to stiff state, the Joint Driver acts as the conventional joint mechanisms (Figure 2.25 (c)). If an external force is applied to a casing, the displacement of the casing is directly transmitted to the leaf spring via the slider, because the main shaft is relative to an another casing (Figure 2.25 (d)).

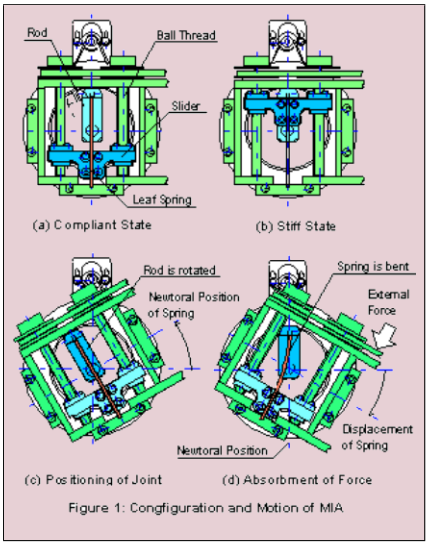

Figure 2.25: *Fundamental motion of the Mechanical Impedance Adjuster (MIA). (figure from Sugano lab. website)*

For adjustment of damping factor, a dry type single disk electromagnetic brake and pseudo-damping control method are used. The brake generates brake forces according to flows of electric current through an electromagnet coil. The brake disk is fixed to the main shaft using a small spring. A pseudo damping effect can be obtained by PWM control of the electric current in proportion to the angular velocity of the joint which is detected by the encoder.

3 Models

In the previous chapter an overview of existing compliant joints have been presented. Exploring their characteristic is possible to verify that even if is there are many feasible arrangements of motors, flexible elements and rigid connections, as investigated in Catalano et al. [2010b], solutions which have been developed can be grouped in three categories: SAFT, antagonistic VSA and serial VSA.

A characterization and the dynamic model of each of this three categories will be presented in this chapter.

3.1 SAFT

In this Thesis we will refer to devices characterized by a driving motor serially connected to the driven link through of deformable transmissions as Single Actuated Flexible Transmission (SAFT). In Fig. 3.1 is shown schematically a SAFT. The deformation ϕ of the transmission is the difference between the link angle q and the motor angle θ ($\phi = q - \theta$). The latter is possibly reflected through a reduction gear with ratio $\gamma \geq 1$ (i.e., $\dot{\theta} = \dot{\theta}_m/\gamma$, where θ_m is the position of the motor as measured by an encoder mounted on its axis[1].

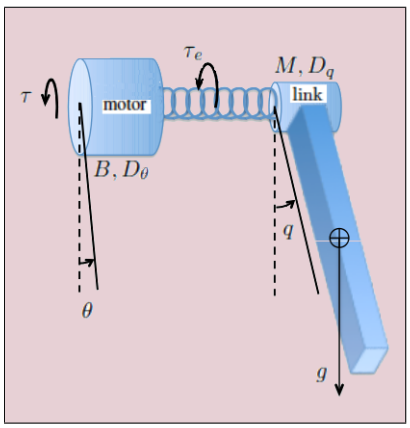

Figure 3.1: *Schematic model of a Single Actuated Flexible Transmission (SAFT).*

Let $U_e(\phi) \geq 0$ be the potential energy associated to the deformation ϕ, with $U_e(\phi) = 0$ if and only if $\phi = 0$. The *flexibility torque* across the trans-

[1] As customary, we model a flexible geared transmission as a rigid reduction gear followed in series by a flexible element.

mission is given by

$$\tau_e(\phi) = \frac{\partial U_e(\phi)}{\partial \phi},$$

which is in general a nonlinear function of ϕ. Without loss of generality, we will assume that

$$\tau_e(0) = 0, \qquad \tau_e(-\phi) = -\tau_e(\phi), \quad \forall \phi, \tag{3.1}$$

i.e., no torque is provided through the undeformed transmission, and the transmission has the same behavior in compression and extension.

When a single motor drives a rigid link, possibly subject to gravity, through a (nonlinear) flexible transmission, the dynamic model takes the form

$$M\ddot{q} + D_q\dot{q} + \tau_e(\phi) + g(q) = \tau_{\text{ext}} \tag{3.2}$$

$$B\ddot{\theta} + D_\theta\dot{\theta} - \tau_e(\phi) = \tau, \tag{3.3}$$

where $M > 0$ and $B = B_m\gamma^2 > 0$ are the link inertia and the reflected motor inertia (with the rotor having inertia B_m), $D_q \geq 0$ and $D_\theta = D_{\theta,m}\gamma^2 \geq 0$ are the viscous friction coefficients at the two sides of the transmission, τ is the motor control torque reflected through the gear ratio ($\tau = \tau_m\gamma$, being τ_m the motor torque on its output axis), and $g(q)$ and τ_{ext} are, respectively, the gravity and the environment/disturbance torques acting on the link.

The stiffness of the transmission is defined as the variation rate of the elastic torque $\tau_e(\phi)$ w.r.t. the deformation ϕ,

$$\sigma(\phi) = \frac{\partial \tau_e(\phi)}{\partial \phi} > 0. \tag{3.4}$$

While slightly different definitions of stiffness can be found in the literature, see, e.g., Ozawa and Kobayashi [2002], Grioli and Bicchi [2011], we consider in (4.5) the internal stiffness of the transmission/flexible joint, usually called *passive stiffness*. Passive stiffness refers thus to the torque needed to deform the transmission. In the absence of gravity ($g(q) \equiv 0$), the passive stiffness coincides with the *external stiffness*

$$\sigma_{\text{ext}}(\phi) = \frac{\partial \tau_{\text{ext}}}{\partial q} = \frac{\partial \tau_{\text{ext}}}{\partial \phi} = \left(\frac{\partial \phi}{\partial \tau_{\text{ext}}}\right)^{-1},$$

which is the inverse of the compliance of the joint, i.e., the deformation of the transmission in response to external torques τ_{ext} applied to the link in *static* conditions (with the motor position θ kept fixed). Such a compliance can be experimentally evaluated.

The model described above can be applied to the SEA and to the SJM.

Extension to multi d.o.f.

Consider a robot manipulator having N elastic joints of constant stiffness and with N driving motors. Let $\boldsymbol{q}$ and $\boldsymbol{\theta}$ be the N-dimensional vectors of link and motor variables, and $\boldsymbol{\phi} = \boldsymbol{\theta} - \boldsymbol{q}$ the vector of transmissions deformation. Under the simplifying modeling assumption of Spong [1987] (Section 1), and including

also viscous effects at the motor and link side, the dynamic model takes the form

$$\boldsymbol{M}(\boldsymbol{q})\ddot{\boldsymbol{q}} + \boldsymbol{c}(\boldsymbol{q},\dot{\boldsymbol{q}}) + \boldsymbol{g}(\boldsymbol{q}) + \boldsymbol{D}_q\dot{\boldsymbol{q}} + \boldsymbol{\tau}_e(\boldsymbol{\phi}) = \boldsymbol{0} \tag{3.5}$$

$$\boldsymbol{B}\ddot{\boldsymbol{\theta}} + \boldsymbol{D}_\theta\dot{\boldsymbol{\theta}} - \boldsymbol{\tau}_e(\boldsymbol{\phi}) = \boldsymbol{\tau}, \tag{3.6}$$

where $\boldsymbol{M} > 0$ is the robot inertia matrix, the constant diagonal matrix $\boldsymbol{B} > 0$ contains the motor inertias, $\boldsymbol{c}$ is the vector of centrifugal and Coriolis terms, $\boldsymbol{g}$ is the gravity vector, $\boldsymbol{\tau}_e > 0$ is the vector of flexibility torques, and $\boldsymbol{D}_q$ and $\boldsymbol{D}_\theta$ are positive semi-definite diagonal matrices of viscous friction coefficients. In case of *elastic* potential $U_e = \frac{1}{2}\boldsymbol{\phi}^T\boldsymbol{K}\boldsymbol{\phi}$ associated to (7.48–7.49), it leads to *linear* elasticity torque vector $\boldsymbol{\tau}_e$ and *constant* device stiffness (diagonal) matrix $\boldsymbol{\sigma}$

$$\boldsymbol{\tau}_e = \left(\frac{\partial U_e}{\partial \boldsymbol{q}}\right)^T = \boldsymbol{K}\boldsymbol{\phi}, \qquad \boldsymbol{\sigma} = \frac{\partial \boldsymbol{\tau}_e}{\partial \boldsymbol{q}} = \boldsymbol{K}.$$

3.2 Antagonistic VSA

The model in (3.2–3.3) can be extended to express the dynamics of an actuator with variable stiffness (VSA). An antagonistic VSA is characterized by two motors working in parallel and antagonistically connected to the driven link through nonlinear transmissions, as shown in fig. 3.2. Although different arrangements are possible, we will consider in the following only the bi-directional one, see Bicchi et al. [2008a]. Depending on the realization, the nonlinearity of the deformation/torque characteristic of the transmissions results either by the use of nonlinear (e.g., cubic or exponential) springs or by the arrangement of linear springs in a nonlinear kinematic mechanism. The two motor-transmission units are modeled with two similar equations of the form (3.3), where each motor-transmission undergoes a deformation $\phi_i = q - \theta_i$, for $i = 1, 2$. The dynamics of an antagonistic VSA is thus

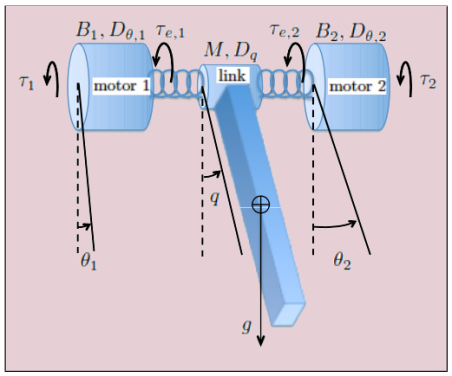

Figure 3.2: *Schematic model of a Variable Stiffness Actuator (VSA) in antagonistic arrangement*

$$M\ddot{q} + D_q\dot{q} + \tau_{e,t}(\boldsymbol{\phi}) + g(q) = \tau_{\text{ext}} \tag{3.7}$$

$$B_i\ddot{\theta}_i + D_{\theta,i}\dot{\theta}_i - \tau_{e,i}(\phi_i) = \tau_i, \quad i = 1, 2. \tag{3.8}$$

In this case, the *total flexibility torque* transmitted to the driven link and the associated (total) *device stiffness* are given by

$$\tau_{e,t}(\boldsymbol{\phi}) = \tau_{e,1}(\phi_1) + \tau_{e,2}(\phi_2) \tag{3.9}$$

and

$$\sigma_t(\boldsymbol{\phi}) = \sigma_1(\phi_1) + \sigma_2(\phi_2), \tag{3.10}$$

where

$$\sigma_i(\phi_i) = \frac{\partial \tau_{e,i}(\phi_i)}{\partial \phi_i} > 0, \quad i = 1, 2, \tag{3.11}$$

are the local stiffnesses of the two transmissions and $\boldsymbol{\phi} = (\phi_1, \phi_2)$. We note the separability of the functions (3.9) and (3.10), whereas in general $\phi_1 \neq \phi_2$. Moreover, most of the times the two motor-transmission units are identical (perfect symmetry). However, our later developments apply directly to the general case. The A-VSA model can be used for the PDAU, DM^2, S2ρ, VSA, VSA-II, VSA-HD and PPAM.

Importance of nonlinear transmission

In antagonistic VSAs is fundamental that at least one of the two transmissions is nonlinear. This necessity can be shown with the follow simple example. Consider two linear transmission in eq. (3.8), respectively with flexibility torque

$$\tau_{e,1}(\phi_1) = K_1 \phi_1 \qquad \text{and} \qquad \tau_{e,2}(\phi_2) = K_2 \phi_2 \,,$$

where K_1 and K_2 are the elastic constant of the two elastic transmissions. The total flexibility torque in eq. (3.7) given by eq. (3.9) is

$$\tau_{e,t}(\boldsymbol{\phi}) = K_1 \phi_1 + K_2 \phi_2 \,,$$

and the total stiffness is derived using eq. (3.11) and eq. (3.10)

$$\sigma_t(\boldsymbol{\phi}) = K_1 + K_2 \,.$$

It results a constant total stiffness, which is not a function of the deformation of the transmission. In other words it cannot be varied. It follows that an antagonist VSA with linear transmissions is not a variable stiffness device.

Extension to multi d.o.f.

A general dynamic model of a N-dof manipulator driven by VSA can be written by compounding the robot link dynamics with the proper motor equations introduced above. Under a similar assumption as used in Spong [1987] (Section 1) for modeling robots with elastic joints of constant stiffness, i.e., that the rotational kinetic energy of the rotors of the two motors at each joint is due only to their own spinning, the dynamic model for a robot with antagonistic VSA takes the form

$$\begin{aligned} \boldsymbol{M}(\boldsymbol{q})\ddot{\boldsymbol{q}} + \boldsymbol{C}(\boldsymbol{q}, \dot{\boldsymbol{q}})\dot{\boldsymbol{q}} + \boldsymbol{D}_{\boldsymbol{q}}\dot{\boldsymbol{q}} + (\boldsymbol{\tau}_{e,1}(\boldsymbol{\phi}) + \boldsymbol{\tau}_{e,2}(\boldsymbol{\phi})) + \boldsymbol{g}(\boldsymbol{q}) &= \boldsymbol{\tau}_{\text{ext}} \\ \boldsymbol{B}_1 \ddot{\boldsymbol{\theta}}_1 + \boldsymbol{D}_1 \dot{\boldsymbol{\theta}}_1 - \boldsymbol{\tau}_{e,1}(\boldsymbol{\phi}) &= \boldsymbol{\tau}_1 \\ \boldsymbol{B}_2 \ddot{\boldsymbol{\theta}}_2 + \boldsymbol{D}_2 \dot{\boldsymbol{\theta}}_2 - \boldsymbol{\tau}_{e,2}(\boldsymbol{\phi}) &= \boldsymbol{\tau}_2, \end{aligned} \tag{3.12}$$

where $\boldsymbol{q} \in \mathbb{R}^N$, $\boldsymbol{\theta} \in \mathbb{R}^N$, $\boldsymbol{\phi} = \boldsymbol{q} - \boldsymbol{\theta}$, $\boldsymbol{M}$ is link inertia matrix, $\boldsymbol{C}$ is the factorization matrix of the Coriolis and centrifugal terms, $\boldsymbol{D}_{\boldsymbol{q}}$ is the (diagonal) viscous friction matrix on the link sides, and $\boldsymbol{g}$ is the gravity vector term. Moreover, for $j = 1, 2$, the matrices $\boldsymbol{B}_j$ and $\boldsymbol{D}_j$ of motor inertias and damping are diagonal, while the dependence of the flexibility torque vectors $\boldsymbol{\tau}_{e,j}$ on $\boldsymbol{\phi}$ is componentwise separable (the k-th components depend only on ϕ_k).

3.3 Serial VSA

A serial VSA, consists of a *principal* motor, used to command the link motion through the flexible transmission, and of a *secondary* motor, used to modify the stiffness of the transmission by changing the operating point on its characteristics (or, equivalently, by shaping the potential energy associated to the deformation). Figure 3.3 shows a schematic model of a serial VSA. The angular position of the secondary motor (called also set-point variable), as reflected through a reduction gear with ratio $\gamma_c \geq 1$, will be denoted by θ_c. In this case, the dynamic model takes the form

$$\begin{aligned} M\ddot{q} + D_q\dot{q} + \tau_e(\theta_c, \phi) + g(q) &= \tau_{\text{ext}} \\ B\ddot{\theta} + D_\theta\dot{\theta} - \tau_e(\theta_c, \phi) &= \tau \\ B_c\ddot{\theta}_c + D_{\theta,c}\dot{\theta}_c + \psi_e(\theta_c, \phi) &= \tau_c, \end{aligned} \tag{3.13}$$

where, together with the notations inherited from (3.2–3.3), $B_c = B_{m,c}\gamma_c^2 > 0$ and $D_{\theta,c} = D_{\theta_{m,c}}\gamma_c^2 > 0$ are, respectively, the reflected inertia and viscous friction coefficient of the secondary motor, and τ_c is its reflected torque ($\tau_c = \tau_{m,c}\gamma_c$). The function $\psi_e(\theta_c, \phi)$ is the *coupled* flexibility torque, representing how the transmission deformation reacts on the secondary motor as a function of the set-point variable. Actually, this is an undesirable dynamic coupling behavior and mechanical solutions that minimize this effect are usually chosen. For this case, the *device stiffness* is defined as

$$\sigma(\theta_c, \phi) = \frac{\partial \tau_e(\theta_c, \phi)}{\partial \phi}, \tag{3.14}$$

since the coupled flexibility torque plays no role.

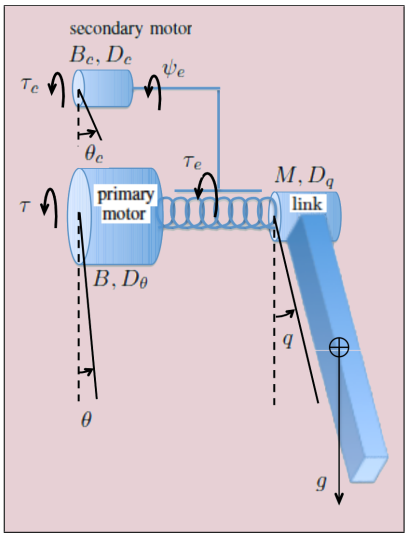

Figure 3.3: *Schematic model of a Variable Stiffness Actuator (VSA) in serial arrangment*

Extension to multi d.o.f.

Similarly to the antagonistic case the Spong [1987] assumption (Section 1) have been used to obtain the model of a N-dof manipulator with Serial VSA

$$\begin{aligned} \boldsymbol{M}(\boldsymbol{q})\ddot{\boldsymbol{q}} + \boldsymbol{C}(\boldsymbol{q}, \dot{\boldsymbol{q}})\dot{\boldsymbol{q}} + \boldsymbol{D_q}\dot{\boldsymbol{q}} + \boldsymbol{\tau}_e(\boldsymbol{\theta}_c, \boldsymbol{\phi}) + \boldsymbol{g}(\boldsymbol{q}) &= \boldsymbol{\tau}_{\text{ext}} \\ \boldsymbol{B}\,\ddot{\boldsymbol{\theta}} + \boldsymbol{D}_\theta\,\dot{\boldsymbol{\theta}} - \boldsymbol{\tau}_e(\boldsymbol{\theta}_c, \boldsymbol{\phi}) &= \boldsymbol{\tau} \\ \boldsymbol{B}_c\,\ddot{\boldsymbol{\theta}}_c + \boldsymbol{D}_{\theta,c}\,\dot{\boldsymbol{\theta}}_c + \boldsymbol{\psi}_e(\boldsymbol{\theta}_c, \boldsymbol{\phi}) &= \boldsymbol{\tau}_c, \end{aligned} \tag{3.15}$$

where $\boldsymbol{q} \in \mathbb{R}^N$, $\boldsymbol{\theta} \in \mathbb{R}^N$, $\boldsymbol{\phi} = \boldsymbol{q} - \boldsymbol{\theta}$, $\boldsymbol{M}$ is link inertia matrix, $\boldsymbol{C}$ is the factorization matrix of the Coriolis and centrifugal terms, $\boldsymbol{D_q}$ is the (diagonal)

viscous friction matrix on the link sides, and $\boldsymbol{g}$ is the gravity vector term. The matrices $\boldsymbol{B}$, $\boldsymbol{B}_c$ and $\boldsymbol{D}_\theta$, $\boldsymbol{D}_{\theta,c}$ are the diagonal inertias and damping matrices for the principal and secondary motor respectively. The flexibility torque vector is $\boldsymbol{\tau}_e(\boldsymbol{\theta}_c, \boldsymbol{\phi})$ and the coupled flexibility torque vector is $\boldsymbol{\psi}_e(\boldsymbol{\theta}_c, \boldsymbol{\phi})$.

4 VSA-II and AwAS

The second part of this Thesis will be centered on the control of VSAs. To prove the effectiveness and performance of our methodologies simulations and experiments will be proposed, using both Antagonistic and Serial VSAs. In this chapter we present a more detailed description of the VSA-II and the AwAS which have been introduced in Chapter 2, and will be used in the second part as test devices.

4.1 VSA-II

The Variable Stiffness Actuator II (VSA-II) Schiavi et al. [2008], developed by the University of Pisa, has been described in Section 2.7. We recall here the dynamic model of the VSA-II introduced in Schiavi et al. [2008]. The notation is slightly modified, and is similar to the one commonly used for elastic joints of constant stiffness (see, Chapter 3).

The VSA-II is an Antagonistic VSA (Section 3.2), tush its dynamic model can be expressed with eq.(3.7-3.8). With reference to the left side of Fig. 4.1,

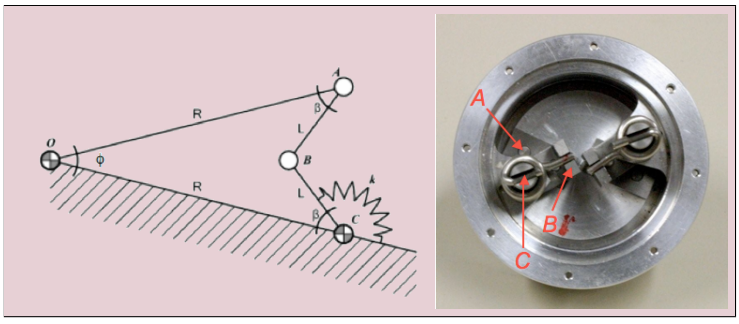

Figure 4.1: *Left: A single four-bar linkage of the VSA-II (modified from Schiavi et al. [2008]). Right: The assembly of two such linkages for one of the two motors (A, B, and C are corresponding points in the two pictures)*

let ϕ be the angle connected to the motor position (input) and β the angle connected to the load (output). It is

$$\beta(\phi) = \arcsin\left(\frac{R}{L}\sin\left(\frac{\phi}{2}\right)\right) - \frac{\phi}{2}. \tag{4.1}$$

A mechanical stop ensures the avoidance of the linkage singularity at $\phi = 0$. Thus, from the geometry $\phi \in (0, \phi_{\max})$, with $\phi_{\max} = 2\arcsin(L/R)$ and $L < R$. The torsional spring of (constant) stiffness k is at rest when $\phi = \beta = 0$. Its potential energy is thus $P(\phi) = \frac{1}{2}k\beta^2(\phi)$ and the torque at the motor end O due to the deflection β is

$$\tau_e(\phi) = \frac{\partial P(\phi)}{\partial \phi} = k\,\beta(\phi)\,\frac{\partial \beta(\phi)}{\partial \phi} \geq 0. \tag{4.2}$$

Therefore, the (nonlinear) stiffness seen at O, as expressed in eq. (4.5) is

$$\sigma(\phi) = \frac{\partial \tau_e(\phi)}{\partial \phi} = k\left(\left(\frac{\partial \beta(\phi)}{\partial \phi}\right)^2 + \beta(\phi)\,\frac{\partial^2 \beta(\phi)}{\partial \phi^2}\right) > \sigma_{\inf}, \tag{4.3}$$

with $\sigma_{\inf} = 0.25\,k\,((R/L) - 1)^2 > 0$. While the explicit expressions of τ_e and σ in (4.2) and (4.3) can be found in Schiavi et al. [2008], the above compact forms will be useful for control implementation. The following developments hold true for any other specific form of the nonlinear geometry $\beta(\phi)$ in (4.1).

In the VSA-II, *two* such pairs of 4-bar mechanisms are combined for each motor and the two motors are assembled in antagonistic mode as in Fig. 4.2. Let θ_1 and θ_2 be the motor positions, and q be the position of the driven link (output load). Replacing ϕ in eq. (4.2) by $\phi_1 = q - \theta_1$ and $\phi_2 = q - \theta_2$, respectively for the motor 1 and 2 at the two sides of the joint, the torque exerted on the load due to the transmission deflections is given by eq. (3.9)

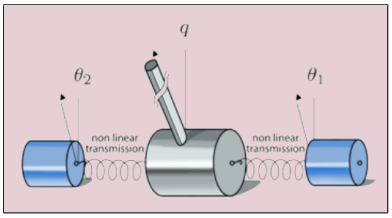

Figure 4.2: *VSA-II antagonistic principle (modified from Schiavi et al. [2008])*

$$\tau_{e,t} = 2\left(\tau_e(\phi_1) + \tau_e(\phi_2)\right), \tag{4.4}$$

where the factor 2 appear due to the two pairs of 4-bar mechanism. The associated (total) stiffness (eq. (3.10)) is

$$\sigma = \sigma_1(\phi_1) + \sigma_2(\phi_2) = 2\left(\sigma(\phi_1) + \sigma(\phi_2)\right), \tag{4.5}$$

where the expression of the functions σ_i, $i = 1, 2$, is given by eq. (4.3).

Consider a 1-dof arm (single link) driven by the VSA-II, moving in the vertical plane, and possibly undergoing collisions. The dynamic model can be derived from eq.(3.7-3.8)

$$\begin{aligned} M\ddot{q} + D_q\dot{q} + mgd\sin q + \tau_{e,t} &= \tau_{\text{ext}}, \\ B\,\ddot{\theta}_1 + D_\theta\,\dot{\theta}_1 - 2\,\tau_e(\phi_1) &= \tau_1 \\ B\,\ddot{\theta}_2 + D_\theta\,\dot{\theta}_2 - 2\,\tau_e(\phi_2) &= \tau_2 \end{aligned} \tag{4.6}$$

where B and M are the inertias of the rotor of the two (identical) DC motors and, respectively, of the link (at the joint axis), D and D_q are the (small) coefficients of viscous friction at the motor sides and at the link side, m and d are the mass of the link and the distance of its center of mass from the joint, g is the gravity acceleration, τ_1 and τ_2 are the control torques produced by the two motors, and τ_{ext} is the torque resulting from a link collision (when present).

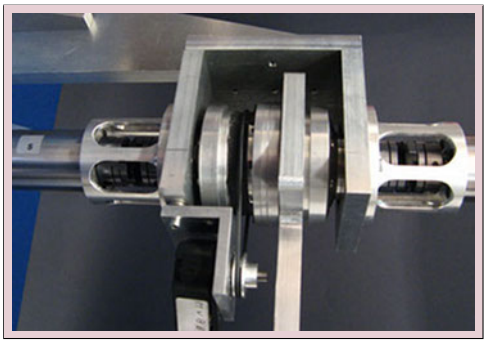

Figure 4.3: *The VSA-II prototype. (modified from Schiavi et al. [2008])*

The model parameters (from Schiavi et al. [2008]) are:

$$
\begin{aligned}
&R/L = 14/8 = 1.75\,,\\
&k = 500 \text{ [N·mm/rad]},\\
&M = 0.1,\ B = 7.3 \text{ [Kg·m·mm]},\\
&D_\theta = 0,\ D_q = 100 \text{ [[N·mm·s/rad]}.
\end{aligned}
$$

4.2 AwAS

The Actuator with Adjustable Stiffness Jafari et al. [2010], developed at the Italian Institute of Technology, and described in Section 2.3, can be modeled as a Serial VSA (see Section 3.3).

The AwAS (Fig. 4.4) actuator adjusts the stiffness at the joint through the variation of the relative distance between a pair of springs and the center of rotation of the joint, using a lever mechanism. The lever arm is adjusted by the secondary motor as

$$r = r_0 - b\theta_c, \tag{4.7}$$

where r_0 is the initial length of the lever arm, θ_c is the angular position of the motor, and b is the transmission ratio between the secondary motor and the ballscrew.

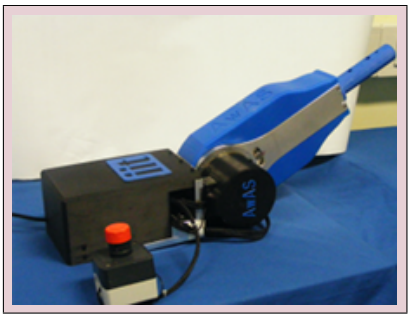

Figure 4.4: *The AwAS prototype (modified from Jafari et al. [2010])*

The dynamics of the AwAS is described by model (4.11), where the flexibility torque $\tau_e(r,\phi)$ and the stiffness $\sigma(r,\phi)$ are expressed as functions of r and are defined by

$$\tau_e(r,\phi) = k_s r^2 \sin 2\phi \tag{4.8}$$

and

$$\sigma(r, \phi) = 2k_s r^2 \cos 2\phi, \tag{4.9}$$

being k_s the stiffness of the springs and r the length of the lever arm, which is the effective distance between the center of rotation of the joint and the springs. Finally, the torque that the transmission applies back to the secondary motor is

$$\psi_e(r, \phi) = -2k_s br \sin^2 \phi. \tag{4.10}$$

With reference to the model (4.11) and eqs. (4.8–4.10), the AwAS model is

$$\begin{aligned} M\ddot{q} + D_q\dot{q} + \tau_e(r, \phi) + g(q) &= \tau_{\text{ext}} \\ B\ddot{\theta} + D_\theta\dot{\theta} - \tau_e(r, \phi) &= \tau \\ B_c\ddot{\theta}_c + D_{\theta,c}\dot{\theta}_c + \psi_e(r, \phi) &= \tau_c, \end{aligned} \tag{4.11}$$

with nominal parameters from Jafari et al. [2010]:

$$\begin{aligned} &M = 0.1,\ B = 2.3 \cdot 10^{-5},\ B_c = 1.29 \cdot 10^{-7}\ [\text{kg·m}^2], \\ &D_q = 0.15,\ D_\theta = 0.001,\ D_{\theta_c} = 0.0141\ [\text{N·m·s/rad}], \\ &\gamma = 50,\ \gamma_c = 23,\ k_s = 14220\ [\text{N/m}],\ r_0 = 0.1\ [\text{m}], \\ &b = 0.0025/2\pi\ [\text{m/rad}]. \end{aligned}$$

Part II

Control

5 Introduction

The control of compliant actuators requires to take into consideration the flexibility of the transmission. In the previous part of this Thesis the importance of the flexibility torque in the modeling of compliant actuators has been shown. This flexibility can be considered from a control point of view as an undesired behavior, and, control laws designed to reduce it can be realized, indeed in this case the capability of compliant joints would not be exploited, and only a loss of performance w.r.t. rigid joint would be obtained. Moreover in case of variable stiffness devices the presence of two control input permits to control two different output, thus control laws specially designed to take advantage of the device capability have to be developed.

To design a control law is fundamental to choose which are the sensed variables. If the use of powerful sensors had been assumed, e.g. torque sensors, it would have simplified the control design, despite that, in this Thesis only the sensors that are common to all compliant devices presented in Chapter 2 are assumed to be used. Namely in our controller we assume to have a position sensor, e.g. encoder, to measure the link position q and a position sensor for each motor to measure the motor angle θ. Using this two values is possible to obtain the deformation of the transmission ϕ which play a key role on the control of compliant joints.

The last remark is about the knowledge of the parameters of the model. In the control laws that will be presented in Chapter 6–7 the knowledge of all parameters of the model will be assumed. While inertia and damping for the motor and the link can be obtained trivially from the motor data sheet and through dedicated experiments, the complete knowledge of the behavior of the flexible transmission is not so simple to obtain, due to the nonlinearity and the complexity of the mechanism. To cope with this problem in Chapter 9 an estimator of the internal stiffness of the joint, which permits to derive all the values, associated to the flexible transmission, needed for the control, will be presented.

6

Feedback Linearization

From the point of view of performance, control design should be aimed at compensating for the static deflection and dynamic vibrations associated to the presence of (constant or time-varying) compliant transmissions, so as to accurately execute fast motions as in the rigid case. For instance, model-based nonlinear feedback control allows to cancel completely these effects in robots with elastic joints of constant stiffness [Spong, 1987, De Luca and Lucibello, 1998]. For some instances of 1-dof arms with variable stiffness actuation, feedback linearization has been proven effective in controlling both the link motion and the desired stiffness in an antagonistic case [Palli et al., 2007] and in one with separate actuation [Choi et al., 2008]. More in general, two classes of multi-dof robots with variable joint stiffness have been considered in [Palli et al., 2008], one where the stiffness can be modified instantaneously by a specific input command and another where this additional control input modulates the stiffness through a second-order mechanical system. Depending on the class type, a dynamic or, respectively, a static feedback linearization law was shown to be sufficient for the simultaneous and decoupled control of the motion and stiffness outputs. Nonetheless, the feasibility of these general control approaches depends on the chosen mechanical implementation of variable stiffness actuation. As a matter of fact, one should check the invertibility of the so-called decoupling matrix of the system on a case-by-case basis.

In this chapter, the feedback linearization control will be presented. In Sect. 6.1 a brief introduction on the feedback linearization theory is given, and this theory is applied to SAFTin Sect.6.2, antagonistic VSA in Sect. 6.3 and serial VSA in Sect. 6.4. The motion control, which permits to track the desired position and possibly the desired stiffness, will be introduced in Sect. 6.5. It follows in Sect. 6.6 simulations with the VSA-II joint.

6.1 Introduction

The idea under the feedback linearization is to cancel *external* nonlinear behaviors of the system using the the input. External means that only the behavior of some outputs can be linearized, generally as many as the inputs. Obviously all other outputs and the internal part of the system will remain nonlinear.

From a mathematical point of view the desired outputs to be linearized have to be differentiate w.r.t. the time until all inputs appear. With this derivation the controlling dynamics of the inputs to the outputs is obtained, in other words how the outputs act to the inputs through the nonlinearity is obtained. Therefore this relation can be inverted for canceling the nonlinearities, making the input output relation linear.

The number of differentiation of the output must be equal to dimension of the state of the system. This guarantees that the feedback linearization controls all internal dynamics of the system, resulting in a stable closed loop system. If this condition is not satisfied some internal dynamics, called *zero dynamic*, are not controlled. In this case a *dynamic* feedback linearization is needed in order to stabilize zero dynamics. In this section it will be shown that compliant actuators can be linearized with a *static* feedback linearization controller, since no zero dynamics are present.

6.2 SAFT

In single actuated flexible transmission is present only one input, the motor torque τ in eq. (3.2) , tush only one output can be feedback linearized. The link position q has been chosen as desired output

$$y = q\,, \tag{6.1}$$

since in classical application the control of the link position is requested.

With reference to the SAFT model (3.2–3.3), assuming that external forces are not present $\tau_{ext} = 0$, the output differentiation is given by

$$\begin{aligned}
y &= q \\
\dot{y} &= \dot{q} \\
\ddot{y} &= \ddot{q} = \frac{-1}{M}\left(\tau_e + D_q\dot{q} + g(q)\right) \\
y^{[3]} &= \frac{-1}{M}\left(\sigma\,\dot{\phi} + D_q\ddot{y} + \dot{g}(q,\dot{q})\right) \\
y^{[4]} &= \frac{-1}{M}\left(\frac{\partial\sigma}{\partial\phi}\dot{\phi}^2 + \sigma\ddot{y} + D_q y^{[3]} + \ddot{g}(q,\dot{q},\ddot{y}) - \frac{\sigma}{B}\left(\tau_e - D_\theta\dot{\theta} + \tau\right)\right) = \\
&= b(\boldsymbol{x}) + \frac{\sigma}{MB}\tau
\end{aligned} \tag{6.2}$$

where b is a function of the state $\boldsymbol{x} = (\theta, q, \dot{\theta}, \dot{q})$. The number of derivation is equal to the dimension of the state of the system, tush no zero dynamics are present. The system can be trivially linearized by inverting the last equation in (6.2)

$$\tau = \frac{MB}{\sigma}\left(v_1 - b(\boldsymbol{x})\right)\,, \tag{6.3}$$

where v_1 is the input of the new linear closed loop system $q^{[4]} = v_1$.

6.3 Antagonistic VSA

In [Schiavi et al., 2008], a simple linear law of the PD type has been used for controlling both the link motion and the device stiffness for antagonistic VSAs. Good results were obtained by suitably combining the control inputs and by defining as controlled outputs the average and the difference of the two motor positions, which are associated respectively to the link position and to the device stiffness. However, this association holds true only at steady-state and in the absence of gravity. A more formal approach is pursued here based on system inversion (or feedback linearization) and considering directly the output of interest, i.e.,

$$\boldsymbol{y} = \begin{pmatrix} y_1 \\ y_2 \end{pmatrix} = \begin{pmatrix} q \\ \sigma \end{pmatrix}, \tag{6.4}$$

under the action of the control input, i.e, the motors torque. The actual computation of a feedback linearization control law depends on the mechanical implementation of the variable stiffness actuation principle. In particular, its applicability relies on the nonsingularity of the decoupling matrix of the system. We will see that the model (3.7-3.8) of a 1-dof arm driven by an antagonistic VSA can be transformed into decoupled chains of input-output integrators (thus, a linear and easily controllable system), provided that the device is pre-loaded to a positive (and typically, moderate) value of stiffness. As a result of the achieved decoupling, each output component in (6.4) can be independently and simultaneously controlled.

The system inversion algorithm formally proceeds on the model by differentiating each output component a finite number of times until at least one of the inputs appear. At this differential level, one can try to invert the system and find the expression of the required input-output decoupling control law. If the sum of the orders of output differentiation is equal to the dimension of the state space, then the same decoupling control law achieves also full linearization of the original system, which is what happens here. It should be stressed that *no* differentiation of measured quantities is actually needed in this control law if the full system state is available. In the following, we assume $\tau_{ext} = 0$ in (3.7-3.8)).

For the first output, we have

$$\begin{aligned} y_1 &= q \\ \dot{y}_1 &= \dot{q} \\ \ddot{y}_1 &= \ddot{q} = \frac{-1}{M}\left(\tau_{e,t} + D_q\dot{q} + g(q)\right) \\ y_1^{[3]} &= \frac{-1}{M}\left(\sigma_1\,\dot{\phi}_1 + \sigma_2\,\dot{\phi}_2 + D_q\ddot{q} + \dot{g}(q)\right) \\ y_1^{[4]} &= b_1(\boldsymbol{x}) + \frac{1}{MB}\left(\sigma_1\,\tau_1 + \sigma_2\,\tau_2\right), \end{aligned} \tag{6.5}$$

where b_1 is a function of the state $\boldsymbol{x} = (\theta_1, \theta_2, q, \dot{\theta}_1, \dot{\theta}_2, \dot{q})$.

In the same way, for the second output

$$\begin{aligned} y_2 &= \sigma \\ \dot{y}_2 &= \dot{\sigma} = \frac{\partial \sigma_1}{\partial \phi_1}\dot{\phi}_1 + \frac{\partial \sigma_2}{\partial \phi_2}\dot{\phi}_2 \\ \ddot{y}_2 &= b_2(\boldsymbol{x}) + \frac{-1}{B}\left(\frac{\partial \sigma_1}{\partial \theta_1}\tau_1 + \frac{\partial \sigma_2}{\partial \theta_2}\tau_2\right), \end{aligned} \tag{6.6}$$

with similar functional dependence for b_2. We can thus write

$$\begin{pmatrix} y_1^{[4]} \\ \ddot{y}_2 \end{pmatrix} = \boldsymbol{b}(\boldsymbol{x}) + \mathcal{A}(\boldsymbol{x}) \begin{pmatrix} \tau_1 \\ \tau_2 \end{pmatrix}, \tag{6.7}$$

where the *decoupling matrix*

$$\mathcal{A}(\boldsymbol{x}) = \boldsymbol{\Gamma} \begin{pmatrix} \sigma_1 & \sigma_2 \\ \dfrac{\partial \sigma_1}{\partial \theta_1} & \dfrac{\partial \sigma_2}{\partial \theta_2} \end{pmatrix} \tag{6.8}$$

is actually only a function of the differences $q - \theta_1$ and $q - \theta_2$ ($\boldsymbol{\Gamma}$ is a constant diagonal, and invertible matrix), and $\boldsymbol{b}(\boldsymbol{x})$ is the vector composed of b_1 and b_2. The determinant of $\mathcal{A}$, evaluated for the mechanical parameters of the VSA-II device, is shown in Fig. 6.1 as a function of its arguments. One can immediately

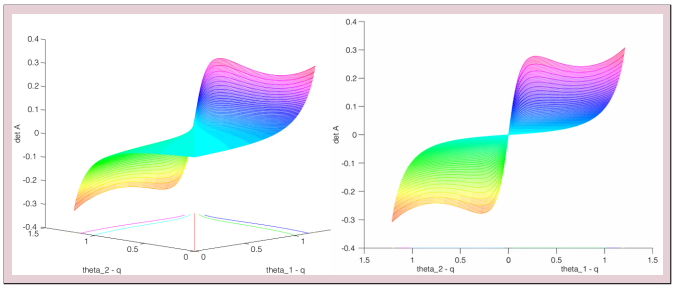

Figure 6.1: *The determinant of the decoupling matrix $\mathcal{A}$ as a function of its arguments $\theta_1 - q$ and $\theta_2 - q$: 3D view (left) and side view (right)*

see that matrix $\mathcal{A}$ is always nonsingular unless $\theta_1 = \theta_2$. Thus, if the VSA is kept always in an operation mode where $\theta_1 \neq \theta_2$, the following control law

$$\begin{pmatrix} \tau_1 \\ \tau_2 \end{pmatrix} = \mathcal{A}^{-1}(\boldsymbol{x}) \left(\begin{pmatrix} v_1 \\ v_2 \end{pmatrix} - \boldsymbol{b}(\boldsymbol{x}) \right) \tag{6.9}$$

solves the decoupling problem, leading to a chain of *four* integrators between the new control input v_1 and the output $y_1 = q$ and a chain of *two* integrators between the new control input v_2 and the output $y_2 = \sigma$. Since the sum $4+2 = 6 = n$, being n the dimension of the system state, the nonlinear state feedback law (6.9) fully linearizes the closed-loop dynamics. Also, gravity compensation is already embedded in the feedback linearizing controller.

In order to guarantee that the condition $\theta_1 \neq \theta_2$ holds at all times, and thus the validity of the proposed control approach, it is sufficient to pre-load the VSA at time $t = 0$ so that $\theta_1(0) - q(0) \neq \theta_2(0) - q(0)$, for any initial value $q(0)$ of the link position. Accordingly, the device will display an initial stiffness $\sigma(0) > 0$. Imposing now, for an arbitrary motion of $q(t)$, a desired evolution of the stiffness $\sigma_d(t)$, with $\sigma_d(0) = \sigma(0)$, which is sufficiently bounded away from zero will thus preserve the nonsingularity of matrix $\mathcal{A}$. In fact, this desired behavior $\sigma_d(t)$ can be perfectly reproduced thanks to the decoupling and output inversion properties of the control law (6.9). For this, it will be sufficient to set $v_2(t) = \ddot{\sigma}_d(t)$, while $v_1(t)$ independently defines the evolution of $q(t)$.

6.4 Serial VSA

With reference to the serial VSA model (3.13) we proceed to differentiate the output of interest (6.4), assuming $\tau_{ext} = 0$.

For the first output, we have

$$\begin{aligned} y_1 &= q \\ \dot{y}_1 &= \dot{q} \\ \ddot{y}_1 &= \ddot{q} = \frac{-1}{M}\left(\tau_e + D_q\dot{q} + g(q)\right) \\ y_1^{[3]} &= \frac{-1}{M}\left(\sigma\dot{\phi} + \frac{\partial\tau_e}{\partial\theta_c}\dot{\theta}_c + D_q\ddot{q} + \dot{g}(q)\right) \\ y_1^{[4]} &= b_1(\boldsymbol{x}) + \frac{1}{M}\left(\sigma\,\frac{\tau}{B} - \frac{\partial\tau_e}{\partial\theta_c}\,\frac{\tau_c}{B_c}\right), \end{aligned} \tag{6.10}$$

where b_1 is a function of the state $\boldsymbol{x} = (\theta_1, \theta_c, q, \dot{\theta}_1, \dot{\theta}_c, \dot{q})$.

In the same way, for the second output

$$\begin{aligned} y_2 &= \sigma \\ \dot{y}_2 &= \dot{\sigma} = \frac{\partial\sigma}{\partial\phi}\,\dot{\phi} + \frac{\partial\sigma}{\partial\theta_c}\,\dot{\theta}_c \\ \ddot{y}_2 &= b_2(\boldsymbol{x}) - \frac{\partial\sigma}{\partial\theta}\,\frac{\tau}{B} + \frac{\partial\sigma}{\partial\theta_c}\,\frac{\tau_c}{B_c}, \end{aligned} \tag{6.11}$$

with similar functional dependence for b_2.

As for the antagonistic case the number of derivation is equal to the dimension of the state vector of the system. We can thus write

$$\begin{pmatrix} y_1^{[4]} \\ \ddot{y}_2 \end{pmatrix} = \boldsymbol{b}(\boldsymbol{x}) + \mathcal{A}(\boldsymbol{x}) \begin{pmatrix} \tau \\ \tau_c \end{pmatrix}, \tag{6.12}$$

where the *decoupling matrix*

$$\mathcal{A}(\boldsymbol{x}) = \boldsymbol{\Gamma} \begin{pmatrix} \sigma & -\dfrac{\partial\tau_e}{\partial\theta_c} \\ -\dfrac{\partial\sigma}{\partial\theta} & \dfrac{\partial\sigma}{\partial\theta_c} \end{pmatrix} \tag{6.13}$$

is actually only a function of ϕ and θ_c ($\boldsymbol{\Gamma}$ is a constant diagonal, and invertible matrix), and $\boldsymbol{b}(\boldsymbol{x})$ is the vector composed of b_1 and b_2. The determinant of $\mathcal{A}$

depends on the parameter of the flexible transmission. Taking into consideration the AwAS model Sect. 4.2 the determinant of $\mathcal{A}$ is

$$\det(\mathcal{A}) = \frac{8k_s^2 b}{MBB_c}(r_0 - b\theta_c)^3, \tag{6.14}$$

which is always different from zero. Therefore pre-compression of the transmission is not needed and the decoupling matrix can be always inverted.

6.5 Motion control

More in general, the control design should be completed by specifying linear control laws v_1 in the SAFTs, and v_1 and v_2 in VSAs that stabilize the system to the desired task, expressed in term of link and stiffness behavior. In order to asymptotically reproduce a desired trajectory $q_d(t)$ for the link position and, simultaneously, a trajectory $\sigma_d(t)$ for the stiffness, we set

$$\begin{aligned} v_1 &= q_d^{[4]} + k_{q,3}(q_d^{[3]} - q^{[3]}) + k_{q,2}(\ddot{q}_d - \ddot{q}) \\ &\quad + k_{q,1}(\dot{q}_d - \dot{q}) + k_{q,0}(q_d - q) \\ v_2 &= \ddot{\sigma}_d + k_{\sigma,1}(\dot{\sigma}_d - \dot{\sigma}) + k_{\sigma,0}(\sigma_d - \sigma), \end{aligned} \tag{6.15}$$

where $k_{\sigma,1} > 0$, $k_{\sigma,0} > 0$, and the gains $k_{q,i}$ are chosen so that $s^4 + k_{q,3}s^3 + k_{q,2}s^2 + k_{q,1}s + k_{q,0}$ is a (Hurwitz) polynomial having all roots in the left-hand side of the complex plane. The actual values of the control gains in (6.15) can be chosen, e.g., by pole placement techniques, yielding exponential convergence of the trajectory tracking errors to zero. The higher-order derivatives of q that appear in (6.15), in the same way as σ and its first derivative, can be directly evaluated as functions of the state of the system by means of eq. (6.2) for SAFTs, eqs. (6.5–6.6) for antagonistic VSAs or eqs. (6.10–6.11) for serial VSAs. Thus, there is never a need to differentiate w.r.t. time the (possibly noisy) measured state variables.

A final remark concerns the requirement of smoothness over time for the desired motion and stiffness trajectories. It is apparent from (6.15) that the link trajectory $q_d(t)$ should be differentiable at least four times, whereas the stiffness trajectory $\sigma_d(t)$ at least two times. If this is the case, the control law (6.9–6.15) will guarantee perfect reproduction for initially matched state conditions, and only exponential tracking otherwise. If a reference trajectory lacks the required smoothness at some point in time, there will be a transient error which is then recovered with the prescribed dynamics imposed by the stabilizing linear control action.

6.6 Simulation results

Antagonistic VSA

The performance of the feedback linearization/decoupling control of Sect. 6.3 is illustrated here by means of numerical simulations with the VSA-II model described in Section 4.1.

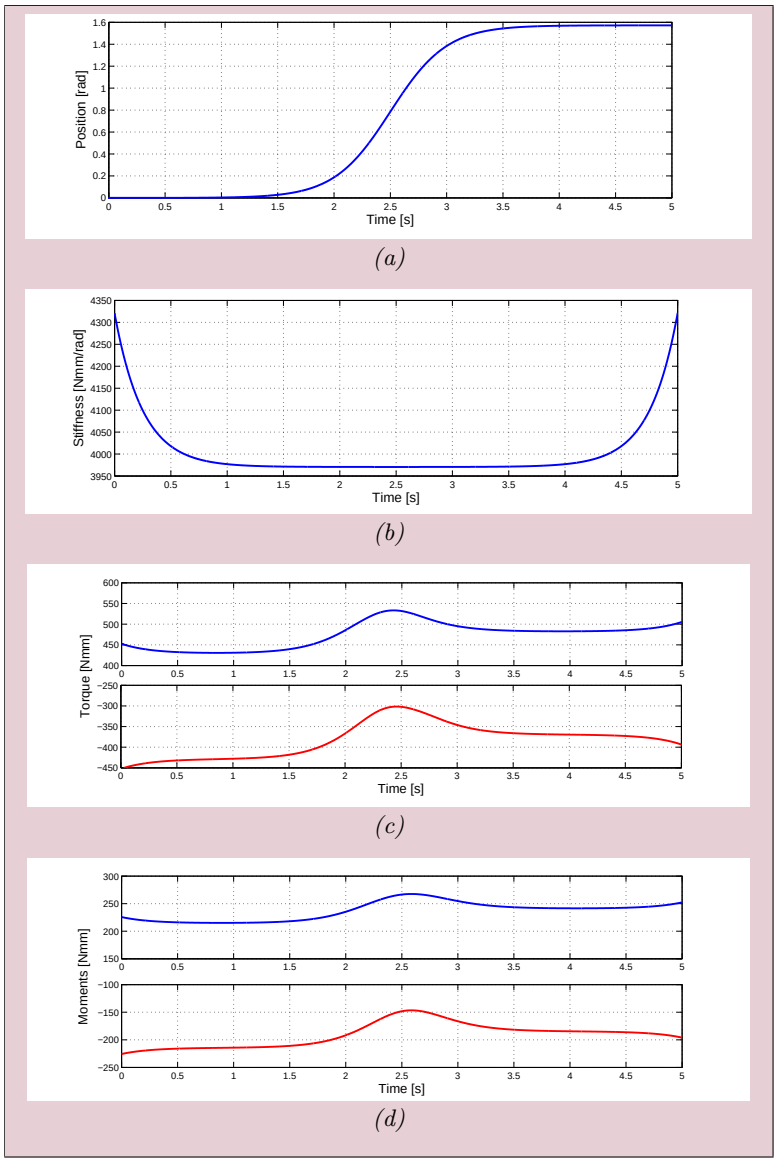

Figure 6.2: *Free motion of the VSA-II using feedback linearization control. Considering matched initial condition: (a) position q; (b) stiffness σ; (c) control torques τ_1 and τ_2; (d) Deflection torques $\tau_{e,1}$ and $\tau_{e,1}$*

In the absence of collisions, the reference trajectories for the position and

stiffness on a finite time interval $[0, T_{\text{tot}}]$ are chosen as follows:

$$\begin{aligned} q_d(t) &= \frac{1}{2\pi} \frac{1}{1+e^{10-4t}} + q_{\text{init}} \\ \sigma_d(t) &= \frac{1}{\dot{q}_d} + \sigma_{\text{init}}. \end{aligned} \tag{6.16}$$

The link should execute an (approximate) rest-to-rest motion of 90° in $T_{\text{tot}} = 5$ s (q_{init} sets the link position start at the downward equilibrium $q = 0$), while the stiffness profile complies with the safety rule "stiff when slow, soft when fast" (σ_{init} sets the desired stiffness at $t = 0$). These reference behaviors are reminiscent of the safe brachistochrone proposed in [Bicchi and Tonietti, 2004], but with conveniently added smoothness.

Figure 6.2 shows the results obtained when the initial state of the system is matched with the reference trajectories and their derivatives. Since the state error is initially zero, this condition is kept throughout the motion/stiffness task, independently from the chosen control gains. Moreover, the imposed initial value for stiffness σ implies $\theta_1(0) \neq \theta_2(0)$. Since the control torques remain always bounded, this condition is kept during the whole motion (thus, the decoupling matrix is never singular).

As a second example, the system is started with an initial position error of 10° and a stiffness error of 50 N·mm/rad with respect to the desired trajectories (6.16). The control gains in the linear stabilizer (6.15) were chosen so as to yield two pairs of real poles in -1 and -10 for the position loop, and a double real pole in -10 for the stiffness loop. After a short transient, both position and stiffness recover the desired trajectory (Fig. 6.3) without a significant additional control effort (not shown).

Serial VSA

The feedback linearization control law for serial VSA proposed in Sect. 6.4 is tested on the AwAS described in Sect 4.2. By using the same rest to rest motion eqs. (6.16) and not matched condition the result shown in FIg. 6.4 is obtained. The model parameters of the AwAS used in the simulation are introduced in Sect 4.2, and the control parameter used in the motion controller eq. (6.15) are $k_{q,3} = 14$, $k_{q,2} = 69$, $k_{q,1} = 140$, $k_{q,0} = 100$, $k_{\sigma,1} = 6$ and $k_{\sigma,1} = 9$. the system is started with an initial position error of 10° and a stiffness error of approximatively 3200 N·mm/rad with respect to the desired trajectories (6.16).

6.7 Conclusions

Using a feedback linearization approach, the actuation capabilities of the device can be fully exploited, under a mild condition for the antagonistic VSA on stiffness pre-loading, which is sufficient to avoid control singularities. The nonlinear controller is able to track precisely and in a stable way fast trajectories, while imposing independently and with similar accuracy a desired stiffness profile on the fly. The control approach proposed can be easily extended to multi d.o.f. manipulator with either antagonistic or serial VSA. The effectiveness of the methodology have been shown with simulations using the VSA-II and the AwAS devices.

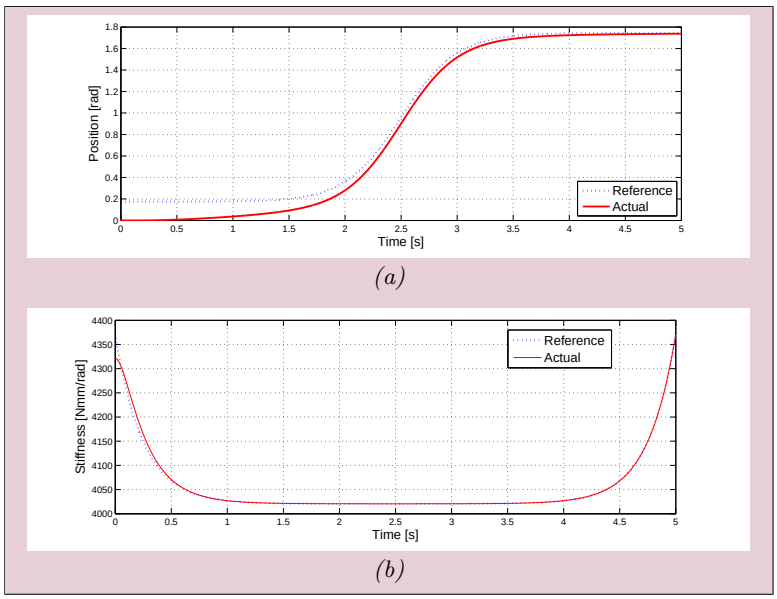

Figure 6.3: *Free motion of the VSA-II using feedback linearization control: (a) position q for an initial error of* $10^\circ \approx 0.2$ *rad; (b) stiffness* σ *for an initial error of* 50 *N·mm/rad*

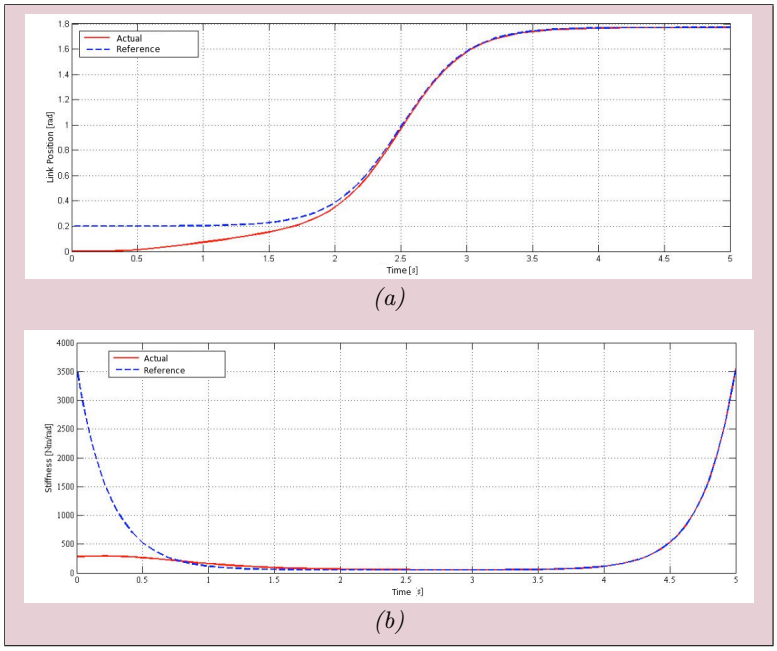

Figure 6.4: *Free motion of the AWAS using feedback linearization control: (a) position q for an initial error of* $10^\circ \approx 0.2$ *rad; (b) stiffness* σ *for an initial error of approx.* 3200 *N·mm/rad*

7 Gravity Cancellation

Robots in physical interaction with humans are conveniently controlled so as to achieve zero-gravity operation Heinzmann and Zelinsky [2003]. This avoids biasing the robot reaction to unintended collisions along the gradient of the gravitational potential, with a uniform and more predictable (thus safer) robot behavior in its whole workspace De Luca et al. [2006].

In this chapter our gravity cancellation algorithm for compliant actuator will be described for all the three typologies of compliant joint : SAFT in Sect. 7.2, antagonistic VSA in Sect. 7.3 and serial VSA in Sect. 7.4. While simulation results are presented in Sect. 7.5 contains simulation. Section 7.6 introduces the extension to multi d.o.f. robots, and, finally, in Section 7.7 the benefits of using our gravity cancellation method is shown by considering a simple PD controller.

7.1 Introduction

Perfect cancellation of gravity is trivial for fully rigid manipulators. In fact, for their standard dynamic model

$$\boldsymbol{M}(\boldsymbol{q})\ddot{\boldsymbol{q}} + \boldsymbol{c}(\boldsymbol{q}, \dot{\boldsymbol{q}}) + \boldsymbol{g}(\boldsymbol{q}) = \boldsymbol{\tau},$$

the choice

$$\boldsymbol{\tau} = \boldsymbol{\tau}_g + \boldsymbol{\tau}_0, \qquad \boldsymbol{\tau}_g = \boldsymbol{g}(\boldsymbol{q})$$

removes gravity from the picture in a complete way (i.e., both statically and dynamically), thanks to the colocation of gravity and input torques (and to the full actuation of the system). The additional command $\boldsymbol{\tau}_0$ is left to the control designer for performing desired tasks, e.g., set-point regulation, trajectory tracking, or reaction to a contact with the environment.

However, robots intended for physical Human-Robot Interaction (pHRI) include compliant elements in their mechanical construction, in order to reduce the possibility of injuries due to unexpected collisions De Santis et al. [2008]. Robot links are designed as lightweight but rigid, while compliance is typically

concentrated in the transmissions at the joints, either with finite constant stiffness $\boldsymbol{K}$, e.g., when using harmonic drives Hirzinger et al. [2001], or with variable (and independently actuated) nonlinear stiffness Bicchi and Tonietti [2004].

The common dynamic model of robots with constant joint elasticity takes the form (3.5–3.6) where actuation torques $\boldsymbol{\tau}$ appear on the motor side of the elastic joints (i.e., performing work on $\boldsymbol{\theta}$), while gravity loading $\boldsymbol{g}(\boldsymbol{q})$ affects primarily the dynamic behavior of the variables on the link side (i.e., $\boldsymbol{q}$). This non-colocation is a major problem for control. Gravity compensation laws have been proposed for regulation tasks, when the link position $\boldsymbol{q}$ has to be asympotically stabilized to a desired constant value $\boldsymbol{q}_d$. A first solution is based on motor PD feedback with *constant* gravity compensation at steady state Tomei [1991]

$$\boldsymbol{\tau}_0 = \boldsymbol{K}_P(\boldsymbol{\theta}_d - \boldsymbol{\theta}) - \boldsymbol{K}_D\dot{\boldsymbol{\theta}}, \qquad \boldsymbol{\tau}_g = \boldsymbol{g}(\boldsymbol{q}_d),$$

with $\boldsymbol{\theta}_d = \boldsymbol{q}_d + \boldsymbol{K}^{-1}\boldsymbol{g}(\boldsymbol{q}_d)$, $\boldsymbol{K}_P > 0$, and $\boldsymbol{K}_D > 0$. In order to show asympotic stability by Lyapunov arguments, the proportional gain should be chosen so that the norm of $\boldsymbol{K}_P$ is larger than a positive constant related to gravity, whereas the stiffness matrix $\boldsymbol{K}$ is assumed to dominate the gradient of $\boldsymbol{g}(\boldsymbol{q})$. Indeed, this compensation cancels gravity only in the final *static* condition. Since the gravity term changes with the robot configuration, an *on-line* compensation has been proposed in De Luca et al. [2005] by evaluating $\boldsymbol{g}$ in $\boldsymbol{\tau}_g$ with a gravity-biased measure of the motor position

$$\boldsymbol{\tau}_g = \boldsymbol{g}(\tilde{\boldsymbol{\theta}}), \qquad \tilde{\boldsymbol{\theta}} = \boldsymbol{\theta} - \boldsymbol{K}^{-1}\boldsymbol{g}(\boldsymbol{q}_d).$$

While the transient performance is largely improved, the theoretical restriction on $\boldsymbol{K}_P$ could not be removed in the Lyapunov analysis. A better result is achieved in Kugi et al. [2008], with a gravity compensation of the form

$$\boldsymbol{\tau}_g = \boldsymbol{g}(\bar{\boldsymbol{q}}(\boldsymbol{\theta})),$$

where, for a measured motor position $\boldsymbol{\theta}$, $\bar{\boldsymbol{q}}(\boldsymbol{\theta})$ is computed by numerically solving the *quasi-static* relation $\boldsymbol{g}(\boldsymbol{q}) + \boldsymbol{K}(\boldsymbol{q} - \boldsymbol{\theta}) = \boldsymbol{0}$. This variant is able to relax the lower bound on $\boldsymbol{K}_P$ so that asymptotic stability can be shown through a modified Lyapunov function. On the other hand, the structural condition on the joint stiffness $\|\boldsymbol{K}\| > \|\partial\boldsymbol{g}(\boldsymbol{q})/\partial\boldsymbol{q}\|$ should still hold.

All the above control laws have the merit of using only feedback from the motor variables $\boldsymbol{\theta}$ and $\dot{\boldsymbol{\theta}}$. However, none of them removes completely the effects of gravity, especially in highly *dynamic* tasks: only a partial compensation, and not a cancellation, of the gravitational load acting on the robot link motion is obtained. In the context of robot reaction to collisions, we also note that a practical solution for compensating gravity in elastic joint robots has been proposed in Haddadin et al. [2008], based on the availability of joint torque sensors. The use of this additional sensor can be interpreted as involving also the link position $\boldsymbol{q}$ in the control law. Furthermore, under the assumption that full state is available, it is known that all robots with elastic joints can be exactly linearized by means of a static Spong [1987] or dynamic state feedback (the latter is needed when some extra inertial terms are included in the model) De Luca and Lucibello [1998]. This structural control property will be further exploited in this chapter.

7.2 SAFT

In this section the gravity cancellation for single actuated flexible transmission is presented. With reference to the SAFT model (3.2–3.3), firstly the simpler case of elastic transmission $\tau_e(\phi) = K\phi$ (with K positive and constant) is considered, then the results will be extended to flexible transmission.

Elastic transmission

Starting from eqs. (3.2–3.3) the SAFT model with elastic transmission is

$$M\ddot{q} + D_q\dot{q} + K\phi + g(q) = 0 \tag{7.1}$$

$$B\ddot{\theta} + D_\theta\dot{\theta} - K\phi = \tau, \tag{7.2}$$

where, for the sake of simplicity, external torques are not considered.

Our control goal is to define a (nonlinear) feedback law $\tau = \tau(q, \theta, \dot{q}, \dot{\theta}, \tau_0)$ in (7.2) such that the behavior of the compensated system matches *in suitable coordinates* that of an identical model but without gravity, i.e.,

$$M\ddot{q}_0 + D_q\dot{q}_0 + K\phi_0 = 0 \tag{7.3}$$

$$B\ddot{\theta}_0 + D_\theta\dot{\theta}_0 - K\phi_0 = \tau_0, \tag{7.4}$$

where the subscript 0 characterizes the variables of the robot *in the absence of gravity*.

It is well known Spong [1987] that system (7.1–7.2) is exactly linearizable by means of a static state feedback into decoupled chains of four integrators, with $\boldsymbol{q}$ and its first three time derivatives being the linearizing coordinates. Indeed, the same holds true also for system (7.3–7.4). Therefore, thanks to the feedback equivalence principle, by imposing the equality

$$q(t) \equiv q_0(t), \qquad \forall t \geq 0 \tag{7.5}$$

one should obtain the desired result without resorting to the complexity of a complete feedback linearization process. One challenge in the application of this simple idea is whether the solution can be found in closed form or not. Below, we show constructively that this is feasible for robots with elastic joints. The same conceptual steps will be followed in all considered instances of transmission flexibility, albeit in some cases the solution will require a numerical procedure.

Differentiating once eq. (7.1) w.r.t. time yields

$$Mq^{[3]} + D_q\ddot{q} + K\phi + \dot{g}(q) = 0$$

Differentiating one more time, recalling that $\phi = q - \theta$, and substituting $\ddot{\theta}$ from (7.2), we obtain

$$Mq^{[4]} + D_q q^{[3]} + K\ddot{q} = \frac{K}{B}\left(\tau - D_\theta\dot{\theta} + K\phi\right) - \ddot{g}(q)\,. \tag{7.6}$$

Noting that the left-hand side of (7.6) is a function of q and its first four derivatives only, we will write it compactly as $f(q, \dot{q}, \ddot{q}, q^{[3]}, q^{[4]})$. Repeating the same computation for the no-gravity model (7.3–7.4) leads to

$$f(q_0, \dot{q}_0, \ddot{q}_0, q_0^{[3]}, q_0^{[4]}) = \frac{K}{B}\left(\tau_0 - D_\theta\dot{\theta}_0 + K\phi_0\right)\,. \tag{7.7}$$

By imposing (7.5), the left-hand sides of (7.6) and (7.7) will be equal, and thus

$$\frac{K}{B}\left(\tau - D_\theta\dot{\theta} + K\phi\right) - \ddot{g}(q) = \frac{K}{B}\left(\tau_0 - D_\theta\dot{\theta}_0 + K\phi_0\right) \tag{7.8}$$

In order to eliminate the presence of the motor variables in (7.8), we use eqs. (7.1) and (7.3). By imposing again (7.5), one has

$$\begin{aligned} K(q-\theta) &= -M\ddot{q} - D_q\dot{q} - g(q) \\ K(q-\theta_0) &= -M\ddot{q} - D_q\dot{q} \end{aligned} \tag{7.9}$$

or

$$\theta = \theta_0 + \frac{1}{K}g(q), \tag{7.10}$$

and then

$$\dot{\theta} = \dot{\theta}_0 + \frac{1}{K}\dot{g}(q). \tag{7.11}$$

Replacing eqs. (7.10–7.11) into (7.8) and simplifying, the solution to our problem is obtained by choosing the control law as

$$\tau = \tau_g + \tau_0 \tag{7.12}$$

with

$$\tau_g = g(q) + \frac{D_\theta}{K}\dot{g}(q) + \frac{B}{K}\ddot{g}(q), \tag{7.13}$$

where

$$\begin{aligned} \dot{g}(q) &= \frac{\partial g(q)}{\partial q}\,\dot{q} \\ \ddot{g}(q) &= \frac{\partial g(q)}{\partial q}\ddot{q} + \sum_{i=1}^{n}\frac{\partial^2 g(q)}{\partial q^2}\,\dot{q}^2. \end{aligned}$$

In addition, matched initial conditions should hold at time $t = 0$:

$$\begin{aligned} q(0) &= q_0(0) & \ddot{q}(0) &= \ddot{q}_0(0) \\ \dot{q}v(0) &= \dot{q}_0(0) & q^{[3]}(0) &= q_0^{[3]}(0). \end{aligned} \tag{7.14}$$

Note that, thanks to the control law (7.12–7.13), the identities (7.14) will be enforced for all $t \geq 0$. The matching conditions (7.14) are not really a restriction. In fact, these conditions can be read in both directions: for a given initial state of the gravity-loaded system, we can always find an equivalent gravity-free system that has its initial state matched. This implies that the link coordinates of the two systems will evolve in the same way under the same command $\boldsymbol{\tau}_0$.

A notable feature is that the control solution can be computed in closed form. Moreover, in static conditions, i.e., with $\dot{q} = \ddot{q} = 0$, the gravity cancellation torque (7.60) becomes $\tau_g = g(q)$, as to be expected. Instead, in dynamic conditions τ_g includes terms that are proportional to the inverse of the joint stiffness K. Thus, the more rigid are the transmissions the less extra dynamic torque is needed for gravity cancellation. In the limit, for $K \to \infty$, we recover the standard gravity cancellation torque of the rigid case also in dynamic conditions.

Indeed, there are still differences in the state behavior between the gravity-free system (7.3–7.4) and system (7.1–7.2) under the gravity cancellation control

law (7.12–7.13). While the two systems will evolve in an identical way when looking at the linearizing coordinates $q(t) \equiv q_0(t)$, the inverse mappings of this evolution in terms of the respective motor variables will be different, as dictated by eqs. (7.10) and (7.11). This should not be surprising from a physical point of view: the gravity-loaded robot needs the presence of a deformation $q-\theta \neq q-\theta_0$ that dynamically balances the gravity on the link side. The control law (7.12–7.13) will only cancel the effects on the link (output) motion, which is what we actually need during robot interaction with the environment or a human.

The torque input τ_0 in (7.12) can be chosen according to the robot primary task, e.g., as in De Luca et al. [2006] for a torque-based robot reaction to detected collisions in pHRI. In this context, perfect gravity cancellation allows a link behavior during transients and at steady-state that is totally unaffected by gravity bias. Furthermore, for a regulation task to a desired link position q_d, it can be shown that the *PD-type* control law

$$\tau_0 = K_P \left(q_d - \theta + K^{-1} g(q)\right) - K_D \left(\dot{\theta} - K^{-1} \frac{\partial g(q)}{\partial q}\, \dot{q}\right),$$

achieves global asymptotic stabilization for *any* $K_P > 0$ and $K_D > 0$, i.e., without the need of a strictly positive lower bound on K_P. This result holds for any $K > 0$, i.e., also for very soft joints. A formal proof of this result for a N-dof manipulator is presented in Sect. 7.7.

Flexible transmission

The results obtained for the elastic case can be extended to SAFT with nonlinear transmission. The dynamic model of a single link moving *under gravity* and driven through such a flexible transmission eqs. (3.2–3.3) is recalled here

$$M\ddot{q} + D_q \dot{q} + g(q) + \tau_e(\phi) = 0 \tag{7.15}$$

$$B\ddot{\theta} + D_\theta \dot{\theta} - \tau_e(\phi) = \tau. \tag{7.16}$$

We wish to define a feedback law $\tau = \tau(q, \theta, \dot{q}, \dot{\theta}, \tau_0)$ in (7.16) so as to match the behavior of some output variable of the model *without gravity*

$$M\ddot{q}_0 + D_q \dot{q}_0 + \tau_e(\phi_0) = 0 \tag{7.17}$$

$$B\ddot{\theta}_0 + D_\theta \dot{\theta}_0 - \tau_e(\phi_0) = \tau_0. \tag{7.18}$$

It is easy to verify that both nonlinear systems (7.15–7.16) and (7.17–7.18) are exactly linearizable by means of a static state feedback into a chain of four integrators, with q and its first three time derivatives as linearizing coordinates. Therefore, the two systems are feedback equivalent and the solution to our problem is obtained by imposing $q(t) = q_0(t)$ for all $t \geq 0$. In particular, from $q^{[4]} = q_0^{[4]}$ we get

$$\begin{aligned} \tau = {} & g(q) + \frac{D_\theta}{\sigma(\phi)}\, \dot{g}(q) + \frac{B}{\sigma(\phi)}\, \ddot{g}(q) \\ & + \frac{\sigma(\phi) - \sigma(\phi_0)}{\sigma(\phi)} \left((B+M)\ddot{q} + (D_q + D_\theta)\dot{q}\right) \\ & + \frac{B}{\sigma(\phi)} \left(\frac{\partial \sigma(\phi)}{\partial \phi}\, \dot{\phi}^2 - \frac{\partial \sigma(\phi_0)}{\partial \phi_0}\, \dot{\phi}_0^2\right) + \frac{\sigma(\phi_0)}{\sigma(\phi)}\, \tau_0 \\ = {} & \tau_g + \alpha_g \tau_0, \end{aligned} \tag{7.19}$$

where $\ddot{q}$ (to be used also in $\ddot{g}(q)$) is computed from (7.15) as

$$\ddot{q} = -\frac{1}{M}\left(D_q\dot{q} + g(q) + \tau_e(\phi)\right).$$

In addition, the initial matching requires

$$\begin{aligned} q(0) &= q_0(0) \qquad & \ddot{q}(0) &= \ddot{q}_0(0) \\ \dot{q}(0) &= \dot{q}_0(0) \qquad & q^{[3]}(0) &= q_0^{[3]}(0). \end{aligned} \tag{7.20}$$

Note that (7.19) collapses into (7.12–7.13) for a transmission with constant stiffness $\sigma = K$. However, differently from the case of linear elasticity, the control law (7.19) contains terms that require the knowledge of the deformation $\phi_0 = q - \theta_0$, and of its rate $\dot{\phi}_0$, pertaining to the model without gravity. Also, the torque τ_0 applied in the gravity-free case needs now to be scaled by the factor $\alpha_g = \sigma(\phi_0)/\sigma(\phi)$.

The value ϕ_0 is computed by solving the nonlinear equation $\tau_e(\phi_0) = -M\ddot{q} - D_q\dot{q}$, which is obtained from (7.17) by taking into account the first three identities in (7.20). Using (7.15), the right-hand side can be written as a function of the *state* (actually, of the configuration variables only) of the gravity-loaded system as

$$\tau_e(\phi_0) = g(q) + \tau_e(\phi) = a(q,\theta). \tag{7.21}$$

Equation (7.21) needs to be solved for ϕ_0 at each time $t \geq 0$ as a function of the current system state. As a representative example, consider a flexible joint transmission with associated potential given by $U_e = \frac{1}{2}K\phi^2 + \frac{1}{4}K_c\phi^4$, with $K > 0$ and $K_c > 0$. The flexibility torque is a cubic function of ϕ and the stiffness has a *quadratic* dependence:

$$\tau_e(\phi) = K\phi + K_c\phi^3, \qquad \sigma(\phi) = K + 3K_c\phi^2. \tag{7.22}$$

At a given (q,θ), equation (7.21) results in the cubic equation $K_c\phi_0^3 + K\phi_0 - a(q,\theta) = 0$, which has always two complex roots and one real (positive or negative) root, thanks to the positivity of K and K_c. The real root is given by

$$\phi_0 = \sqrt[3]{\frac{1}{2}\frac{a(q,\theta)}{K_c} + b(q,\theta)} + \sqrt[3]{\frac{1}{2}\frac{a(q,\theta)}{K_c} - b(q,\theta)},$$

where $b(q,\theta) = \sqrt{\frac{1}{27}\left(\frac{K}{K_c}\right)^3 + \frac{1}{4}\left(\frac{a(q,\theta)}{K_c}\right)^2} > 0$. For more general stiffness profiles, a solution to (7.21) should be searched numerically.

Once ϕ_0 has been found, the value of $\dot{\phi}_0$ that appears in the control law (7.19) is obtained by time differentiation of (7.21) (or, equivalently, from the fourth identity in (7.20)) as

$$\dot{\phi}_0 = \frac{1}{\sigma(\phi_0)}\left(\sigma(\phi)\dot{\phi} + \frac{\partial g(q)}{\partial q}\,\dot{q}\right). \tag{7.23}$$

As a result, the gravity cancellation control law (7.19) can be computed in closed form from full state measurements in the case of cubic stiffness (and for other simple nonlinear dependencies). Note that for multi-dof robots with nonlinear flexible joints one needs to solve n similar equations of the form (7.21), whereas (7.23) is replicated component-wise.

7.3 Antagonistic VSA

The same approach can be used for antagonistic VSA. Recalling the antagonistic VSA model (3.7–3.8)

$$M\ddot{q} + D_q\dot{q} + g(q) + \tau_e(\phi_1) + \tau_e(\phi_2) = 0 \tag{7.24}$$

$$B\ddot{\theta}_1 + D_\theta\dot{\theta}_1 - \tau_e(\phi_1) = \tau_1 \tag{7.25}$$

$$B\ddot{\theta}_2 + D_\theta\dot{\theta}_2 - \tau_e(\phi_2) = \tau_2, \tag{7.26}$$

where τ_1 and τ_2 are the torques supplied by the two motors. Without loss of generality, we have assumed in (7.24–7.26) a full symmetry for the two actuation/transmission systems. Accordingly, the total stiffness σ_t of the device is given by the separable function

$$\sigma_t(\phi_1, \phi_2) = \frac{\partial(\tau_e(\phi_1) + \tau_e(\phi_2))}{\partial q} = \sigma(\phi_1) + \sigma(\phi_2). \tag{7.27}$$

As before, the target behavior is specified by a dynamic system of the same form (7.24–7.26), but with $g(q) \equiv 0$ and all its variables labeled by a 0 subscript.

Since the system has two inputs, according to the feedback equivalence principle, we should determine *two* independent system output functions that play the role of linearizing coordinates in a feedback linearization scheme. Based on the results in Chapter 6 , these two outputs are the link position q and the total stiffness σ_t. In fact, differentiating once (7.24) w.r.t. time gives

$$Mq^{[3]} + D_q\ddot{q} + \dot{g}(q) + \sigma(\phi_1)\dot{\phi}_1 + \sigma(\phi_2)\dot{\phi}_2 = 0. \tag{7.28}$$

DIfferentiating once more, using (7.25–7.26), and rearraging terms, we obtain

$$\begin{aligned} Mq^{[4]} + D_q q^{[3]} + \ddot{g}(q) + \frac{\partial\sigma(\phi_1)}{\partial\phi_1}\dot{\phi}_1^2 + \frac{\partial\sigma(\phi_2)}{\partial\phi_2}\dot{\phi}_2^2 + \sigma_t\ddot{q} \\ = \sigma(\phi_1)\ddot{\theta}_1 + \sigma(\phi_2)\ddot{\theta}_2 \\ = \frac{1}{B}\begin{pmatrix} \sigma(\phi_1) & \sigma(\phi_2) \end{pmatrix}\begin{pmatrix} \tau_1 + \tau_e(\phi_1) - D_\theta\dot{\theta}_1 \\ \tau_2 + \tau_e(\phi_2) - D_\theta\dot{\theta}_2 \end{pmatrix}. \end{aligned} \tag{7.29}$$

Similarly, by differentiating (7.27) w.r.t. time, we have

$$\dot{\sigma}_t = \frac{\partial\sigma(\phi_1)}{\partial\phi_1}\dot{\phi}_1 + \frac{\partial\sigma(\phi_2)}{\partial\phi_2}\dot{\phi}_2 \tag{7.30}$$

and, by rearraging terms and using again (7.25–7.26),

$$\begin{aligned} -\ddot{\sigma}_t + \frac{\partial^2\sigma(\phi_1)}{\partial\phi_1^2}\dot{\phi}_1^2 + \frac{\partial^2\sigma(\phi_2)}{\partial\phi_2^2}\dot{\phi}_2^2 + \left(\frac{\partial\sigma(\phi_1)}{\partial\phi_1} + \frac{\partial\sigma(\phi_2)}{\partial\phi_2}\right)\ddot{q} \\ = \frac{\partial\sigma(\phi_1)}{\partial\phi_1}\ddot{\theta}_1 + \frac{\partial\sigma(\phi_2)}{\partial\phi_2}\ddot{\theta}_2 \\ = \frac{1}{B}\begin{pmatrix} \dfrac{\partial\sigma(\phi_1)}{\partial\phi_1} & \dfrac{\partial\sigma(\phi_2)}{\partial\phi_2} \end{pmatrix}\begin{pmatrix} \tau_1 + \tau_e(\phi_1) - D_\theta\dot{\theta}_1 \\ \tau_2 + \tau_e(\phi_2) - D_\theta\dot{\theta}_2 \end{pmatrix}. \end{aligned} \tag{7.31}$$

It can be shown that the decoupling matrix associated to the output vector (q, σ_t) is proportional to the matrix

$$\boldsymbol{\mathcal{A}}(\phi_1, \phi_2) = \begin{pmatrix} \sigma(\phi_1) & \sigma(\phi_2) \\ \dfrac{\partial \sigma(\phi_1)}{\partial \phi_1} & \dfrac{\partial \sigma(\phi_2)}{\partial \phi_2} \end{pmatrix},$$

which is generically *nonsingular*, except when $\theta_1 = \theta_2$ (a condition that can always be avoided by suitably pre-charging the actuation system). Therefore, the outputs q, together with its first three derivatives, and σ_t, with its first derivative, are linearizing coordinates for system (7.24–7.26).

Comparing the expressions (7.29) and (7.31) with those of the gravity-free case (with a 0 subscript), the solution to the problem of dynamic gravity cancellation is given by the control torques τ_1 and τ_2

$$\begin{aligned} \begin{pmatrix} \tau_1 \\ \tau_2 \end{pmatrix} = & \begin{pmatrix} D_\theta \, \dot{\theta}_1 - \tau_e(\phi_1) \\ D_\theta \, \dot{\theta}_2 - \tau_e(\phi_2) \end{pmatrix} + \boldsymbol{\mathcal{A}}^{-1}(\phi_1, \phi_2) \cdot \\ & \left\{ \boldsymbol{\mathcal{A}}(\phi_{10}, \phi_{20}) \left(\begin{pmatrix} \tau_{10} \\ \tau_{20} \end{pmatrix} + \begin{pmatrix} \tau_e(\phi_{10}) - D_\theta \, \dot{\theta}_{10} \\ \tau_e(\phi_{20}) - D_\theta \, \dot{\theta}_{20} \end{pmatrix} \right) \right. \\ & \left. + B \begin{pmatrix} \ddot{g}(q) + \displaystyle\sum_{i=1}^{2} \left(\frac{\partial \sigma(\phi_i)}{\partial \phi_i} \, \dot{\phi}_i^2 - \frac{\partial \sigma(\phi_{i0})}{\partial \phi_{i0}} \, \dot{\phi}_{i0}^2 \right) \\ \displaystyle\sum_{i=1}^{2} \left(\frac{\partial \sigma(\phi_i)}{\partial \phi_i} - \frac{\partial \sigma(\phi_{i0})}{\partial \phi_{i0}} \right) \ddot{q} \\ + \displaystyle\sum_{i=1}^{2} \left(\frac{\partial^2 \sigma(\phi_i)}{\partial \phi_i^2} \, \dot{\phi}_i^2 - \frac{\partial^2 \sigma(\phi_{i0})}{\partial \phi_{i0}^2} \, \dot{\phi}_{i0}^2 \right) \end{pmatrix} \right\}, \end{aligned} \tag{7.32}$$

where the link acceleration $\ddot{q}$ (to be used also in $\ddot{g}(q)$) is computed from (7.24) as

$$\ddot{q} = -\frac{1}{M} \left(D_q \dot{q} + g(q) + \tau_e(\phi_1) + \tau_e(\phi_2) \right).$$

In addition, an initial state matching given by

$$q(0) = q_0(0) \quad \dot{q}(0) = \dot{q}_0(0) \quad \ddot{q}(0) = \ddot{q}_0(0) \quad q^{[3]}(0) = q_0^{[3]}(0)$$

and

$$\begin{aligned} \sigma_t(0) = \sigma_t(\phi_1(0), \phi_2(0)) &= \sigma_t(\phi_{10}(0), \phi_{20}(0)) = \sigma_{t0}(0) \\ \dot{\sigma}_t(0) &= \dot{\sigma}_{t0}(0) \end{aligned}$$

should hold between the gravity-loaded and the gravity-free system. Note that the above identities will hold for all $t \geq 0$ thanks to the chosen control law.

The control law (7.32) physically replaces all terms that are affected by gravity (motor variables, flexible deformation torques, partial derivatives of the stiffness functions) with those of the gravity-free target system. For the considered single-dof VSA-based joint, the dynamic gravity cancellation law is very similar to a feedback linearization law from the point of view of complexity. However, these two controllers will differ consistently when considering multi-dof VSA robotic systems.

Beside measurements of the state of the gravity-loaded system, in order to evaluate (7.32) we need also knowledge of the deformations ϕ_{i0}, $i = 1, 2$, and of their rates $\dot{\phi}_{i0}$, $i = 1, 2$, pertaining to the target system without gravity. Note that from ϕ_{i0}, we directly obtain also $\theta_{i0} = q - \phi_{i0}$. Similarly to Sect. 7.2, the deformations ϕ_{10} and ϕ_{20} are determined by solving the coupled system of two nonlinear equations

$$\begin{aligned} \tau_e(\phi_{10}) + \tau_e(\phi_{20}) &= -M\ddot{q} - D_q\dot{q} = a_1(q, \theta_1, \theta_2) \\ \sigma(\phi_{10}) + \sigma(\phi_{20}) &= \sigma_t(q, \theta_1, \theta_2), \end{aligned} \tag{7.33}$$

where the right-hand sides of (7.33) are expressed in terms of current state measurements using (7.24) and (7.27). Due to the symmetry, if (ϕ_a, ϕ_b) is a solution of (7.33) then (ϕ_b, ϕ_a) is a solution as well.

In general, system (7.33) needs to be solved numerically. Some additional insight is provided in the case of *cubic* flexibility torques, see (7.22). We have then

$$K(\phi_{10} + \phi_{20}) + K_c(\phi_{10}^3 + \phi_{20}^3) = a_1(q, \theta_1, \theta_2) \tag{7.34}$$

$$2K + 3K_c(\phi_{10}^2 + \phi_{20}^2) = \sigma_t(q, \theta_1, \theta_2). \tag{7.35}$$

Since by definition

$$\frac{\sigma_t - 2K}{3K_c} := R^2 \geq 0,$$

the solutions to equation (7.35) can be parametrized by a scalar $\alpha \in [0, 2\pi)$ as $\phi_{10} = R\cos\alpha$ and $\phi_{20} = R\sin\alpha$. Replacing these in (7.34) yields the single trigonometric equation in α

$$(\cos\alpha + \sin\alpha) + \frac{\sigma_t - 2K}{3K}\left(\cos^3\alpha + \sin^3\alpha\right) = \frac{a_1}{KR}. \tag{7.36}$$

Figure 7.1 shows a plot of one of the two branches of the expression on the left-hand side of (7.36), obtained for $K = 100$, $K_c = 500$, and $\sigma_t = 220$. The horizontal line corresponds to the case $a_1 = 10$, and the associated root α provides the solution $\phi_{10} = 0.1136$ and $\phi_{20} = -0.0209$ [rad]. It can be seen that equation (7.36) is sufficiently smooth, and thus easily solvable by a numerical root finder (e.g., the `fzero` routine of Matlab). Assume now that the device stiffness σ_t can be changed within the interval $(2K, 4K)$, i.e., from its minimum physical value to a 100% increase. It can be shown that a pair of α solutions to (7.36) always exist in this interval for σ_t, provided that $|a_1| < \sqrt{2}KR\,[1 + 0.5(\sigma_t - 2K)/(3K)]$.

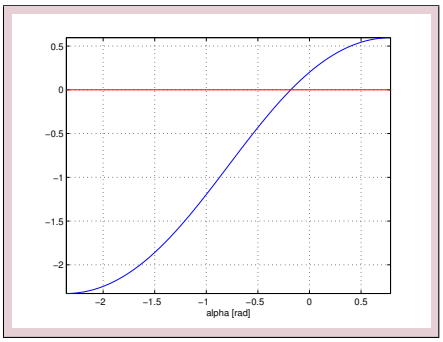

Figure 7.1: *A typical functional form of eq. (7.36) and a possible solution*

It should be stressed that the existence of pairs of solutions is not a source of problems. In fact, system (7.33) will be solved at every (discretized) instant $t \geq 0$. Once a specific solution has been chosen at $t = 0$, the process is repeated

on line and a local numerical search around the previous solution generates a single update.

Finally, having determined ϕ_{10} and ϕ_{20}, their rates are obtained by time differentiation of (7.33) as

$$\begin{aligned}\begin{pmatrix}\dot{\phi}_{10}\\ \dot{\phi}_{20}\end{pmatrix} &= \boldsymbol{\mathcal{A}}^{-1}(\phi_{10},\phi_{20})\begin{pmatrix}-Mq^{[3]}-D_q\ddot{q}\\ \dot{\sigma}_t\end{pmatrix}\\ &= \boldsymbol{\mathcal{A}}^{-1}(\phi_{10},\phi_{20})\begin{pmatrix}\sigma(\phi_1)\dot{\phi}_1+\sigma(\phi_2)\dot{\phi}_2+\frac{\partial g(q)}{\partial q}\dot{q}\\ \frac{\partial\sigma(\phi_1)}{\partial\phi_1}\dot{\phi}_1+\frac{\partial\sigma(\phi_2)}{\partial\phi_2}\dot{\phi}_2\end{pmatrix},\end{aligned}$$

where (7.28) and (7.30) have been used to express all quantities in terms of the original VSA system state only.

7.4 Serial VSA

As for the antagonistic VSA the gravity cancellation can be applied to the serial VSA. We recall here the serial VSA model (3.13)

$$M\ddot{q}+D_q\dot{q}+\tau_e(\theta_c,\phi)+g(q) = 0 \tag{7.37}$$

$$B\ddot{\theta}+D_\theta\dot{\theta}-\tau_e(\theta_c,\phi) = \tau \tag{7.38}$$

$$B_c\ddot{\theta}_c+D_{\theta,c}\dot{\theta}_c+\psi_e(\theta_c,\phi) = \tau_c, \tag{7.39}$$

Since the system has two inputs, according to the feedback equivalence principle, we should determine *two* independent system output functions that play the role of linearizing coordinates in a feedback linearization scheme. Based on the results in Chapter 6, as for the antagonistic VSA (Sect. 7.3) , these two outputs are the link position q and the total stiffness σ.

In fact, differentiating once (7.37) w.r.t. time gives

$$Mq^{[3]}+D_q\ddot{q}+\sigma\dot{\phi}+\frac{\partial\tau_e}{\partial\theta_c}\dot{\theta}_c+\dot{g}=0 \tag{7.40}$$

DIfferentiating once more, using (7.38–7.39), and rearraging terms, we obtain

$$\begin{aligned}&Mq^{[4]}+D_qq^{[3]}+\sigma\ddot{q}+\frac{\partial\sigma}{\partial\phi}\dot{\phi}^2+\frac{\partial\sigma}{\partial\theta_c}\dot{\phi}\dot{\theta}_c+\\ &\frac{\partial^2\tau_e}{\partial\theta_c^2}\dot{\theta}_c^2+\frac{\partial^2\tau_e}{\partial\theta_c\partial\phi}\dot{\theta}_c\dot{\phi}+\ddot{g}=\\ &\qquad\begin{pmatrix}\frac{\sigma}{B} & -\frac{\partial\tau_e}{\partial\theta_c}\frac{1}{B_c}\end{pmatrix}\begin{pmatrix}\tau+\tau_e-D_\theta\dot{\theta}\\ \tau_c-\psi_e-D_{\theta,c}\dot{\theta}_c\end{pmatrix}\end{aligned} \tag{7.41}$$

Similarly, by differentiating (3.14) w.r.t. time, we have

$$\dot{\sigma}=\frac{\partial\sigma}{\partial\phi}\dot{\phi}+\frac{\partial\sigma}{\partial\theta_c}\dot{\theta}_c \tag{7.42}$$

and, by rearranging terms and using again (7.38–7.39),

$$\begin{aligned}\ddot{\sigma} \;=\; & \frac{\partial^2\sigma}{\partial\phi^2}\dot{\phi}^2 + \frac{\partial^2\sigma}{\partial\phi\partial\theta_c}\dot{\phi}\dot{\theta}_c + \frac{\partial^2\sigma}{\partial\theta_c^2}\dot{\theta}_c^2 + \frac{\partial^2\sigma}{\partial\theta_c\partial\phi}\dot{\theta}_c\dot{\phi} + \frac{\partial\sigma}{\partial\phi}\ddot{q} + \\ & \begin{pmatrix} -\dfrac{\sigma}{\partial\phi}\dfrac{1}{B} & \dfrac{\partial\sigma}{\partial\theta_c}\dfrac{1}{B_c} \end{pmatrix} \begin{pmatrix} \tau + \tau_e - D_\theta\dot{\theta} \\ \tau_c - \psi_e - D_{\theta,c}\dot{\theta}_c \end{pmatrix}.\end{aligned} \tag{7.43}$$

Is not surprising that the decoupling matrix associated to the output vector (q, σ) is the same of eq. (6.13)

$$\mathcal{A}(\phi, \theta_c) = \mathbf{\Gamma} \begin{pmatrix} \sigma & -\dfrac{\partial\tau_e}{\partial\theta_c} \\ -\dfrac{\partial\sigma}{\partial\theta} & \dfrac{\partial\sigma}{\partial\theta_c} \end{pmatrix} \tag{7.44}$$

The gravity cancellation control for serial VSA is then

$$\begin{aligned}\begin{pmatrix} \tau \\ \tau_c \end{pmatrix} \;=\; & \begin{pmatrix} D_\theta\dot{\theta} - \tau_e \\ D_{\theta,c}\dot{\theta}_c + \psi_e \end{pmatrix} + \mathcal{A}^{-1}(\phi, \theta_c)\cdot \\ & \left\{ \mathcal{A}(\phi_0, \theta_{c,0}) \begin{pmatrix} \tau_0 + \tau_e(\theta_{c,0}, \phi_0) - D_\theta\dot{\theta}_0 \\ \tau_{c,0} - \psi_e(\theta_{c,0}, \phi_0) - D_{\theta,c}\dot{\theta}_{c,0} \end{pmatrix} + \right. \\ & \left. \begin{pmatrix} B & 0 \\ 0 & B_c \end{pmatrix} \begin{pmatrix} \bar{b}_1(\boldsymbol{x}) - \bar{b}_1(\boldsymbol{x}_0) + \ddot{g}(q) \\ \bar{b}_2(\boldsymbol{x}) - \bar{b}_2(\boldsymbol{x}_0) \end{pmatrix} \right\},\end{aligned} \tag{7.45}$$

where $\bar{\boldsymbol{b}}(\boldsymbol{\gamma}) = (\bar{b}_1(\boldsymbol{\gamma}), \bar{b}_1(\boldsymbol{\gamma}))$ is a function of the system state which is $\boldsymbol{x} = (q, \theta, \theta_c, \dot{q}, \dot{\theta}, \dot{\theta}_c)$ for the system with gravity and $\boldsymbol{x}_0 = (q, \theta_0, \theta_{c,0}, \dot{q}, \dot{\theta}_0, \dot{\theta}_{c,0})$ for the system without gravity.

A similar approach used for the antagonistic VSA, in eq. (7.33), can be used to obtain ϕ_0 and $\theta_{c,0}$ necessary to compute the gravity cancellation control (7.45). Namely the system of two nonlinear equation

$$\begin{aligned}\tau_e(\theta_{c,0}, \phi_0) \;&=\; -M\ddot{q} - D_q\dot{q} \\ \sigma(\theta_{c,0}, \phi_0) \;&=\; \sigma(\theta_c, \phi)\end{aligned} \tag{7.46}$$

have to be solved.

7.5 Simulation results

SAFT with elastic transmission

To illustrate the performance of the control law (7.12–7.13), a simulation of a link with gravity term $g(q) = mdg_0 \sin q$ is performed. Where m is the mass of the link, d is the distance of its center of mass from the joint, and g_0 is the gravity acceleration. The explicit expression of the dynamic gravity cancellation term τ_g in (7.13) is then

$$\begin{aligned}\tau_g = mdg_0 \Big\{ & \left(1 - \tfrac{B}{K}\,\dot{q}^2\right) \sin q - \tfrac{B}{M}\tfrac{mdg_0}{K}\,\sin q \cos q \\ & + \tfrac{MD_\theta - BD_q}{KM}\,\dot{q}\cos q + \tfrac{B}{M}(\theta - q)\cos q \Big\}.\end{aligned} \tag{7.47}$$

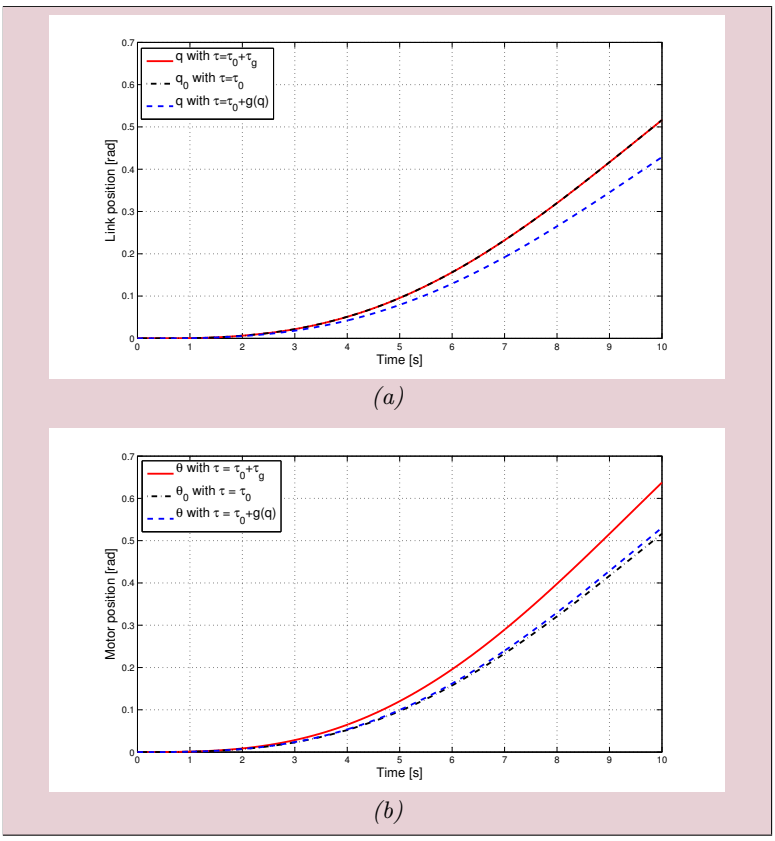

Figure 7.2: *Comparison of link (a) and motor (b) position for a single elastic joint without gravity under τ_0 [dot-dashed, black], and with gravity under τ_0 and a link-based compensation $g(q)$ [dashed, blue] or under τ_0 and the dynamic cancellation law τ_g in (7.47) [continuous, red]*

Using $M = 8.333$, $B = 50$ [N·mm·s^2/rad], $m = 0.1$ [kg], $d = 250$ [mm], $D_q = 0.1$, $D_\theta = 1$ [N·mm·s/rad], and $K = 100$ [N·mm/rad] as data, we simulated the two systems starting at rest from the downward equilibrium, and applying an open-loop torque $\tau_0 = \sin 0.1\pi t$ for $T = 10$ s. Figure 7.2 shows the obtained evolution of the link (a) and motor (b) angles in the absence or presence of gravity. For the latter case, we have considered also the use of a simpler link-based compensation $g(q)$ in place of the dynamic cancellation law τ_g given by (7.47). From Fig. 7.2(a), it can be seen that $q(t) = q_0(t)$ exactly in the case of dynamic cancellation, while an error is present when using $g(q)$. On the other hand, $\theta(t) \neq \theta_0(t)$ (both with dynamic cancellation and link-based compensation) despite the initial states of the systems with and without gravity were fully matched at $t = 0$, with no initial joint deformation (see Fig. 7.2(b)). The total torques (i.e., including τ_0) for the link-based gravity compensation and for its perfect cancellation are reported in Fig. 7.3, showing that the dynamic torque contribution is indeed non-negligible.

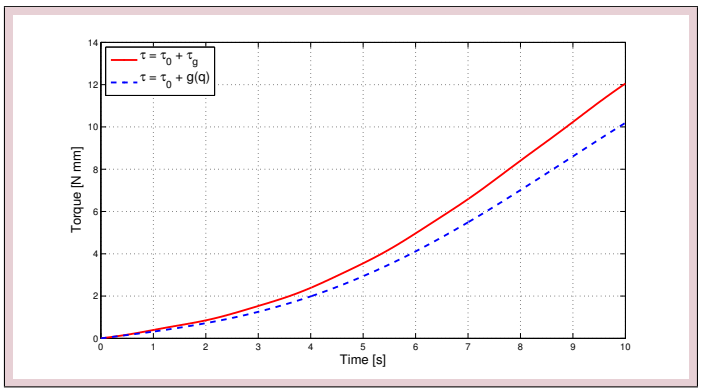

Figure 7.3: *Total applied torques with $g(q)$ only [dashed, blue] and with τ_g in (7.47) [continuous, red] for the motion of Fig. 7.2*

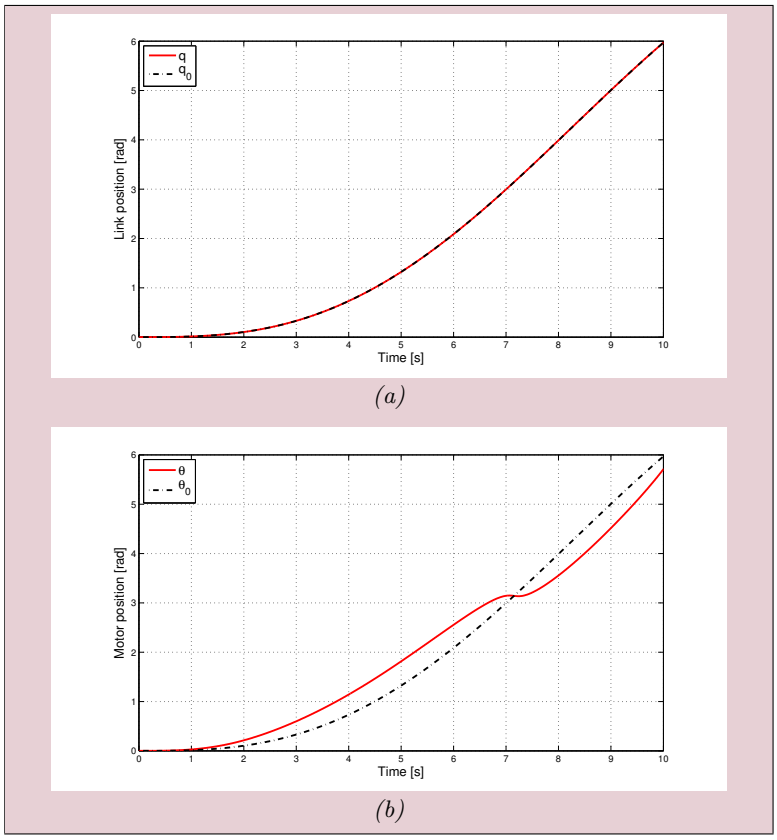

Figure 7.4: *Comparison of link (a) and motor (b) position for a single nonlinear flexible joint without gravity under τ_0 [dot-dashed, black], and with gravity under the dynamic cancellation law (7.19) [continuous, red]*

SAFT with nonlinear transmission

We simulated a joint with cubic flexibility torque $\tau_e(\phi)$ having $K = 100$ [N·mm/rad] and $K_c = 500$ [N·mm/rad]. With these data, the joint stiffness $\sigma(\phi)$ increases by

about 45% w.r.t. its value at $\phi = 0$ when the joint deformation is $|\phi| = 0.18$ [rad]. All other model parameters, the initial conditions, and the open-loop input torque are the same as in the previous simulation. Figure 7.4 shows the evolution of the link (a) and motor (b) angles obtained in the absence or in the presence of gravity under the dynamic gravity cancellation law (7.19).

Antagonistic VSA with cubic transmission

We have simulated the dynamic gravity cancellation law (7.32) for a symmetric antagonistic joint with cubic flexibility torques, using the numerical same numerical data of previous examples, duplicated as needed. In the present case, the input torques τ_{10} and τ_{20} have been chosen of the bang-bang type as in Fig. 7.5(c). Figure 7.5 shows the validity of the proposed scheme: both the link position (a) and the device stiffness (b) have identical evolutions in the absence of gravity and when gravity is present but dynamically canceled. Note that the stiffness variation during motion is as large as 2.5 [Nm/rad]. The total applied torques are shown in Fig. 7.6.

Antagonistic VSA: the VSA-II

We report also a numerical result on gravity cancellation for the VSA-II described in Sect. 4.1. Figure 7.7 shows the obtained evolution when using the same open-loop torque input of Fig. 7.5(c) and the numerical data from Schiavi et al. [2008], De Luca et al. [2009]. The total applied torques are reported in Fig. 7.8.

7.6 Extension to Multi d.o.f.

Consider a robot manipulator having n elastic joints of constant stiffness and with n driving motors. Recalling the model of a multi d.o.f. manipulator actuated by SAFT eqs. (3.5–3.6), and considering transmissions with constant stiffness

$$\boldsymbol{M}(\boldsymbol{q})\ddot{\boldsymbol{q}} + \boldsymbol{c}(\boldsymbol{q},\dot{\boldsymbol{q}}) + \boldsymbol{g}(\boldsymbol{q}) + \boldsymbol{D}_q\dot{\boldsymbol{q}} + \boldsymbol{K}(\boldsymbol{q}-\boldsymbol{\theta}) = \boldsymbol{0} \tag{7.48}$$

$$\boldsymbol{B}\ddot{\boldsymbol{\theta}} + \boldsymbol{D}_\theta\dot{\boldsymbol{\theta}} + \boldsymbol{K}(\boldsymbol{\theta}-\boldsymbol{q}) = \boldsymbol{\tau}, \tag{7.49}$$

Our control goal is to define a (nonlinear) feedback law $\boldsymbol{\tau} = \boldsymbol{\tau}(\boldsymbol{q},\boldsymbol{\theta},\dot{\boldsymbol{q}},\dot{\boldsymbol{\theta}},\boldsymbol{\tau}_0)$ in (7.49) such that the behavior of the compensated system matches *in suitable coordinates* that of an identical model but without gravity, i.e.,

$$\boldsymbol{M}(\boldsymbol{q}_0)\ddot{\boldsymbol{q}}_0 + \boldsymbol{c}(\boldsymbol{q}_0,\dot{\boldsymbol{q}}_0) + \boldsymbol{D}_q\dot{\boldsymbol{q}}_0 + \boldsymbol{K}(\boldsymbol{q}_0-\boldsymbol{\theta}_0) = \boldsymbol{0} \tag{7.50}$$

$$\boldsymbol{B}\ddot{\boldsymbol{\theta}}_0 + \boldsymbol{D}_\theta\dot{\boldsymbol{\theta}}_0 + \boldsymbol{K}(\boldsymbol{\theta}_0-\boldsymbol{q}_0) = \boldsymbol{\tau}_0, \tag{7.51}$$

where the subscript 0 characterizes the variables of the robot *in the absence of gravity*.

It is well known Spong [1987] that system (7.48–7.49) is exactly linearizable by means of a static state feedback into decoupled chains of four integrators, with $\boldsymbol{q}$ and its first three time derivatives being the linearizing coordinates.

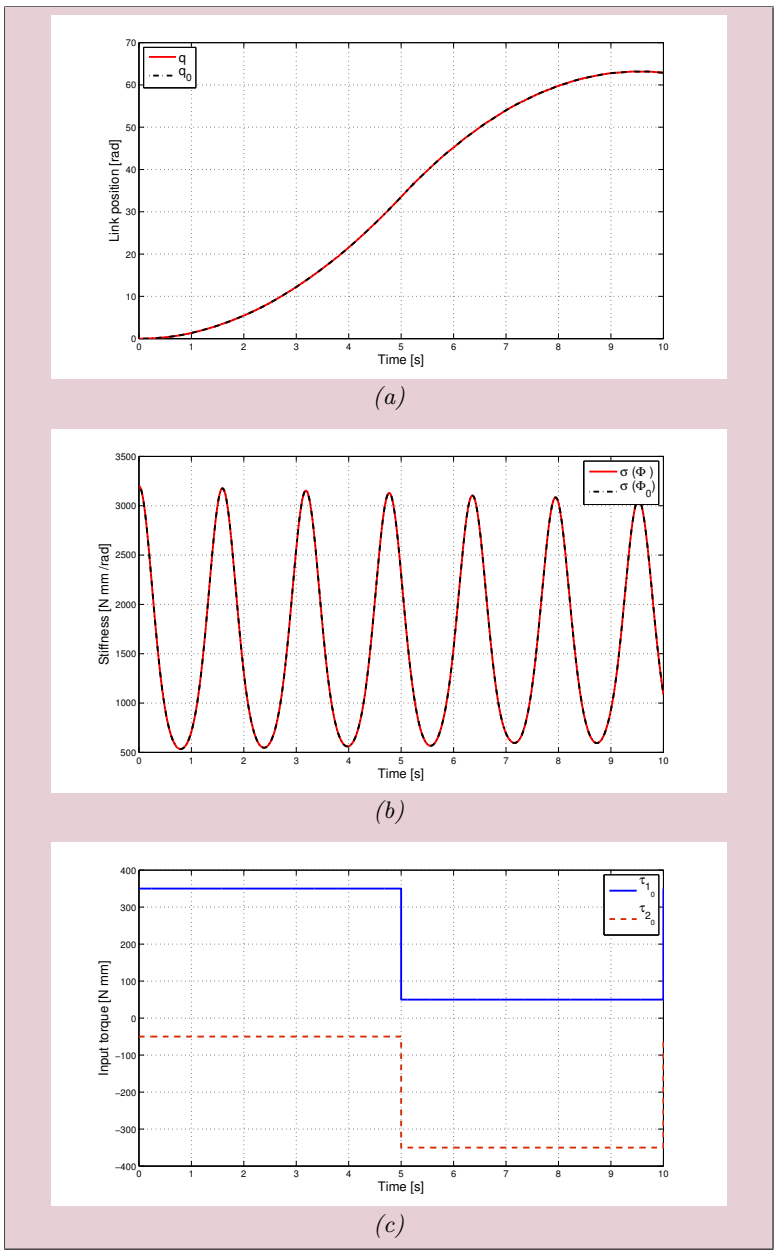

Figure 7.5: *Comparison of link position (a) and device stiffness (b) for a variable stiffness antagonistic joint with cubic flexibility torques without gravity [dot-dashed, black], and with gravity under the dynamic cancellation law (7.32) [continuous, red] when the bang-bang torque inputs τ_{10} and τ_{10} (c) are applied*

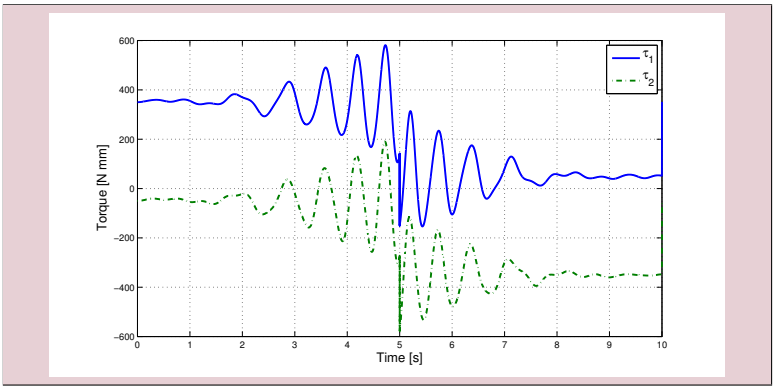

Figure 7.6: *Total applied torques (7.32) for the link motion and device stiffness evolution of Fig. 7.5*

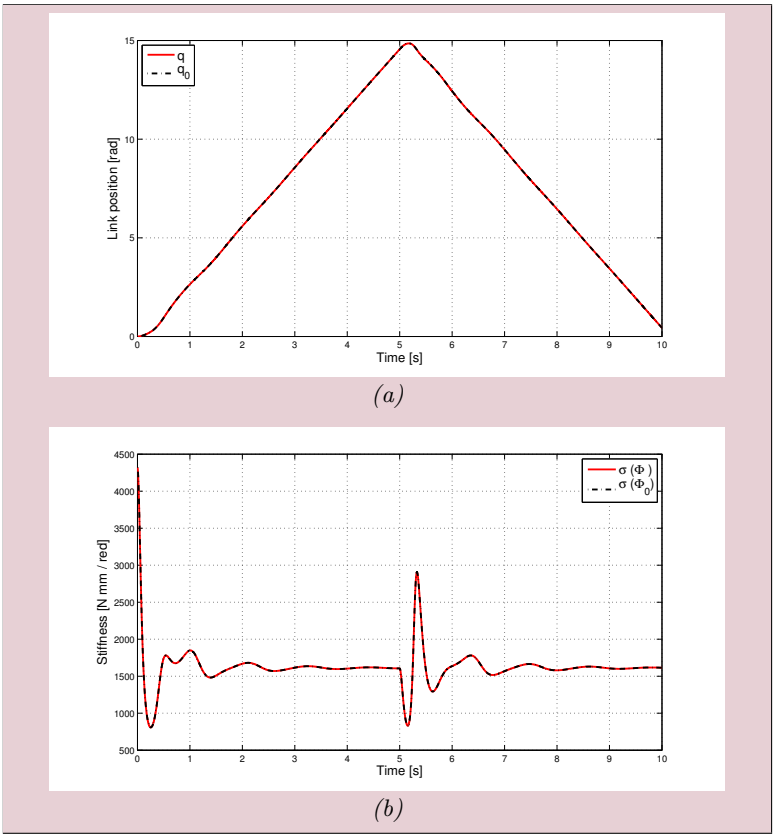

Figure 7.7: *Comparison of link position (a) and device stiffness (b) for the VSA-II without gravity [dot-dashed, black], and with gravity under the dynamic cancellation law [continuous, red] when the bang-bang torque inputs τ_{10} and τ_{10} of Fig. 7.5(c) are applied*

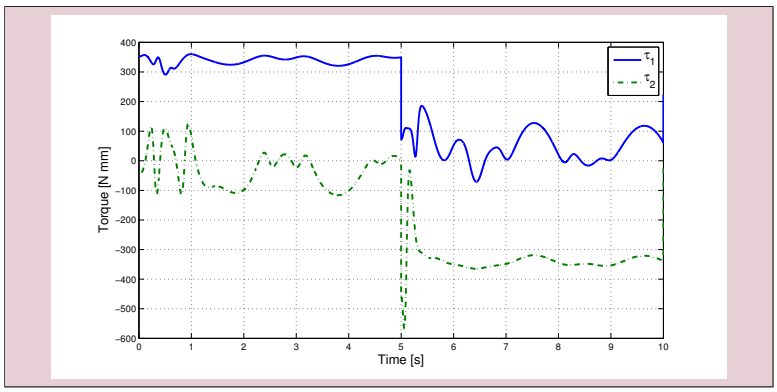

Figure 7.8: *Total applied torques for the link motion and device stiffness evolution of Fig. 7.7*

Indeed, the same holds true also for system (7.50–7.51). Therefore, thanks to the feedback equivalence principle, by imposing the equality

$$\boldsymbol{q}(t) \equiv \boldsymbol{q}_0(t), \qquad \forall t \geq 0 \tag{7.52}$$

As shown in Sect. 7.2 one should obtain the desired result without resorting to the complexity of a complete feedback linearization process. Using the same approach of the single d.o.f. case eq. (7.48) is differentiating once w.r.t. time yielding

$$\boldsymbol{M}(\boldsymbol{q})\boldsymbol{q}^{[3]} + (\dot{\boldsymbol{M}}(\boldsymbol{q}) + \boldsymbol{D}_q)\ddot{\boldsymbol{q}} + \dot{\boldsymbol{c}}(\boldsymbol{q}, \dot{\boldsymbol{q}}) + \dot{\boldsymbol{g}}(\boldsymbol{q}) + \boldsymbol{K}(\dot{\boldsymbol{q}} - \dot{\boldsymbol{\theta}}) = \boldsymbol{0},$$

with the notation $\boldsymbol{q}^{[i]} = d^i\boldsymbol{q}/dt^i$. Differentiating one more time, and substituting $\ddot{\boldsymbol{\theta}}$ from (7.49), we obtain

$$\begin{aligned} \boldsymbol{M}(\boldsymbol{q})\boldsymbol{q}^{[4]} + (2\dot{\boldsymbol{M}}(\boldsymbol{q}) + \boldsymbol{D}_q)\boldsymbol{q}^{[3]} + \ddot{\boldsymbol{M}}(\boldsymbol{q})\ddot{\boldsymbol{q}} + \ddot{\boldsymbol{c}}(\boldsymbol{q}, \dot{\boldsymbol{q}}) + \boldsymbol{K}\ddot{\boldsymbol{q}} \\ = \boldsymbol{K}\boldsymbol{B}^{-1}\left(\boldsymbol{\tau} - \boldsymbol{D}_\theta\dot{\boldsymbol{\theta}} - \boldsymbol{K}(\boldsymbol{\theta} - \boldsymbol{q})\right) - \ddot{\boldsymbol{g}}(\boldsymbol{q}). \end{aligned} \tag{7.53}$$

Noting that the left-hand side of (7.53) is a function of $\boldsymbol{q}$ and its first four derivatives only, we will write it compactly as $\boldsymbol{f}(\boldsymbol{q}, \ddot{\boldsymbol{q}}, \ddot{\boldsymbol{q}}, \boldsymbol{q}^{[3]}, \boldsymbol{q}^{[4]})$. Repeating the same computation for the no-gravity model (7.50–7.51) leads to

$$\boldsymbol{f}(\boldsymbol{q}_0, \ddot{\boldsymbol{q}}_0, \ddot{\boldsymbol{q}}_0, \boldsymbol{q}_0^{[3]}, \boldsymbol{q}_0^{[4]}) = \boldsymbol{K}\boldsymbol{B}^{-1}\left(\boldsymbol{\tau}_0 - \boldsymbol{D}_\theta\dot{\boldsymbol{\theta}}_0 - \boldsymbol{K}(\boldsymbol{\theta}_0 - \boldsymbol{q})\right). \tag{7.54}$$

By imposing (7.52), the left-hand sides of (7.53) and (7.54) will be equal, and thus

$$\begin{aligned} \boldsymbol{K}\boldsymbol{B}^{-1}\left(\boldsymbol{\tau} - \boldsymbol{D}_\theta\dot{\boldsymbol{\theta}} - \boldsymbol{K}(\boldsymbol{\theta} - \boldsymbol{q})\right) - \ddot{\boldsymbol{g}}(\boldsymbol{q}) \\ = \boldsymbol{K}\boldsymbol{B}^{-1}\left(\boldsymbol{\tau}_0 - \boldsymbol{D}_\theta\dot{\boldsymbol{\theta}}_0 - \boldsymbol{K}(\boldsymbol{\theta}_0 - \boldsymbol{q})\right). \end{aligned} \tag{7.55}$$

In order to eliminate the presence of the motor variables in (7.55), we use eqs. (7.48) and (7.50). By imposing again (7.52), one has

$$\begin{aligned} \boldsymbol{K}(\boldsymbol{\theta} - \boldsymbol{q}) &= \boldsymbol{M}(\boldsymbol{q})\ddot{\boldsymbol{q}} + \boldsymbol{c}(\boldsymbol{q}, \dot{\boldsymbol{q}}) + \boldsymbol{D}_q\dot{\boldsymbol{q}} + \boldsymbol{g}(\boldsymbol{q}) \\ \boldsymbol{K}(\boldsymbol{\theta}_0 - \boldsymbol{q}) &= \boldsymbol{M}(\boldsymbol{q})\ddot{\boldsymbol{q}} + \boldsymbol{c}(\boldsymbol{q}, \dot{\boldsymbol{q}}) + \boldsymbol{D}_q\dot{\boldsymbol{q}}, \end{aligned} \tag{7.56}$$

or

$$\boldsymbol{\theta} = \boldsymbol{\theta}_0 + \boldsymbol{K}^{-1}\boldsymbol{g}(\boldsymbol{q}), \tag{7.57}$$

and then

$$\dot{\boldsymbol{\theta}} = \dot{\boldsymbol{\theta}}_0 + \boldsymbol{K}^{-1}\dot{\boldsymbol{g}}(\boldsymbol{q}). \tag{7.58}$$

Replacing eqs. (7.57–7.58) into (7.55) and simplifying, the solution to our problem is obtained by choosing the control law as

$$\boldsymbol{\tau} = \boldsymbol{\tau}_g + \boldsymbol{\tau}_0 \tag{7.59}$$

with

$$\boldsymbol{\tau}_g = \boldsymbol{g}(\boldsymbol{q}) + \boldsymbol{D}_\theta \boldsymbol{K}^{-1}\dot{\boldsymbol{g}}(\boldsymbol{q}) + \boldsymbol{B}\boldsymbol{K}^{-1}\ddot{\boldsymbol{g}}(\boldsymbol{q}), \tag{7.60}$$

where

$$\dot{\boldsymbol{g}}(\boldsymbol{q}) = \frac{\partial \boldsymbol{g}(\boldsymbol{q})}{\partial \boldsymbol{q}}\,\dot{\boldsymbol{q}}$$

$$\ddot{\boldsymbol{g}}(\boldsymbol{q}) = \frac{\partial \boldsymbol{g}(\boldsymbol{q})}{\partial \boldsymbol{q}}\boldsymbol{M}^{-1}(\boldsymbol{q})\big(\boldsymbol{K}(\boldsymbol{\theta}-\boldsymbol{q}) - \boldsymbol{c}(\boldsymbol{q},\dot{\boldsymbol{q}}) - \boldsymbol{g}(\boldsymbol{q}) - \boldsymbol{D}_q\dot{\boldsymbol{q}}\big) + \sum_{i=1}^{n}\frac{\partial^2 \boldsymbol{g}(\boldsymbol{q})}{\partial \boldsymbol{q}\,\partial q_i}\,\dot{\boldsymbol{q}}\,\dot{q}_i.$$

In addition, matched initial conditions should hold at time $t = 0$:

$$\begin{aligned} \boldsymbol{q}(0) &= \boldsymbol{q}_0(0) \qquad & \ddot{\boldsymbol{q}}(0) &= \ddot{\boldsymbol{q}}_0(0) \\ \dot{\boldsymbol{q}}(0) &= \dot{\boldsymbol{q}}_0(0) \qquad & \boldsymbol{q}^{[3]}(0) &= \boldsymbol{q}_0^{[3]}(0). \end{aligned} \tag{7.61}$$

Note that, thanks to the control law (7.59–7.60), the identities (7.61) will be enforced for all $t \geq 0$.

We remark that, despite of the need of inverting the robot inertia matrix $\boldsymbol{M}(\boldsymbol{q})$, the gravity cancellation torque (7.60) is much simpler than the expression of a feedback linearization control law, which involves in fact also the time derivatives of the model terms $\boldsymbol{M}(\boldsymbol{q})$ and $\boldsymbol{c}(\boldsymbol{q},\dot{\boldsymbol{q}})$ up to the second order.

The torque input $\boldsymbol{\tau}_0$ in (7.59) can be chosen according to the robot primary task, e.g., as in De Luca et al. [2006] for a torque-based robot reaction to detected collisions in pHRI. In this context, perfect gravity cancellation allows a link behavior during transients and at steady-state that is totally unaffected by gravity bias. Furthermore, for a regulation task to a desired link position $\boldsymbol{q}_d$, it can be shown that the *PD-type* control law

$$\boldsymbol{\tau}_0 = \boldsymbol{K}_P\left(\boldsymbol{q}_d - \boldsymbol{\theta} + \boldsymbol{K}^{-1}\boldsymbol{g}(\boldsymbol{q})\right) - \boldsymbol{K}_D\Big(\dot{\boldsymbol{\theta}} - \boldsymbol{K}^{-1}\frac{\partial \boldsymbol{g}(\boldsymbol{q})}{\partial \boldsymbol{q}}\,\dot{\boldsymbol{q}}\Big),$$

achieves global asymptotic stabilization for *any* $\boldsymbol{K}_P > 0$ and $\boldsymbol{K}_D > 0$, i.e., without the need of a strictly positive lower bound on $\boldsymbol{K}_P$. This result holds for any $\boldsymbol{K} > 0$, i.e., also for very soft joints. A formal proof of this result is presented in Sect. 7.7.

7.7 A New PD-type Regulator for Robots with Elastic Joints

Consider again the gravity-loaded system (7.48–7.49) in the absence of dissipative terms[1], i.e.,

$$\boldsymbol{M}(\boldsymbol{q})\ddot{\boldsymbol{q}} + \boldsymbol{S}(\boldsymbol{q},\dot{\boldsymbol{q}})\dot{\boldsymbol{q}} + \boldsymbol{g}(\boldsymbol{q}) + \boldsymbol{K}(\boldsymbol{q}-\boldsymbol{\theta}) = \boldsymbol{0} \tag{7.62}$$

$$\boldsymbol{B}\ddot{\boldsymbol{\theta}} + \boldsymbol{K}(\boldsymbol{\theta}-\boldsymbol{q}) = \boldsymbol{\tau}, \tag{7.63}$$

where any factorization $\boldsymbol{c}(\boldsymbol{q},\dot{\boldsymbol{q}}) = \boldsymbol{S}(\boldsymbol{q},\dot{\boldsymbol{q}})\dot{\boldsymbol{q}}$ can be used for the Coriolis/centrifugal vector. We address the problem of asymptotic stabilization of a desired (closed-loop) equilibrium state

$$\boldsymbol{q} = \boldsymbol{q}_d, \quad \boldsymbol{\theta} = \boldsymbol{\theta}_d := \boldsymbol{q}_d + \boldsymbol{K}^{-1}\boldsymbol{g}(\boldsymbol{q}_d), \quad \dot{\boldsymbol{q}} = \dot{\boldsymbol{\theta}} = \boldsymbol{0}. \tag{7.64}$$

The desired motor position $\boldsymbol{\theta}_d$ is obtained from the static analysis (i.e., setting $\dot{\boldsymbol{q}} = \ddot{\boldsymbol{q}} = \boldsymbol{0}$) of equation (7.62) at the desired link position $\boldsymbol{q}_d$.

Taking advantage of the dynamic gravity cancellation law, we present a new regulation controller realizing the task. The complete control law is defined as

$$\boldsymbol{\tau} = \boldsymbol{\tau}_g + \boldsymbol{\tau}_0, \tag{7.65}$$

where $\boldsymbol{\tau}_g$ is given by (7.60) (having set $\boldsymbol{D}_\theta = \boldsymbol{O}$)

$$\boldsymbol{\tau}_g = \boldsymbol{g}(\boldsymbol{q}) + \boldsymbol{B}\boldsymbol{K}^{-1}\ddot{\boldsymbol{g}}(\boldsymbol{q}), \tag{7.66}$$

and $\boldsymbol{\tau}_0$ is chosen as the *PD-type control law*

$$\boldsymbol{\tau}_0 = \boldsymbol{K}_P(\boldsymbol{q}_d - \boldsymbol{\theta} + \boldsymbol{K}^{-1}\boldsymbol{g}(\boldsymbol{q})) - \boldsymbol{K}_D(\dot{\boldsymbol{\theta}} - \boldsymbol{K}^{-1}\dot{\boldsymbol{g}}(\boldsymbol{q})). \tag{7.67}$$

The following result holds.

Theorem 1 *The desired state (7.64) for system (7.62–7.63) with control law (7.65–7.67) is the unique equilibrium state of the closed-loop system. Moreover, if*

$$\boldsymbol{K}_P > 0, \qquad \boldsymbol{K}_D > 0,$$

the desired state is globally asymptotically stable.

Proof The proof is based on Lyapunov analysis and LaSalle theorem. First, we show that there is a unique equilibrium state for the closed-loop system, i.e., a unique equilibrium configuration $(\boldsymbol{q}_e, \boldsymbol{\theta}_e)$ with zero velocities $\dot{\boldsymbol{q}}$ and $\dot{\boldsymbol{\theta}}$. By setting $\ddot{\boldsymbol{q}} = \ddot{\boldsymbol{\theta}} = \boldsymbol{0}$ in the closed-loop equations given by (7.62–7.63) and (7.65–7.67), any equilibrium configuration should satisfy

$$\begin{aligned} \boldsymbol{g}(\boldsymbol{q}_e) + \boldsymbol{K}(\boldsymbol{q}_e - \boldsymbol{\theta}_e) &= \boldsymbol{0} \\ \boldsymbol{K}(\boldsymbol{q}_e - \boldsymbol{\theta}_e) + \boldsymbol{g}(\boldsymbol{q}_e) + \boldsymbol{K}_P(\boldsymbol{q}_d - \boldsymbol{\theta}_e + \boldsymbol{K}^{-1}\boldsymbol{g}(\boldsymbol{q}_e)) &= \boldsymbol{0}. \end{aligned}$$

[1] Neglecting dissipative terms (e.g., viscous friction on the motor and link sides) is the worst situation from the point of view of stability of the robotic system. Their inclusion would make the analysis simpler.

Subtracting the two equations leads to

$$\boldsymbol{\theta}_e = \boldsymbol{q}_d + \boldsymbol{K}^{-1}\boldsymbol{g}(\boldsymbol{q}_e),$$

while the first equation yields

$$\boldsymbol{\theta}_e = \boldsymbol{q}_e + \boldsymbol{K}^{-1}\boldsymbol{g}(\boldsymbol{q}_e).$$

By comparison, it follows that the the unique equilibrium is

$$\boldsymbol{q}_e = \boldsymbol{q}_d, \qquad \boldsymbol{\theta}_e = \boldsymbol{q}_d + \boldsymbol{K}^{-1}\boldsymbol{g}(\boldsymbol{q}_d) = \boldsymbol{\theta}_d.$$

Let a Lyapunov candidate be defined by the following quadratic function:

$$\begin{aligned} V = \tfrac{1}{2}\Big(&\dot{\boldsymbol{q}}^T\boldsymbol{M}(\boldsymbol{q})\dot{\boldsymbol{q}} + \left(\dot{\boldsymbol{\theta}} - \boldsymbol{K}^{-1}\dot{\boldsymbol{g}}(\boldsymbol{q})\right)^T\boldsymbol{B}\left(\dot{\boldsymbol{\theta}} - \boldsymbol{K}^{-1}\dot{\boldsymbol{g}}(\boldsymbol{q})\right) \\ &+ \left(\boldsymbol{q} - \boldsymbol{\theta} + \boldsymbol{K}^{-1}\boldsymbol{g}(\boldsymbol{q})\right)^T\boldsymbol{K}\left(\boldsymbol{q} - \boldsymbol{\theta} + \boldsymbol{K}^{-1}\boldsymbol{g}(\boldsymbol{q})\right) \\ &+ \left(\boldsymbol{q}_d - \boldsymbol{\theta} + \boldsymbol{K}^{-1}\boldsymbol{g}(\boldsymbol{q})\right)^T\boldsymbol{K}_P\left(\boldsymbol{q}_d - \boldsymbol{\theta} + \boldsymbol{K}^{-1}\boldsymbol{g}(\boldsymbol{q})\right)\Big). \end{aligned}$$

As the sum of positive definite quadratic terms, V is positive definite. Moreover, $V = 0$ if and only if

$$\dot{\boldsymbol{q}} = \boldsymbol{0}, \quad \dot{\boldsymbol{\theta}} - \boldsymbol{K}^{-1}\frac{\partial \boldsymbol{g}(\boldsymbol{q})}{\partial \boldsymbol{q}}\dot{\boldsymbol{q}} = \boldsymbol{0} \quad \Rightarrow \quad \dot{\boldsymbol{\theta}} = \boldsymbol{0}$$

and

$$\left.\begin{aligned} \boldsymbol{q} - \boldsymbol{\theta} + \boldsymbol{K}^{-1}\boldsymbol{g}(\boldsymbol{q}) &= \boldsymbol{0} \\ \boldsymbol{q}_d - \boldsymbol{\theta} + \boldsymbol{K}^{-1}\boldsymbol{g}(\boldsymbol{q}) &= \boldsymbol{0} \end{aligned}\right\} \Rightarrow \left\{\begin{aligned} \boldsymbol{q} &= \boldsymbol{q}_d \\ \boldsymbol{\theta} &= \boldsymbol{q}_d + \boldsymbol{K}^{-1}\boldsymbol{g}(\boldsymbol{q}_d). \end{aligned}\right.$$

Therefore, the desired state is the unique minimum of V. Dropping for compactness dependencies, the time derivative of V is

$$\begin{aligned} \dot{V} = &\dot{\boldsymbol{q}}^T\boldsymbol{M}\ddot{\boldsymbol{q}} + \tfrac{1}{2}\dot{\boldsymbol{q}}^T\dot{\boldsymbol{M}}\dot{\boldsymbol{q}} + \left(\dot{\boldsymbol{\theta}} - \boldsymbol{K}^{-1}\dot{\boldsymbol{g}}\right)^T\boldsymbol{B}\left(\ddot{\boldsymbol{\theta}} - \boldsymbol{K}^{-1}\ddot{\boldsymbol{g}}\right) \\ &+ \left(\boldsymbol{q} - \boldsymbol{\theta} + \boldsymbol{K}^{-1}\boldsymbol{g}\right)^T\boldsymbol{K}\left(\dot{\boldsymbol{q}} - \dot{\boldsymbol{\theta}} + \boldsymbol{K}^{-1}\dot{\boldsymbol{g}}\right) \\ &- \left(\boldsymbol{q}_d - \boldsymbol{\theta} + \boldsymbol{K}^{-1}\boldsymbol{g}\right)^T\boldsymbol{K}_P\left(\dot{\boldsymbol{\theta}} - \boldsymbol{K}^{-1}\dot{\boldsymbol{g}}\right). \end{aligned}$$

The closed-loop equations (7.62–7.63) with (7.65–7.67) can be conveniently rewritten in the form

$$\boldsymbol{M}\ddot{\boldsymbol{q}} = \boldsymbol{K}(\boldsymbol{\theta} - \boldsymbol{q}) - \boldsymbol{S}\dot{\boldsymbol{q}} - \boldsymbol{g}$$

$$\boldsymbol{B}\left(\ddot{\boldsymbol{\theta}} - \boldsymbol{K}^{-1}\ddot{\boldsymbol{g}}\right) = \boldsymbol{K}(\boldsymbol{q} - \boldsymbol{\theta}) + \boldsymbol{g} + \boldsymbol{K}_P\left(\boldsymbol{q}_d - \boldsymbol{\theta} + \boldsymbol{K}^{-1}\boldsymbol{g}\right) - \boldsymbol{K}_D\left(\dot{\boldsymbol{\theta}} - \boldsymbol{K}^{-1}\dot{\boldsymbol{g}}\right).$$

Substituting these into the expression of $\dot{V}$ and simplifying terms yields

$$\begin{aligned} \dot{V} = &\dot{\boldsymbol{q}}^T\left(\boldsymbol{K}(\boldsymbol{\theta} - \boldsymbol{q}) + \tfrac{1}{2}\left(\dot{\boldsymbol{M}} - 2\boldsymbol{S}\right)\dot{\boldsymbol{q}} - \boldsymbol{g}\right) \\ &+ \left(\dot{\boldsymbol{\theta}} - \boldsymbol{K}^{-1}\dot{\boldsymbol{g}}\right)^T\Big(\boldsymbol{K}(\boldsymbol{q} - \boldsymbol{\theta}) + \boldsymbol{g} \\ &\qquad + \boldsymbol{K}_P\left(\boldsymbol{q}_d - \boldsymbol{\theta} + \boldsymbol{K}^{-1}\boldsymbol{g}\right) - \boldsymbol{K}_D\left(\dot{\boldsymbol{\theta}} - \boldsymbol{K}^{-1}\dot{\boldsymbol{g}}\right)\Big) \\ &+ \left(\boldsymbol{K}(\boldsymbol{q} - \boldsymbol{\theta}) + \boldsymbol{g}\right)^T\left(\dot{\boldsymbol{q}} - \dot{\boldsymbol{\theta}} + \boldsymbol{K}^{-1}\dot{\boldsymbol{g}}\right) \\ &- \left(\boldsymbol{q}_d - \boldsymbol{\theta} + \boldsymbol{K}^{-1}\boldsymbol{g}\right)^T\boldsymbol{K}_P\left(\dot{\boldsymbol{\theta}} - \boldsymbol{K}^{-1}\dot{\boldsymbol{g}}\right) \\ = &-\left(\dot{\boldsymbol{\theta}} - \boldsymbol{K}^{-1}\dot{\boldsymbol{g}}\right)^T\boldsymbol{K}_D\left(\dot{\boldsymbol{\theta}} - \boldsymbol{K}^{-1}\dot{\boldsymbol{g}}\right) \leq 0, \end{aligned}$$

where the general relation $\dot{\boldsymbol{q}}^T \left(\dot{\boldsymbol{M}} - 2\boldsymbol{S} \right) \dot{\boldsymbol{q}} = \boldsymbol{0}$ has been used. Thus, it is

$$\dot{V} = 0 \quad \Leftrightarrow \quad \dot{\boldsymbol{g}}(\boldsymbol{q}) - \boldsymbol{K}\dot{\boldsymbol{\theta}} = \boldsymbol{0}.$$

We proceed by using LaSalle arguments. The desired state satisfies indeed $\dot{V} = 0$, and thus $V(t) \equiv 0$. We should verify whether there are other system trajectories that are invariant with respect to the set of states where $\dot{V} = 0$. When $\dot{V} = 0$, note first that

$$\frac{d}{dt} \left(\boldsymbol{g}(\boldsymbol{q}) - \boldsymbol{K}\boldsymbol{\theta} \right) = \boldsymbol{0} \quad \Rightarrow \quad \boldsymbol{g}(\boldsymbol{q}) - \boldsymbol{K}\boldsymbol{\theta} = \boldsymbol{k}_1,$$

where $\boldsymbol{k}_1$ is a constant vector. Moreover, the model equation (7.63) with $\boldsymbol{\tau}$ as in (7.65–7.67) becomes

$$\boldsymbol{B}\,\ddot{\boldsymbol{\theta}} + \boldsymbol{K}(\boldsymbol{\theta} - \boldsymbol{q}) = \boldsymbol{g}(\boldsymbol{q}) + \boldsymbol{B}\boldsymbol{K}^{-1}\ddot{\boldsymbol{g}}(\boldsymbol{q}) + \boldsymbol{K}_P(\boldsymbol{q}_d - \boldsymbol{\theta} + \boldsymbol{K}^{-1}\boldsymbol{g}(\boldsymbol{q})),$$

or, by simple manipulation,

$$\boldsymbol{B}\boldsymbol{K}^{-1} \frac{d}{dt} \left(\boldsymbol{K}\dot{\boldsymbol{\theta}} - \dot{\boldsymbol{g}}(\boldsymbol{q}) \right) = \left(\boldsymbol{I} + \boldsymbol{K}_P\boldsymbol{K}^{-1} \right) \left[\boldsymbol{g}(\boldsymbol{q}) - \boldsymbol{K}\boldsymbol{\theta} \right] + \boldsymbol{K}\boldsymbol{q} + \boldsymbol{K}_P\boldsymbol{q}_d.$$

For a closed-loop system trajectory remaining in the set of states such that $\dot{V} = 0$, the left-hand side of this equation must be zero. Since the term in square brackets on the right-hand side is constant, it follows that

$$\boldsymbol{K}\boldsymbol{q} + \boldsymbol{K}_P\boldsymbol{q}_d = \boldsymbol{k}_2,$$

and hence $\boldsymbol{q}$ is constant by itself. As a consequence, $\boldsymbol{\theta}$ is also a constant, and thus $\dot{\boldsymbol{q}} = \dot{\boldsymbol{\theta}} = \boldsymbol{0}$. Therefore, the only invariant trajectory of the closed-loop system that is compatible with $\dot{V} = 0$ is an equilibrium state. Since $\boldsymbol{q} = \boldsymbol{q}_d$, $\boldsymbol{\theta} = \boldsymbol{\theta}_d$, with $\dot{\boldsymbol{q}} = \dot{\boldsymbol{\theta}} = \boldsymbol{0}$, is the unique equilibrium, then the desired state is globally asymptotically stable thanks to LaSalle theorem. This completes the proof[2]. ∎

A series of remarks are in order:

- The expression of the control law (7.67) is logically derived from a pure PD scheme on the motor variables $\boldsymbol{\theta}_0$ and $\dot{\boldsymbol{\theta}}_0$ of the gravity-free system,

$$\begin{aligned} \boldsymbol{\tau}_0 &= \boldsymbol{K}_P(\boldsymbol{\theta}_{d0} - \boldsymbol{\theta}_0) - \boldsymbol{K}_D\dot{\boldsymbol{\theta}}_0 \\ &= \boldsymbol{K}_P(\boldsymbol{q}_d - \boldsymbol{\theta} + \boldsymbol{K}^{-1}\boldsymbol{g}(\boldsymbol{q})) - \boldsymbol{K}_D(\dot{\boldsymbol{\theta}} - \boldsymbol{K}^{-1}\dot{\boldsymbol{g}}(\boldsymbol{q})), \end{aligned}$$

  using the relations (7.57–7.58) between motor variables of the gravity-free system and of the gravity-loaded system under the action of dynamic gravity cancellation, and noting that the motor reference for the PD is $\boldsymbol{\theta}_{d0} = \boldsymbol{q}_d$ since gravitational effects are canceled by $\boldsymbol{\tau}_g$. Another way of interpreting terms in the control law (7.65–7.67) is to note that the motor reference $\boldsymbol{\theta}_d = \boldsymbol{q}_d + \boldsymbol{K}^{-1}\boldsymbol{g}(\boldsymbol{q}_d)$ in the PD law with *constant* gravity compensation of Tomei [1991] is replaced by its *on-line* version $\boldsymbol{q}_d + \boldsymbol{K}^{-1}\boldsymbol{g}(\boldsymbol{q})$.

[2] The introduced constants are $\boldsymbol{k}_1 = -\boldsymbol{K}\boldsymbol{q}_d$, $\boldsymbol{k}_2 = (\boldsymbol{K} + \boldsymbol{K}_P)\boldsymbol{q}_d$.

- The PD term in the control law, i.e., eq. (7.67), needs feedback from the full state of the robot, just as the term $\boldsymbol{\tau}_g$. This is the same requisite of exact linearization laws by static state feedback. Conversely, energy-based Lyapunov designs for elastic joint robots use only motor feedback. The proposed controller realizes thus a compromise, eliminating the gravity-dependent dynamic terms by means of a full state feedback but avoiding the need of complete cancellation of the dynamics of the elastic joint robot.

- Using gravity cancellation, there is no need of a positive lower bound on the joint stiffness $\boldsymbol{K}$, as opposed to the previous literature Tomei [1991], De Luca et al. [2005], Kugi et al. [2008]. While in practice joint stiffness always dominates the gradient of gravity torques in industrial robots with elastic joints (e.g., using harmonic drives), this relaxation can be of interest for actuation systems with variable stiffness (see Sect. **??**), where very low values of stiffness may be desirable to limit injuries due to accidental collisions between robot and humans.

- Looking at the proof of Theorem 1, it is easy to see that the desired state would still be the unique equilibrium for the closed-loop system when reducing the gravity-term in the controller to $\boldsymbol{\tau}_g = \boldsymbol{g}(\boldsymbol{q})$. However, a Lyapunov-based proof of global asymptotic stability with such a term added to a PD controller is not available.

Simulation results

We present some simulation results that show the typical behavior obtained under the action of the PD-type control law (7.67) with the gravity cancellation (7.66). A single link with elastic joint is considered, using the same numerical data of Sect. 7.5. The link is commanded to move from the downward equilibrium $q = 0$ to $q_d = \pi/2$. The PD (scalar) gains were chosen as $k_P = 100$ and $k_D = 80$. These values were conveniently tuned in the absence of gravity. Figure 7.9 shows the comparative evolution of the relevant variables in the two situations of no gravity and presence of gravity with gravity cancellation. The link motion in Fig. 7.9(a) is exactly the same, as expected. The motor position has a different evolution in the two cases (Fig. 7.9(b)), due to the need to charge the elastic joint for dynamically balancing gravity on the link. The total applied motor torque is also different (Fig. 7.9(c)): in fact, it should vanish at steady state when gravity is absent, whereas it should at least provide the static gravity torque at final destination in the other case. The new control law is able to regulate the link to the desired position even if the joint stiffness is here very small, in particular lower than the maximum gradient of the gravity term ($K = 100 < 245.25 = mdg_0$). Note that the small oscillations experienced by the link while approaching the goal are due to the poor transient performance achievable by motor PD feedback in the absence of gravity, and not to the nature of the dynamic gravity cancellation law: the only role of τ_g is to allow the exact reproduction of the link behavior in the absence of gravity, no matter how good or bad this is. The very low value of joint stiffness is partly responsible for this behavior. In fact, Figure 7.10 shows the results under the same PD gains when increasing the joint stiffness to $K = 500$. The improvement in the transient behavior is quite apparent.

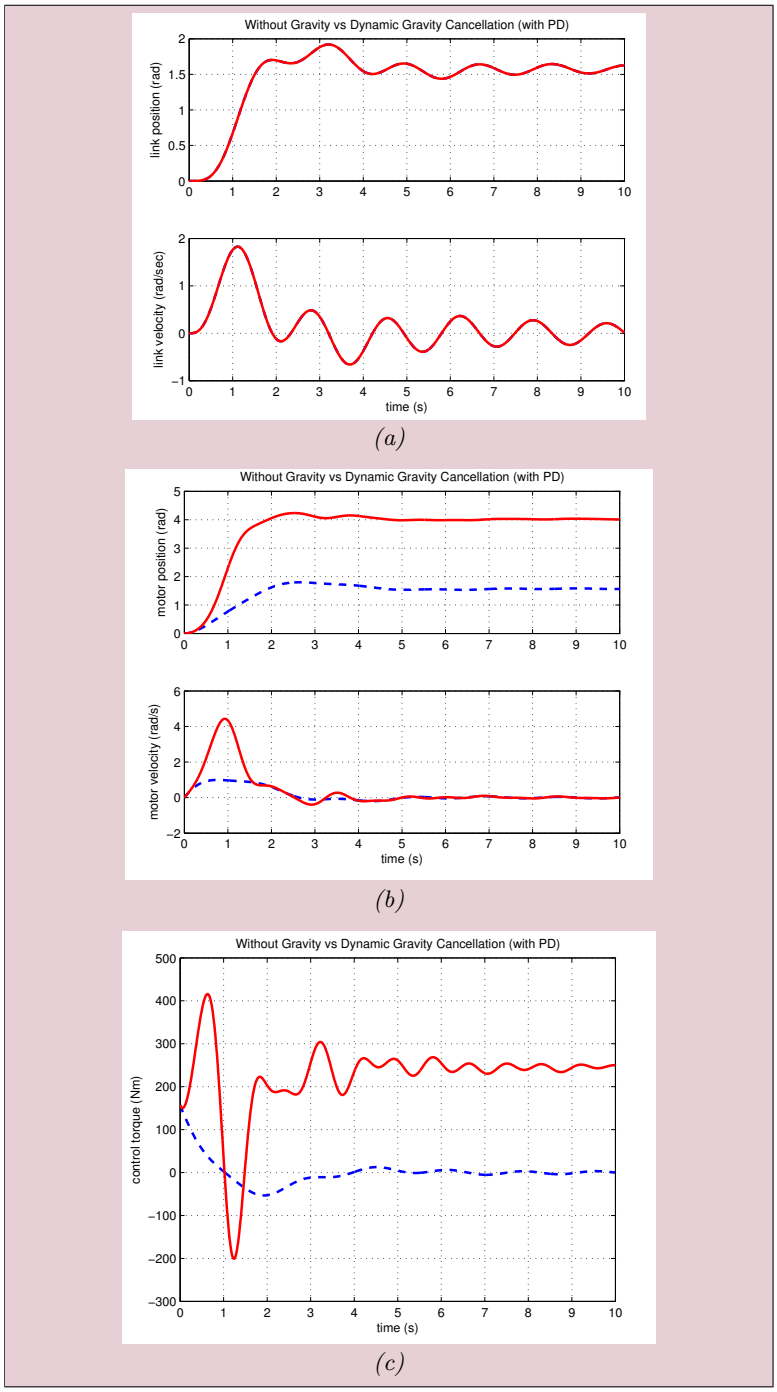

Figure 7.9: *Comparison of link variables (a), motor variables (b), and control torques (c) for a single link with elastic joint without gravity under PD control on the motor side [dashed, blue], and with gravity under the PD-type control law with dynamic cancellation (7.65–7.67) [continuous, red]; the joint stiffness is* $K = 100$

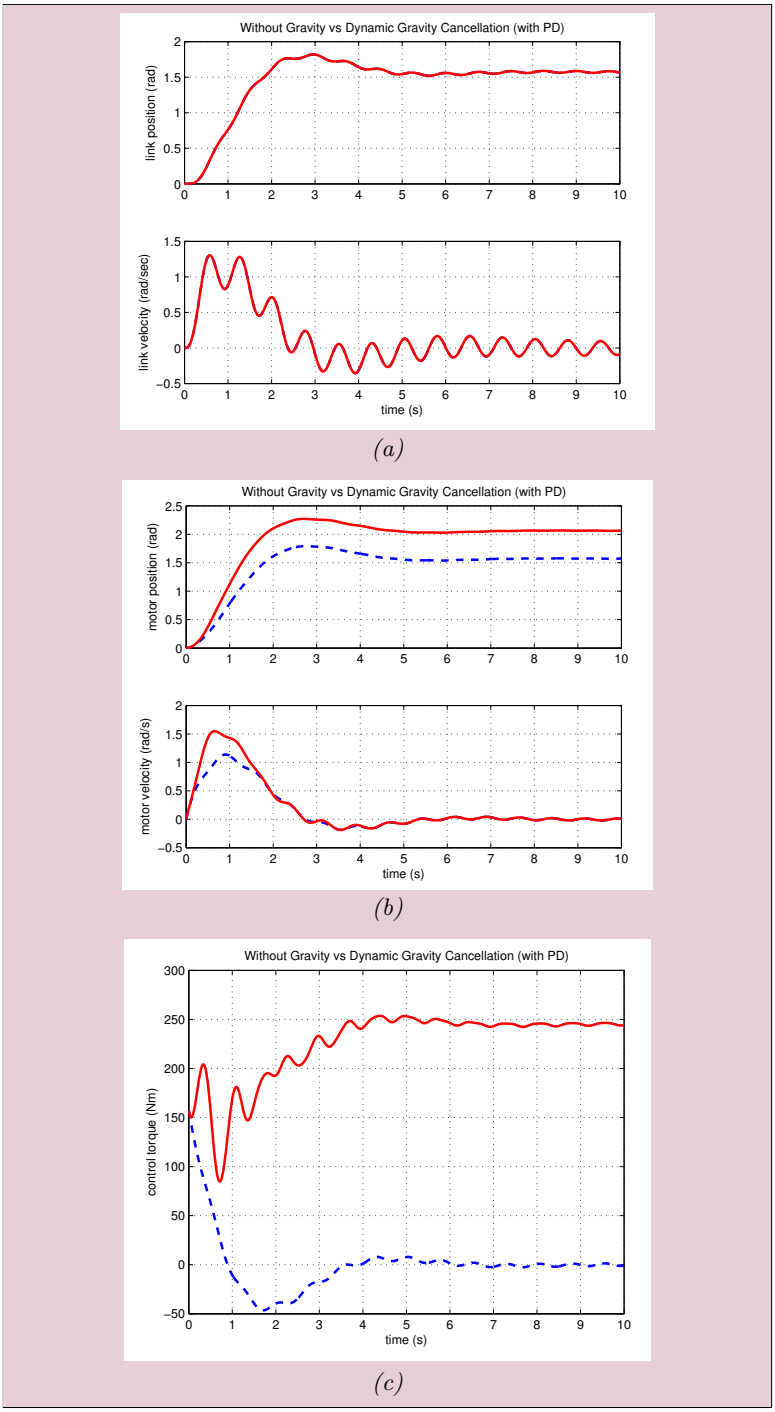

Figure 7.10: *Comparison of link variables (a), motor variables (b), and control torques (c) for a single link with elastic joint without gravity under PD control on the motor side [dashed, blue], and with gravity under the PD-type control law with dynamic cancellation (7.65–7.67) [continuous, red]; the joint stiffness is* $K = 500$

7.8 Conclusions

We have considered the problem of perfect cancellation of dynamic gravity effects acting on the link motion of robot manipulators having flexible transmissions. The cases of flexible transmissions having constant or nonlinear stiffness characteristics with single actuation at each joint, and of variable nonlinear stiffness with (double) antagonistic actuation or serial actuation have been analyzed. Based on the feedback equivalence principle, nonlinear control laws have been designed that allow the outputs of the gravity-loaded to behave as those of a reference model where gravity is absent. In the case of VSA-based manipulators, this includes the dynamic shaping of both the link motion and the evolution of the device stiffness. Dynamic gravity cancellation involves in general the on-line computation of inertial terms, but the presented control laws are still much simpler than those needed for feedback linearization. The control laws solving the problem have been obtained either in closed algebraic form or by using simple numerical techniques. In particular, a parallel simulation of the gravity-free system to be matched is never required.

The presented results can be used for different control purposes. For set-point regulation tasks, a PD-type state feedback law has been designed on top of the gravity cancellation law in the case of robots with elastic joints. Global asymptotic stability has been shown using Lyapunov techniques, without the need of a strictly positive lower bound neither on the proportional gain nor on the joint stiffness. In a similar way, we foresee that enhanced regulation controllers could be obtained with relative ease also for VSA-based manipulators, where the link position as well as the device stiffness need to be asymptotically stabilized to a desired constant value.

The proposed dynamic gravity cancellation is also useful in safe physical human-robot interaction. In general, unexpected collisions may occur at any time during motion and the compliant robot should react as soon as the impact is detected (e.g., with a sensorless residual-based method as in De Luca et al. [2006]). Through the permanent cancellation of the gravitational loads on the robot links, a physical torque-based reaction strategy can be designed so that the controlled robot rapidly flees away from the danger area in a gravity-unbiased dynamic fashion. This subject is currently under investigation.

8 Collision Detection and Reaction

A FUNDAMENTAL task for the robot controller is the handling of collisions, which include their fast and reliable detection and the switching to a safe reaction strategy once a collision has been detected. Human-robot collisions may happen in general at any location along the robot structure. While external vision systems or proximity sensing and additional force/torque sensors are indeed helpful for the anticipation or avoidance of collisions, a simpler and more cost-effective detection approach should rely only on the available proprioceptive sensors of the robot (encoders) and on the use of its nominal dynamic model. For rigid robots, such collision detectors have been designed, e.g., in [Morinaga and Kosuge, 2003, De Luca and Mattone, 2005]. In particular, the momentum-based approach proposed in [De Luca and Mattone, 2005] regards the collision as a system fault [De Luca and Mattone, 2003] and generates a residual vector that can be used both for detection and for the successive reaction. Moreover, this detection scheme can be easily extended to the case of robots with joint elasticity, provided that joint torque sensors are available [De Luca et al., 2006]. No such results are available for detecting collisions in the case of variable stiffness actuation.

Upon recognition of a collision, the simplest reaction strategy is to stop the robot [Suita et al., 1995, Yamada et al., 1997], which is safe but leaves the human user in an unpleasant state of danger, next to the robot arm. Canceling gravity through control [Heinzmann and Zelinsky, 2003] allows to let the robot float in space, reacting in response to the impact forces in an unbiased way. More active strategies, where the residual vector is used to define a direction of safe reflex motion of the robot, have been proposed and successfully experimented in [De Luca et al., 2006, Haddadin et al., 2008], both in the case of rigid and of elastic joints. The definition of effective strategies of reaction to collisions for manipulators with variable stiffness actuation is still an open research issue.

In this chapter a residual-based collision detector for SAFT (Sect. 8.2), antagonistic VSA (Sect. 8.3) and serial VSA (Sect. 8.4) will be proposed. In Section 8.5 a reaction strategy will be presented, and simulation using the VSA-II will be shown in Sect. 8.6.

8.1 Introduction

Consider now the possible occurrence of a link collision with a human or an obstacle. In presented models (3.2–3.3) (SAFT), (3.7–3.8) (antagonistic VSA) and (3.13) (serial VSA) , it will be $\tau_{ext}(t) \not\equiv 0$ for $t \geq t_K$, where t_K is the instant of first impact.

We would like to detect collisions without the need of additional sensors beyond the encoders available at the joints, possibly allowing the numerical differentiation of position measurements in order to obtain velocities. As mentioned in the introduction, the momentum-based method obtains such a result in rigid robots [De Luca and Mattone, 2005] and in robots with elastic joints of constant stiffness [De Luca et al., 2006]. In the latter case, with the availability of a joint torque sensor one can directly extend the result from the rigid situation.

8.2 SAFT

Since the link dynamics of compliant joints (3.2), (3.7) or the first equation of (3.13) are formally equivalent to the link dynamics of a robot with elastic joints, a first solution would be to design the so-called *residual* allowing to detect collision based only on this equation and on the properties of the link momentum $p = M\dot{q}$. However, this would need sensors for measuring the nonlinear transmission torques $\tau_{e,i}$. A more viable but equivalent solution is proposed next. Denote the *sum* of the components of the momentum vector of the robot system by

$$p_{\text{sum}} = B\dot{\theta} + M\dot{q}, \tag{8.1}$$

and define the following residual:

$$r = K_I \left(p_{\text{sum}} - \int_0^t (r + \tau + D_\theta - D_q - g(q))\, ds \right), \tag{8.2}$$

where K_I is a free design parameter. Using the SAFT model (3.2–3.3), and $r(0) = 0$ for a system initially at rest, it is easy to check that the residual r satisfies

$$\dot{r} = K_I \left(\tau_{ext} - r \right), \tag{8.3}$$

resulting in a fist-order, stable filter of the unknown collision torque τ_{ext}. For a large K_I, the residual r follows closely the time behavior of τ_{ext}, and in particular returns to zero when the contact is lost. Indeed, to cope with sensor noise and/or model uncertainties that would otherwise generate false alarms, a compatible value of K_I should be used in conjunction with some small positive threshold r_{coll}: collision will be actually detected only at a time instant $t_D > t_K$ when $|r| > r_{\text{coll}}$. Note finally that the computation of the residual (8.2) is completely independent from the (possibly time-varying) stiffness of the device and from the torques due to deflection of the transmissions. This is an appealing result from an implementation point of view. Moreover, the collision detector works in the same way no matter how the control torque τ is generated (which is good, e.g., when switching control laws from free motion to collision reaction).

8.3 Antagonistic VSA

The residual for the antagonistic VSA can be extended from the SAFT case (8.2) by using the *sum* of the components of the momentum vector of the robot system

$$p_{\text{sum}} = B(\dot{\theta}_1 + \dot{\theta}_2) + M\dot{q}, \tag{8.4}$$

and define similarly to the SEA case the following residual:

$$r = K_I \left(p_{\text{sum}} - \int_0^t (r + \tau_1 + \tau_2 - \tau_D - g(q))\, ds \right), \tag{8.5}$$

where the dissipative terms in the model have been collected in $\tau_D = D_q\dot{q} + D(\dot{\theta}_1 + \dot{\theta}_2)$, and $r(0) = 0$ for a system initially at rest.

Using (3.7–3.8), it is easy to check that the residual r satisfies

$$\dot{r} = K_I \left(\tau_{ext} - r \right), \tag{8.6}$$

resulting a stable first-order filter of the external force τ_{ext} with the same characteristic of the SAFT residual.

8.4 Serial VSA

For the sake of completeness we present the residual collision detector also for the serial VSA, but it is immediate to note from the serial VSA model (3.13) that, since the secondary motor influence only the flexibility torque $\tau_e(\theta_c, \phi)$ by varying the set point θ_c, and the residual (8.2) is completely independent from $\tau_e(\theta_c, \phi)$, the same residual based collision detector used for the SAFT actuators can be used for the serial VSA as well.

8.5 Reaction Strategy

We propose a reaction strategy to be activated upon recognition of a collision. In the present 1-dof case, the situation is trivial because the link can only reverse motion and go in the opposite direction of the detected contact. Anyway, we provide here a general solution that can be used also for the multi-dof case. A first approach could be to switch the control law and apply maximum torque with the two motors, so as to move away from the impact area as fast as possible. However, control on the device stiffness would be given up in this way and this may have a negative effect on the interaction forces during the short time between the detection instant t_D and when the link starts executing the commanded reaction. Therefore, it seems more convenient to keep the same feedback linearizing controller (6.9) and to change only (part of) the linear design of $\boldsymbol{v} = (v_1, v_2)$ in eq. (6.15). In particular, we set

$$v_1 = -k_{q,3}\, q^{[3]} - k_{q,2}\, \ddot{q} - k_{q,1}\, \dot{q} + k_R\, r, \tag{8.7}$$

where $k_R > 0$, and the other coefficients are chosen such that $s^3 + k_{q,3}s^2 + k_{q,2}s + k_{q,1}$ is a Hurwitz polynomial. The rationale of this law is to have the link be pushed away by an amplified collision torque ($k_R r \simeq k_R \tau_{ext}$), while

stabilizing motion to $\dot{q}_d = 0$. After losing contact, r will rapidly go to zero and the link will be slowed down until reaching a rest position away from the collision area. The rest position will depend on the amplitude of the impact force and on the gains chosen in (8.7). Moreover, the same structure (6.15) will be kept for v_2, but dropping the reference value σ_d to the lowest feasible level of stiffness. This will guarantee the softest compliant behavior of the device in the post-impact phase. Thanks to the decoupling obtained by the control law, in nominal conditions there will be no cross-effects due to the switching of v_1 and v_2. However, when external contact is present[1] and/or due to uncertainty in the dynamic parameters, a nonlinear and coupled behavior still results, see, e.g., [Ozawa and Kobayashi, 2002], which can be evaluated by simulation.

8.6 Simulation results

Next, the same rest to rest simulation with the VSA-II presented in Sect. 6.6, but with the presence of a fixed compliant obstacle is considered. The obstacle is located approximately midway along the motion trajectory, and the collision occurs around $t_K = 2.6$ s.

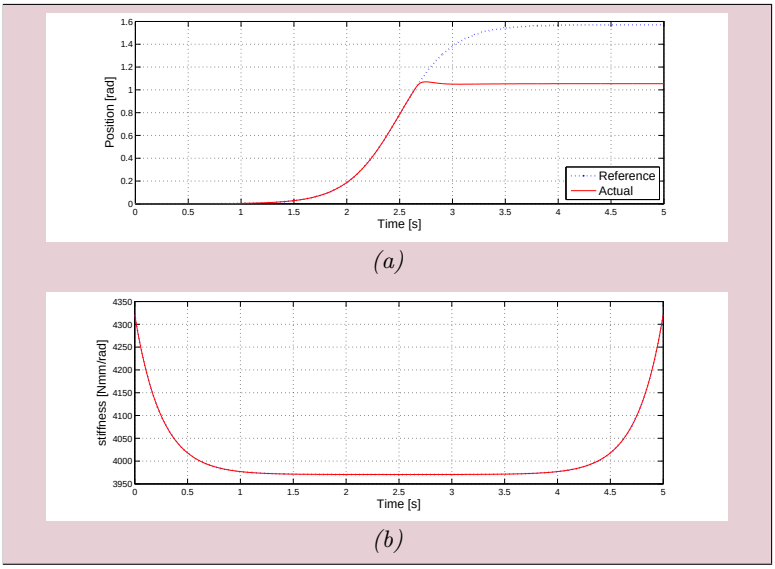

Figure 8.1: *VSS-II collision without reaction: (a) link position q; (b) stiffness σ;*

Without activating the reaction strategy, the link would hit the obstacle, bounce several times against it, and then finally stops in contact after the reference motion trajectory ends (Fig. 8.1(a)). The control torques would exceed the motor capabilities while the deflection torques would undergo fast oscillations, with potential damage of the device. Nonetheless, the stiffness σ would be (nominally) unaffected from this behavior, as a result of the decoupled dynamics enforced by the control law (Fig. 8.1(b)). Figure 8.2 shows the unmeasured

[1] In fact, the unknown collision torque has been neglected in the control design: a non-zero τ_{ext} will affect in $\ddot{q}$ and higher position derivatives as well as $\ddot{\sigma}$ in eqs. (6.5–6.6).

external torque τ_{ext} compared with the residual r. It is possible to note that after the collision the obstacle remain clamped, this behavior can be dangerous and a reaction is needed. Note that the residual is an estimation of the external torque.

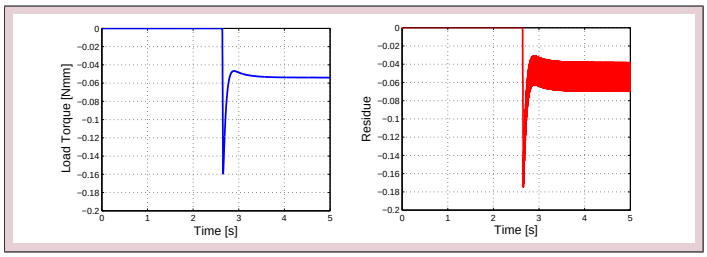

Figure 8.2: *VSS-II collision without reaction: unmeasured external torque τ_{ext} (left) and residual r (right)*

The results obtained with a detection gain $K_I = 10^3$, a reaction gain $k_R = 2 \cdot 10^5$, and the other gains in eq. (8.7) chosen so as to have three real poles placed in $\{-110, -87, -23\}$, are shown in Figs. 8.3–8.5. After the impact, the

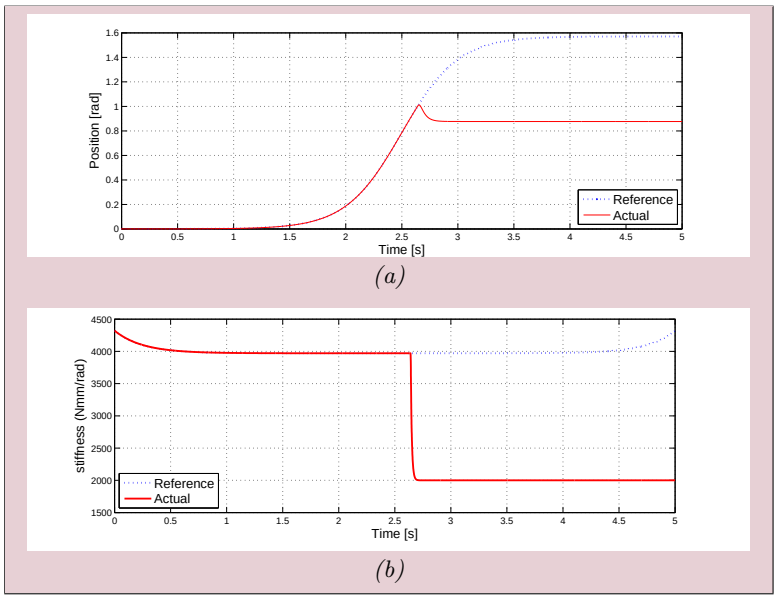

Figure 8.3: *VSS-II collision and reaction: (a) link position q; (b) stiffness σ;*

reaction strategy moves the link back by about 8° (this displacement would be larger for smaller gains), while the desired stiffness is controlled so as to drop down to 2000 N·mm/rad (Fig. 8.3). The residual in Fig. 8.4, computed from eq. (8.6), closely follows the (unmeasured) joint torque resulting from link collision. The control switching is response to the detected collision is evident on the applied torques, which are driven in fact during the reaction phase by the value of r through eq. (8.7). Note that the steady-state torques in Fig. 8.5 are those needed to hold the link under gravity in the final rest position: these gravity torques are automatically provided by the feedback linearizing law.

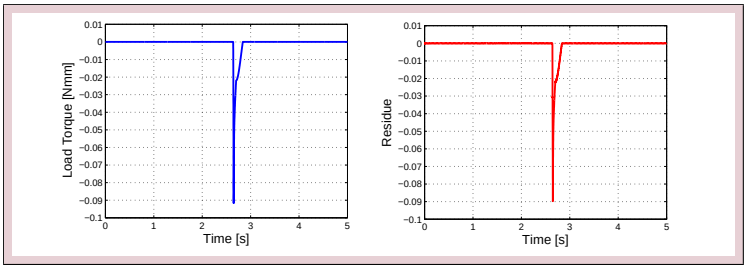

Figure 8.4: *Evolution of the collision torque τ_K (left) and of the residual r (right): the robot reaction reduces to zero both quantities*

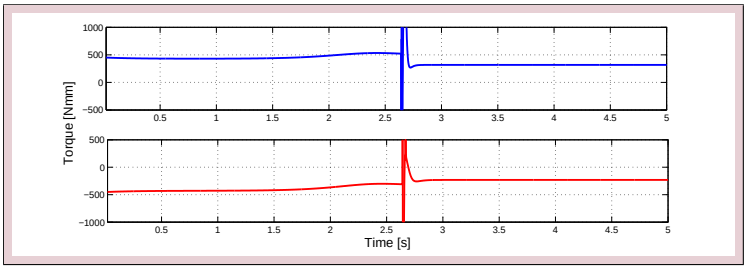

Figure 8.5: *Control torques τ_1 and τ_2 in case of collision and reaction*

8.7 Extension to the multi-dof case

The theoretical developments presented for a 1-dof arm actuated either by a SEA, an antagonistic VSA or a serial VSA can be easily extended to the case of N-dof manipulators having each rotational joint. In this section, a couple of representative results are sketched for the antagonistic VSA.

Taking into consideration the multi d.o.f. model for antagonistic VSAs expressed by eqs. (3.12), collision detection can be achieved using the sum of the generalized momentum vectors pertaining to the motors and to the robot links,

$$\boldsymbol{p}_{\text{sum}} = \boldsymbol{B}(\dot{\boldsymbol{\theta}}_1 + \dot{\boldsymbol{\theta}}_2) + \boldsymbol{M}(\boldsymbol{q})\dot{\boldsymbol{q}}, \tag{8.8}$$

and defining the residual vector $\boldsymbol{r}$ as

$$\begin{aligned} \boldsymbol{r} \;=\; \boldsymbol{K}_I \Big(\boldsymbol{p}_{\text{sum}} - \int_0^t \Big(& \boldsymbol{r} + \boldsymbol{C}^T(\boldsymbol{q}, \dot{\boldsymbol{q}})\dot{\boldsymbol{q}} - \boldsymbol{g}(\boldsymbol{q}) \\ & + \boldsymbol{\tau}_1 + \boldsymbol{\tau}_2 - \boldsymbol{D}(\dot{\boldsymbol{\theta}}_1 + \dot{\boldsymbol{\theta}}_2) \Big)\, ds \Big), \end{aligned} \tag{8.9}$$

with $\boldsymbol{K}_I > \boldsymbol{O}$. Using the dynamic properties of the Lagrangian dynamics [De Luca et al., 2006], it can be shown that

$$\dot{\boldsymbol{r}} = \boldsymbol{K}_I \left(\boldsymbol{\tau}_K - \boldsymbol{r} \right). \tag{8.10}$$

As in the scalar case, the residual (8.9) does not require any knowledge about the flexibility (stiffness and deflection torques) of the joints.

This results can be obtained straightforwardly for the SEA and the serial VSA using the same approach.

8.8 Conclusion

A momentum-based observer has been designed so as to promptly detect unexpected collisions without extra joint/transmission torque sensors and independently from the current stiffness value of the device. Based on the residual signal, and taking advantage of the decoupling control in operation, a collision reaction law has been proposed that drives the arm away from the contact area and safely stops it, while dropping suddenly the stiffness to the lowest feasible level. This is useful for minimizing the effects of interaction forces in the early post-impact phase. Simulation results obtained with the VSA-II, using the feedback linearization controler described in Chapter 6 have been proposed.

9 Stiffness Estimation

All the above control schemes require an accurate knowledge of the nonlinear stiffness of the compliant joint. However, there are no sensors available for a direct measurement of the varying stiffness on line (i.e., during robot operation). The device stiffness is usually computed from position and/or joint torque sensor data, based on a nominal mathematical model. This method is especially critical for VSA-based manipulators since:

i) the stiffness characteristic curve is intrinsically nonlinear;

ii) the mathematical model can be a complex function of the deformation of the transmissions, subject to kinematic and dynamic uncertainties;

iii) the stiffness is a variable parameter that should be set explicitly under control.

The last issue implies an intrinsic weakness for any feedback control scheme, with or without a stiffness estimation procedure. As a matter of fact, the absence of a direct measurement of the controlled (stiffness) output, a control law can at best assign the desired reference behavior to the nominal output (or to the estimated output), but not to the actual one (the ground truth is missing). Therefore, the robustness of an estimation method with respect to perturbations is particularly needed in such cases.

In this chapter our stiffness estimator is described. SAFT, antagonistic VSA and serial VSA are respectively considered in Sect. 9.2, Sect. 9.3 and Sect. 9.4. Section 9.5 deals with the poor excitation problem, while Section 9.7 shows how to choose the estimator parameter and the robustness of the estimation is evaluated. Simulation results using the VSA-II and the AwAS are proposed in Sect. 9.6, and Experiment with the AwAS are shown is Sect. 9.8. Finally, in Sect. 9.9, the presented stiffness estimator is used in simulation to control a VSA-II using the feedback linearization low described in Chapter 6.

9.1 Introduction

While many papers have dealt with stiffness estimation in contact situations between the end-effector of a rigid robot and the environment or human Diolaiti et al. [2005], Verscheure et al. [2009], Coutinho and Cortesao [2010], Ludvig and Kearney [2009], less work appears to have been devoted the estimation of variable, nonlinear stiffness of a single or multiple actuated flexible joints. With the recent diffusion of several new devices, there is now a growing interest in the development of on-line stiffness estimation methods for VSA. In Serio et al. [2011], a stiffness estimator has been introduced based on the knowledge of the applied external torque, which is measured by a sensor. An extended Kalman filter is used to estimate simultaneously the transmission stiffness and the link inertia and damping. However, the method uses the time derivative of the measured flexibility torque and an interaction loop is present between the two used observers, leading respectively to high noise sensitivity and poor excitation conditions. These drawbacks have been alleviated in Grioli and Bicchi [2010, 2011], but the presented stiffness estimators are still based on the knowledge of the flexibility torque and rely on the use of a joint torque sensor. In Flacco and De Luca [2011a], we have developed a stiffness estimator for a single flexible transmission or for double flexible transmissions in antagonist arrangement that does not use joint torque sensing. From the reconstructed flexibility torque of the transmission, stiffness was estimated either by using a black-box regressor or by a least squares method applied in batch mode and based on a model where the unknown system coefficients appear in a nonlinear way. The first variant works on line and requires minimal a priori information. However, it can be used only for a point-wise stiffness estimation and does not allow differentiation of an identified stiffness function which is needed in advanced control laws for VSA devices such as De Luca et al. [2009]. The second variant produces better results, but was not intended for on-line implementation.

In this chapter, we present a unifying and updated review of the on-line stiffness estimation method proposed in our more recent works Flacco and De Luca [2011b], Flacco et al. [2011], which improved the original ideas of Flacco and De Luca [2011a]. The method consists of two stages. In a first stage, we design a residual-based estimator of the flexibility torque of the nonlinear transmission. This allows to avoid the need of joint torque sensing. In a second stage, we use a Recursive Least Squares (RLS) estimator based on a generic, but linearly parameterized model of the transmission stiffness. This also allows to generate a functional estimation of the stiffness, which can be used for further elaborations in a closed-loop system based, e.g., on feedback linearization control. Starting from this basic result, we are able to address with minor modifications but in a straightforward way the problem of estimating the stiffness of VSA devices both in antagonistic and in serial configurations. In fact, the two-stage estimation is fully designed *on the motor side* of a robot transmission, leading to three relevant features:

i) only motor and link position measurements and motor dynamic parameters are used;

ii) the approach can be replicated as needed for each flexible transmission that is affecting the device stiffness of a VSA (antagonistic or serial);

iii) in multi-dof VSA-driven robot arms, the method can be similarly implemented in a fully decentralized way.

In order to achieve a more robust behavior, the first stage is refined by using a modified version of a discrete-time kinematic Kalman filter (see, e.g., Jeon and Tomizuka [2007]), which avoids the need of numerical differentiation of motor position measurements for computing the residual and is able to handle encoder quantization errors, one of the critical problems in implementations. Moreover, the second stage relies on a enhanced RLS algorithm, based on Bittanti et al. [1990], that improves robustness and ensures convergence or at least stability of the stiffness estimation also in conditions of poor excitation, as when the flexible transmissions undergo relatively small deformations.

With reference to the models (3.2-3.3), (3.7–3.8), and (3.13), respectively for a single actuated flexible transmission, for an antagonistic and for a serial VSA, our goal is to estimate on line the varying device stiffness for each case, without the use of additional (e.g., joint torque) sensors beyond the encoders placed at the link and motor(s) sides, nor of time derivatives of these position measurements. From the structure of $\sigma_t(\boldsymbol{\phi})$ in (3.10) and of the motor equations in (3.8), as well as from the dependence of $\sigma(\theta_c, \phi)$ in (3.14) and the principal motor equation in (3.13), it is immediate to see that a unified approach can be followed by addressing first the estimation of a single transmission stiffness on the motor side, and then extending the method to the other cases. The same argument applies also for the multi-dof robot case, provided that we can take advantage of the decentralized structure of the motor equations.

9.2 SAFT

According to the final considerations of the previous section, we will develop the method on a single flexible transmission with a single motor. The estimation is performed in two stages, first by estimating the flexibility torque $\tau_e(\phi)$ using a residual-based technique, then by using this result to estimate on line the stiffness $\sigma(\phi)$ with a Recursive Least Squares algorithm based on a parameterized model.

Residual for flexibility torque estimation

With reference to eqs. (3.2–3.3), a *residual* signal can be generated that provides a filtered version of the unmeasured flexibilty torque $\tau_e(\phi)$t. Denoting as $p = B\dot{\theta}$ the generalized momentum of the motor, the residual is defined as

$$r_e = K_I \left(p + D_\theta \theta - \int_0^t (\tau + r_e)\, ds \right), \tag{9.1}$$

where $K_I > 0$ is a free design parameter. From eq. (3.3), it is easy to check that the residual r_e satisfies

$$\dot{r}_e = K_I \left(\tau_e(\phi) - r_e \right), \tag{9.2}$$

resulting in a first-order, stable filter of the unknown flexibility torque. A discrete-time implementation of the residual (9.1) at $t = kT$ is

$$\begin{aligned} I_\tau(k) &= I_\tau(k-1) + \frac{\tau(k)+\tau(k-1)}{2}\,T \\ r(k) &= K_I\left(B\dot{\theta}(k) + D_\theta\theta(k) - I_\tau(k)\right) \\ r_e(k) &= \frac{2-TK_I}{2+TK_I}\,r_e(k-1) + \frac{2\,(r(k)-r(k-1))}{2+TK_I}, \end{aligned} \tag{9.3}$$

where T is the sampling time.

It should be noted that the flexibility torque is estimated using only the motor parameters B and D_θ, which can be obtained by the motor data sheet. The motor torque τ is obtained from the known commanded voltage/current, using the motor electrical model and its data sheet. The motor position θ is measured by an encoder and its velocity $\dot{\theta}$ (needed in p) is obtained numerically.

However, the discretization and the presence of encoder quantization may introduce excessive noise when computing the motor angular velocity by numerical differentiation. A possible solution for avoiding the use of motor velocity $\dot{\theta}$ is to define a second-order residual as

$$r_{e_2} = K_1\left[B\theta + \int_0^t \left(D_\theta\theta - \int_0^t (\tau + r_{e_2})\,ds\right) dl\right] - K_2\int_0^t r_{e_2} ds, \tag{9.4}$$

where $K_1 > 0$ and $K_2 > 0$ are two free design parameters. It is straightforward to verify that the residual r_{e_2} satisfies

$$\ddot{r}_{e_2} = K_1\left(\tau_e(\phi) - r_{e_2}\right) - K_2\dot{r}_{e_2}, \tag{9.5}$$

resulting in a second-order, stable filter of the unknown flexibility torque weighted. The estimation convergence is obtained thanks to the presence of the damping factor $K_2\dot{r}_{e_2}$. While appealing, the use of a second-order residual presents two main disadvantages: the associated digital filter has a delay of two steps instead of one, and the second design parameter K_2 is not so easy to tune.

An alternative solution is to use a Modified Kinematic Kalman Filter (MKKF). Let x be an angular position and $\dot{x}$ the associated angular velocity. In order to estimate $\boldsymbol{\xi}(k) = (x(k)\,\dot{x}(k))^T$ with a kinematic Kalman filter (KKF), the following system is considered

$$\boldsymbol{\xi}(k) = \begin{pmatrix} 1 & T \\ 0 & 1 \end{pmatrix}\boldsymbol{\xi}(k-1) + \boldsymbol{\mu} \tag{9.6}$$

$$z(k) = \begin{pmatrix} 1 & 0 \end{pmatrix}\boldsymbol{\xi}(k) + \nu, \tag{9.7}$$

where $z(k)$ is the noisy measure (the encoder angle in our case) and the zero mean Gaussian noises $\boldsymbol{\mu}$ and ν have, respectively, covariance matrix $\boldsymbol{Q}$ and variance R. In the state equation (9.6), acceleration is not considered and $\boldsymbol{\mu}$ represents the noise due also to this absence. Setting $\boldsymbol{\Gamma} = \left(T^2/2\ T\right)^T$, the covariance matrix of $\boldsymbol{\mu}$ is $\boldsymbol{Q} = V_a\,\boldsymbol{\Gamma}\boldsymbol{\Gamma}^T$, where V_a is the variance associated to the state. While the variance R of the measures is usually set to a constant value, in the proposed modified KKF it is chosen as a function of the estimated

velocity, since the noise due to encoder quantization is significant at low speed and negligible at high speed. In particular, we used

$$R(k) = \frac{V_{\max} - V_{\min}}{1 + e^{(|\dot{x}(k)|w_s - 1)\alpha}} + V_{\min}, \tag{9.8}$$

where $V_{\max}$ and $V_{\min}$ are the maximum and minimum variances considered, $w_s = (2\pi/\Delta)/T$, being $2\pi/\Delta$ the encoder resolution, and α is a shaping factor (see Sect. 9.6 for the resulting effects). In the rest of the paper, whenever we refer to an angular position and/or velocity, we will be considering their evaluation obtained with the MKKF.

Stiffness estimation based on RLS

In this second stage, the flexibility torque $\tau_e(\phi)$ is approximated by a nonlinear parametric model function $f(\phi, \boldsymbol{\alpha})$, typically chosen as linear in the unknown n-dimensional parameter vector $\boldsymbol{\alpha}$, using a Recursive Least Squares (RLS) algorithm. From computed or measured data, we set the relationship

$$\widehat{\tau}_e(\phi(k)) = f(\phi(k), \boldsymbol{\alpha}) = \boldsymbol{F}^T(k)\boldsymbol{\alpha}, \tag{9.9}$$

where $\phi(k)$ is the deformation measured at time $t = kT$ and $\widehat{\tau}_e(\phi(k))$ may be either the *measured* flexibility torque, if a joint torque sensor is available, or otherwise its *estimate* given by the residual $r_e(k)$ in eq. (9.3). The n-dimensional vector $\boldsymbol{F}$, i.e., the Jacobian of $f(\phi, \boldsymbol{\alpha})$ w.r.t. the parameter $\boldsymbol{\alpha}$, is usually given by polynomial terms in ϕ.

The on-line minimization of the sum of the squares of the estimation errors up to time $t = kT$

$$E(k) = \sum_{i=1}^{k} \left(\widehat{\tau}_e(\phi(i)) - \boldsymbol{F}^T(i)\boldsymbol{\alpha}\right)^2, \tag{9.10}$$

provides the current estimate $\widehat{\boldsymbol{\alpha}}(k)$ by the RLS algorithm as follows:

$$\begin{aligned}
\epsilon(k) &= \widehat{\tau}_e(\phi(k)) - \boldsymbol{F}^T(k)\widehat{\boldsymbol{\alpha}}(k-1) \\
\rho(k) &= \boldsymbol{F}^T(k)\boldsymbol{P}(k-1)\boldsymbol{F}(k) \\
\boldsymbol{K}(k) &= \frac{\boldsymbol{P}(k-1)\boldsymbol{F}(k)}{1 + \rho(k)} \\
\widehat{\boldsymbol{\alpha}}(k) &= \widehat{\boldsymbol{\alpha}}(k-1) + K(k)\epsilon(k) \\
\boldsymbol{P}(k) &= \boldsymbol{P}(k-1) - \boldsymbol{K}(k)\boldsymbol{F}^T(k)\boldsymbol{P}(k-1).
\end{aligned} \tag{9.11}$$

The algorithm (9.11), initialized with an a priori estimate $\widehat{\boldsymbol{\alpha}}(0)$ of the parameters and a covariance matrix $\boldsymbol{P}(0) > 0$, updates the previous estimation based on the current error $\epsilon(k)$ between the residual/measure and the predicted transmission flexibility torque. The larger the covariance, the larger will be the update of the parameters. Therefore, the covariance matrix $\boldsymbol{P}$ is initialized with large values in case of poor a priori knowledge about the parameters. $\boldsymbol{P}$ typically decreases at each step and there will be no significant parameter updates when the updating factor becomes too small. The degree of the polynomial $f(\phi(k), \boldsymbol{\alpha})$ should be adequate for capturing the nonlinearity of the transmission flexibility torque. Otherwise, the RLS algorithm will not track efficiently the data or, even if it converges ($\boldsymbol{P}$ is small), a non-negligible residual estimation error would result.

Finally, the stiffness estimation is obtained directly from $f(\phi(k), \widehat{\boldsymbol{\alpha}}(k))$ as

$$\widehat{\sigma}(\phi(k)) = \left(\frac{\partial \boldsymbol{F}(k)}{\partial \phi(k)}\right)^T \widehat{\boldsymbol{\alpha}}(k). \tag{9.12}$$

In particular, we consider the case when the relationship (9.9) is *linear* in the parameters $\boldsymbol{\alpha}$, i.e.,

$$f(\phi, \boldsymbol{\alpha}) = \boldsymbol{F}^T(\phi)\boldsymbol{\alpha} = \sum_{h=0}^{n-1} \alpha_h f_h(\phi). \tag{9.13}$$

For a single or a double antagonistic flexible transmission, taking into account the physical assumption (3.1) on the flexibility torque, we choose as basis functions in (9.13) only *odd* powers of ϕ up to the order $2h-1$,

$$f_h(\phi) = \phi^{2h+1}, \quad h = 0, \ldots, n-1, \tag{9.14}$$

and eq. (9.12) becomes

$$\widehat{\sigma}(\phi) = \sum_{h=0}^{n-1} (2h+1)\, \alpha_h\, \phi^{2h}. \tag{9.15}$$

In the same way, the derivative of the stiffness w.r.t. the transmission deformation is obtained as

$$\frac{\partial \widehat{\sigma}(\phi)}{\partial \phi} = \sum_{h=1}^{n-1} (4h^2 + 2h)\, \alpha_h\, \phi^{2h-1}. \tag{9.16}$$

This and a similar closed-form expression for the second derivative are very useful for the feedback linearization Chapter 6 and for the gravity cancellation Chapter 7.

9.3 Antagonistic VSA

Being the two transmissions which compose the antagonistic VSA decoupled eqs. (3.8), and considering that the total stiffness is the sum of the stiffness of the two transmissions eq. (3.10), the stiffness of each transmission can be estimated separately and independently, and then the total stiffness can be obtained from the relation (3.10).

9.4 Serial VSA

With reference to Fig. 9.1, consider now an adjustable stiffness actuator modeled by eqs. (3.13). The estimation of the flexibility torque $\tau_e(\theta_c, \phi)$ is obtained using eq. (9.1) as before, since the principal motor side dynamics is identical and the dependence of τ_e also on θ_c plays no role in the definition of the residual. For stiffness estimation, the RLS algorithm (9.11) is used but, departing from the antagonistic VSA case (9.13), the linear parameterization of the flexibility

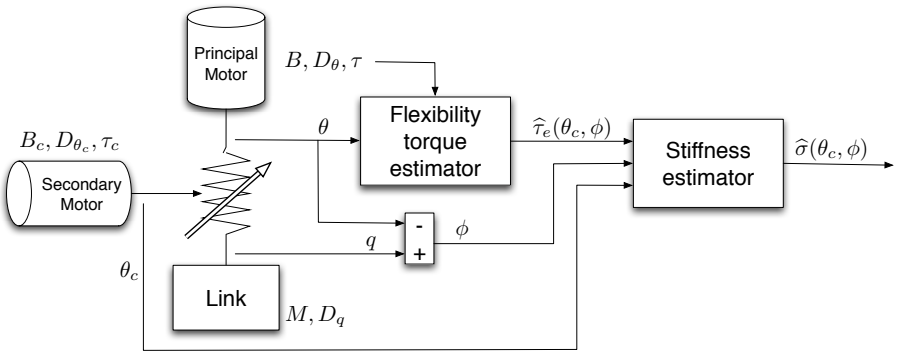

Figure 9.1: *Two-stage stiffness estimator for an actuator with adjustable stiffness in serial configuration*

torque should be introduced more carefully in order to take into account the dependence from the position of the secondary motor.

We assume that the presence of the secondary motor does not affect assumption (3.1), or

$$\tau_e(\theta_c, 0) = 0, \quad \tau_e(\theta_c, -\phi) = -\tau_e(\theta_c, \phi), \quad \forall \theta_c, \phi. \tag{9.17}$$

In fact, the set-point variable θ_c of the secondary motor does not change the symmetric nature of the transmission, but will affect the shape of the flexibility torque in a separable way as

$$\tau_e(\theta_c, \phi) = \ell(\theta_c) h(\phi), \tag{9.18}$$

i.e., with a *positive* functional factor that depends on θ_c multiplying the flexibility term due to the deformation ϕ. A behavior like the one in (9.18) is highly desirable in the design of VSA systems and is observed in all adjustable stiffness devices we are aware of. As a consequence, in the parametric approximation of τ_e, we will consider the following two polynomials for $h(\phi)$ and $\ell(\theta_c)$:

$$h(\phi, \boldsymbol{\alpha}) = \sum_{i=0}^{n-1} \alpha_i \, \phi^{2i+1}, \tag{9.19}$$

$$\ell(\theta_c, \boldsymbol{\beta}) = \sum_{j=0}^{m-1} \beta_j \, \theta_c^j. \tag{9.20}$$

For the sake of simplicity we do not force positivity of the factor $\ell(\theta_c)$, which would lead to the need of adding constraints in the RLS algorithm without effective improvement of the estimate. In the estimation process, we do not need a separate (and non trivial) estimation of the $n + m$ unknown parameters in vectors $\boldsymbol{\alpha}$ and $\boldsymbol{\beta}$, but we linearly re-parameterize the problem in terms of the $n \cdot m$ scalar parameters

$$\eta_{i,j} = \alpha_i \, \beta_j. \tag{9.21}$$

Based on eq. (9.18), the function f fitting τ_e will thus be

$$f(\theta_c, \phi, \boldsymbol{\eta}) = \sum_{i=0}^{n-1} \sum_{j=0}^{m-1} \eta_{i,j} \, \theta_c^j \, \phi^{2i+1} = \boldsymbol{F}^T(\theta_c, \phi) \, \boldsymbol{\eta}. \tag{9.22}$$

The Jacobian of $f(\theta_c, \phi, \boldsymbol{\eta})$ w.r.t. the new parameter vector $\boldsymbol{\eta}$ is given by

$$\boldsymbol{F}^T(\theta_c, \phi) = \begin{pmatrix} \phi & \phi^3 & \dots & \phi^{2n-1} \\ \theta_c\phi & \theta_c\phi^3 & \dots & \theta_c\phi^{2n-1} \\ \dots & \dots & \dots & \dots \\ \theta_c^{m-1}\phi & \theta_c^{m-1}\phi^3 & \dots & \theta_c^{m-1}\phi^{2n-1} \end{pmatrix}. \tag{9.23}$$

Considering a discrete-time implementation, the estimation of the unknown parameter $\widehat{\boldsymbol{\eta}}$ is obtained using (9.11), where $\widehat{\boldsymbol{\alpha}}(k)$ is obviously replaced by $\widehat{\boldsymbol{\eta}}(k)$. Therefore, the stiffness estimate at time $t = kT$ is given again by the relation (9.12) suitably modified, i.e.,

$$\begin{aligned} \widehat{\sigma}(\theta_c(k), \phi(k)) &= \frac{\partial f(\theta_c(k), \phi(k))}{\partial \phi(k)} = \left(\frac{\partial \boldsymbol{F}(k)}{\partial \phi(k)}\right)^T \widehat{\boldsymbol{\eta}}(k) \\ &= \sum_{i=0}^{n-1} \sum_{j=0}^{m-1} (2i+1)\, \widehat{\eta}_{i,j}(k)\, \theta_c^j(k)\, \phi^{2i}(k). \end{aligned} \tag{9.24}$$

9.5 Handling poor excitation conditions

For a robust parameter estimation, it is important that the input signal changes sufficiently so that the collected data contain enough information about the characteristics of the function to be estimated. This is related to the concept of *persistent excitation* of signals. The RLS algorithm applied to antagonistic VSAs is not very sensitive to poor excitation, because the deformation of the two transmissions are significant in order to simultaneously control both link motion and stiffness. Instead in serial VSA the deformation can be minimal. Therefore, in this case the persistent excitation requirement is a very critical issue for stiffness estimation. Since the RLS estimation may become unstable in the presence of poor excitation, we propose a modified RLS based on the results of Bittanti et al. [1990], which are briefly recalled.

Assume that measured data y are generated at $t = kT$ as

$$y(k) = \boldsymbol{F}^T(k)\overline{\boldsymbol{\alpha}}, \tag{9.25}$$

where $\overline{\boldsymbol{\alpha}}$ is the true but unknown parameter vector. In the parameter estimation error $\widetilde{\boldsymbol{\alpha}} = \widehat{\boldsymbol{\alpha}} - \overline{\boldsymbol{\alpha}}$, it is possible to discriminate a component $\widetilde{\boldsymbol{\alpha}}_U$ that belongs to the so-called unexcitation subspace and a component $\widetilde{\boldsymbol{\alpha}}_E$ that belongs to its orthogonal complement $\Omega_E = \Omega_U^{\perp}$, the excitation subspace. Consider the following modification to the RLS algorithm (9.11) used for the estimate $\widehat{\boldsymbol{\alpha}}$

$$\begin{aligned} \widehat{\boldsymbol{\alpha}}(k) &= \widehat{\boldsymbol{\alpha}}(k-1) + a(k)\boldsymbol{K}(k)\epsilon(k) \\ \boldsymbol{P}(k) &= \boldsymbol{P}(k-1) - a(k)\boldsymbol{K}(k)\boldsymbol{F}^T(k)\boldsymbol{P}(k-1), \end{aligned} \tag{9.26}$$

where the scalar $a(k)$ is a time-varying function.

Under the data generation assumption (9.25), it has been proven in Bittanti et al. [1990] that, if there exists a scalar $c > 0$ such that

$$\frac{a(k)}{1 + \rho(k) - a(k)\rho(k)} \geq c, \qquad \forall k, \tag{9.27}$$

then, for every given $\widehat{\boldsymbol{\alpha}}(0)$ and $\boldsymbol{P}(0) > 0$:

1. $\|\widetilde{\boldsymbol{\alpha}}(k)\| \leq \lambda, \quad \forall k$, being λ a suitable constant;

2. $\lim_{k\to\infty} \widetilde{\boldsymbol{\alpha}}_E(k) = \mathbf{0}$.

Provided that $a(k)$ can be chosen so as to verify condition (9.27), we obtain thus practical convergence of the parameter estimation even in poor excitation cases. Given a constant $c > 0$, the *stability factor* $a(k)$ is then simply chosen as

$$a(k) = \frac{c + c\rho(k)}{1 + c\rho(k)}. \tag{9.28}$$

Summarizing, the enhanced RLS algorithm is obtained from (9.11), by replacing the last two equations therein with (9.26) and using (9.28).

9.6 Simulation results

To test the effectiveness of the estimator we performed extensive discrete-time simulations, both for the VSA-II and the AwAS (see Chapter 4). Actuators under realistic conditions are modeled, e.g., considering the encoder quantization, a noisy motor torque τ used in the residual computation (9.1) as well as a noisy sensed torque $\tau_e(\phi)$, which can be used in alternative to the residual as input $\widehat{\tau}_e(\phi)$ to the RLS algorithm (9.11). A tilda denotes the noisy signals, i.e.,

$$\widetilde{\tau} = \tau + \nu_\tau, \tag{9.29}$$
$$\widetilde{\tau}_e(\phi) = \tau_e(\phi) + \nu_{\tau_e}, \tag{9.30}$$

where ν_τ and ν_{τ_e} are zero mean gaussian noises.

To show the robustness of our algorithm, we performed the stiffness estimation in three modalities, using three different signals as input $\widehat{\tau}_e(\phi)$ of the RLS algorithm. In the MODEL modality, we used as input the flexibility torque obtained from eq. (4.8) with the nominal system data[1]. In the SENSOR modality, we used as input the flexibility torque measured by a noisy joint torque sensor, see eq. (9.30). Finally, in the RESIDUAL modality we fed the RLS algorithm with the residual that estimates the flexibility torque. In this last modality, the residual (9.1) has been evaluated using the principal motor position θ and velocity $\dot{\theta}$ obtained by processing the encoder data with the MKKF presented in Sect. 9.2, as well as the noisy motor torque (9.29). Summarizing, for the three modalities we have:

$$\begin{aligned} \widehat{\tau}_e(\phi) &= \tau_e(\phi) && \text{MODEL} \\ \widehat{\tau}_e(\phi) &= \widetilde{\tau}_e(\phi) && \text{SENSOR} \\ \widehat{\tau}_e(\phi) &= r_e && \text{RESIDUAL} \end{aligned} \tag{9.31}$$

To quantify the different stiffness estimation, we have considered two performance indices, namely the mean square error (MSE) and the mean square

[1] In simulations, this flexibility torque is indeed also the actual one.

relative error percentage (MSREP) over p samples,

$$\text{MSE} = \frac{\sum_{k=0}^{p}\left[\left(\sigma(k)-\widehat{\sigma}(k)\right)^2\right]}{p}, \tag{9.32}$$

$$\text{MSREP} = \frac{\sum_{k=0}^{p}\left[\left(\frac{\sigma(k)-\widehat{\sigma}(k)}{\sigma(k)}\right)^2\right]}{p}100. \tag{9.33}$$

Antagonistic VSA: VSA-II

The estimator has been tested in realistic simulations performed with Simulink, using the VSAII introduced in Sect. 7.5.

We have included in the simulations the presence of encoders with $\Delta = 4059$ pulses/turn for measuring q, θ_1 and θ_2. The two motor are controlled respectively with a torque $\tau_1 = 10\sin 0.1\pi$ and $\tau_2 = 10\sin 0.2\pi$, and the simulation were run with a sampling time $T = 1$ ms. The simulation starts from the initial configuration $q(0) = \theta_1(0) = \theta_2(0) = 0$ [rad] and with the system at rest. The chosen MKKF parameters in eq. (9.8) were $V_{\max} = 10^5$, $V_{\min} = 10^4$, and $\alpha = 6$, obtained by considering a nominal minimum and maximum velocity which rely on a minimum and maximum variance. The remaining estimation parameters were: $K_I = 300$, in eq. (9.1), which represent the filter bandwidth of the residual; $\boldsymbol{P}(0) = 10^6\boldsymbol{I}_{n\times n}$ in eq. (9.11); $n = 4$ in eqs. (9.14) ; and $c = 10^{-5}$ in eq. (9.28). No a-priori knowledge is supposed for the parameters of the polynomial function eqs. (9.14), i.e., $\boldsymbol{\alpha}(0) = \boldsymbol{0}$.

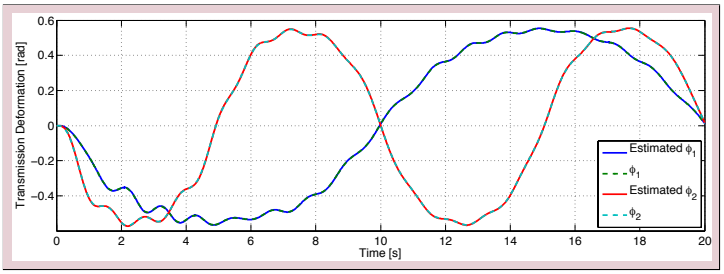

Figure 9.2: *Actual deformations ϕ_1 and ϕ_2 (dashed) of the two transmissions of the VSA-II and their very accurate estimations (solid, almost superposed) obtained using the MKKF on the measured position of the link and motors*

Figure 9.2 shows the time behavior of the transmission deformation of the two transmissions ϕ_1 and ϕ_2 during the simulation. The estimation obtained using our MKKF for link and motors position show the effectiveness of our algorithm.

Figure 9.3 compares the noisy measure of the flexibility torque $\tau_e(\phi)$ and its estimation obtained using the residual, with its actual (nominal) evolution. In particular, both the measured torque and the estimation of the flexibility torque obtained directly from the residual (9.1) are quite noisy under the assumed operative conditions. However, a reliable (filtered and centered) flexibility torque estimation is obtained when feeding the residual into the RLS algorithm.

Finally, the time evolutions of the stiffness estimated in the different modalities are reported in Fig. 9.4, compared to the actual evolution. From the plot

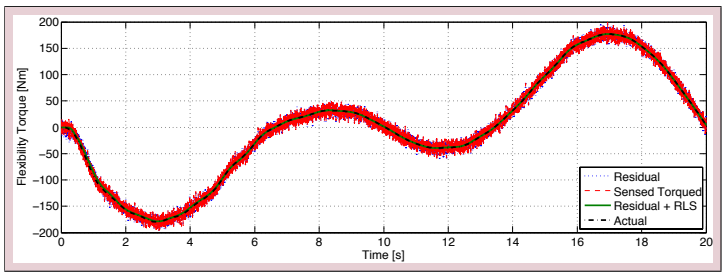

Figure 9.3: *Comparison of the total flexibility torque of the VSA-II transmissions: Actual $\tau_e(\phi)$ (dashed, black), estimated from the residual as γr_e (dotted, blue), measured by a noisy torque sensor as $\widetilde{\tau}_e(\phi)$ (dashed, red), and obtained from the RLS algorithm as $f(\phi, \widehat{\boldsymbol{\alpha}})$ using the residual in input (solid, green)*

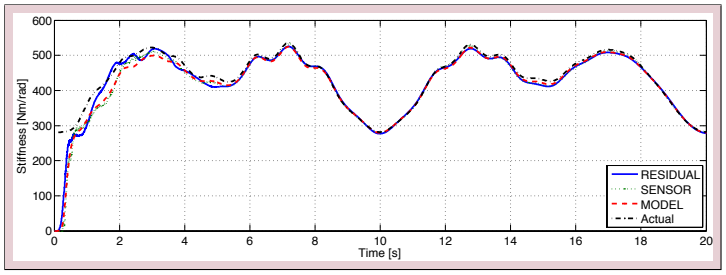

Figure 9.4: *Comparison of the total stiffness $\sigma_t(\boldsymbol{\phi})$ of the VSA-II: Actual (dot-dashed, black), MODEL estimation (dashed, red), SENSOR estimation (dotted, green), and RESIDUAL estimation (solid, blue). All methods provide a good stiffness estimation after a short learning phase*

is possible to perceive the fast convergence speed and the good steady tracking of the actual stiffness despite the presence of encoder quantization and measure noises. This results are confirmed by the performance indices in Tab. 9.1.

Serial VSA: AwAS

With reference to the AwAS model introduced in Sect. 4.2, and including in the simulations the presence of encoders with $\Delta = 40000$ pulses/turn for measuring q and θ, and with $\Delta_c = 1024$ for θ_c. The simulations were run with sampling time $T = 1$ ms, using as torque inputs for the principal and secondary motor $\tau = 0.3 \sin 0.2\pi$ and $\tau_c = 8 \sin 0.2\pi$ [Nm], from the initial configuration $q(0) = \theta(0) = 0$, $\theta_c(0) = -30/b$ [rad] and with the system at rest. The MKKF parameters in eq. (9.8) were $V_{\max} = 10^5$, $V_{\min} = 10^4$, and $\alpha = 6$, and the residual parameter in eq. (9.1) was $K_I = 300$, as in the VSA-II case; $\boldsymbol{P}(0) = 10^{20}\boldsymbol{I}_{n\times m}$ in eq. (9.11); $n = 6$ and $m = 3$ in eqs. (9.19) and (9.20); and $c = 10^{-20}$ in eq. (9.28). Therefore, the parameter vector $\boldsymbol{\eta}$ has dimension $n{\cdot}m = 18$, and we set $\widehat{\boldsymbol{\eta}}(0) = \mathbf{0}$. The orders of the polynomial functions m and n are selected on the basis of the nominal model. However, higher orders can be selected to better fit the nonlinearities.

Figure 9.5 shows the time behavior of the transmission deformation ϕ during the simulation. Note that its maximum value is very small (of the order

Estimation	MSE	MSREP
MODEL	19.28	0.0312 %
SENSOR	22.36	0.0314 %
RESIDUAL	75.84	0.0375 %

Table 9.1: *Performance of estimations of the total VSA-II stiffness in simulation*

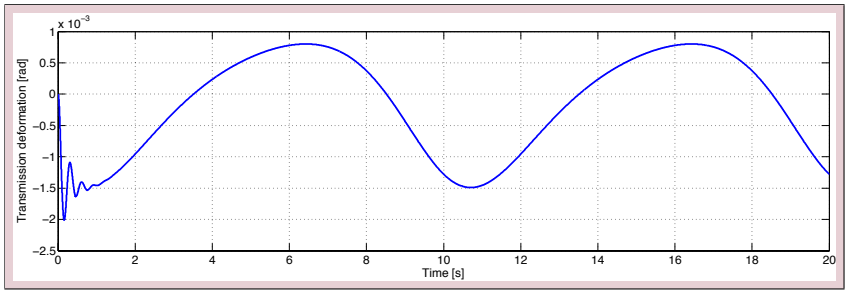

Figure 9.5: *Transmission deformation ϕ in simulation*

0.001 rad) and we are thus in a situation of very poor excitation for the RLS algorithm.

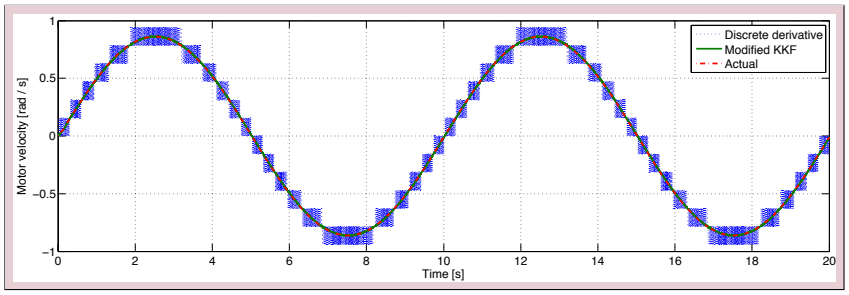

Figure 9.6: *Motor angular velocity $\dot{\theta}$: Actual (dot-dashed, red), obtained with numerical differentiation (dotted, blue), and estimated with MKKF (solid, green)*

The need for MKKF processing of the encoder data follows from the results in Fig. 9.6. The principal motor velocity $\dot{\theta}$ obtained by numerical differentiation of the encoder position data suffers from the presence of quantization.

Figure 9.7 compares two different estimations and the noisy measure of the flexibility torque $\tau_e(\theta_c, \phi)$ with its actual (nominal) evolution. In particular, both the measured torque and the estimation of the flexibility torque obtained directly from the residual (9.1) are quite noisy under the assumed operative conditions. However, a reliable (filtered and centered) flexibility torque estimation is obtained when feeding the residual into the RLS algorithm and using the estimated parameter vector $\widehat{\boldsymbol{\eta}}$ in eq. (9.22).

Finally, the time evolutions of the stiffness estimated in the different modalities are reported in Fig. 9.8, compared to the actual evolution. From the results in Tab. 9.2, all methods perform similarly well. Being these simulation results, the MODEL stiffness estimate is indeed very accurate despite the presence of

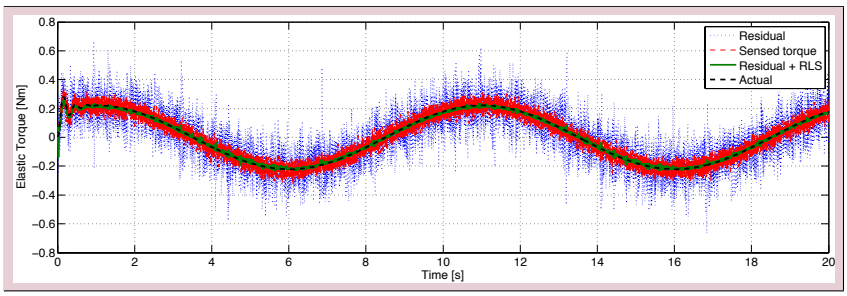

Figure 9.7: *Comparison of the flexibility torque of the AwAS transmission: Actual $\tau_e(\theta_c, \phi)$ (dashed, black), estimated from the residual as γr_e (dotted, blue), measured by a noisy torque sensor $\widetilde{\tau}_e(\theta_c, \phi)$ (dashed, red), and obtained from the RLS algorithm as $f(\theta_c, \phi, \widehat{\boldsymbol{\eta}})$ using the residual in input (solid, green)*

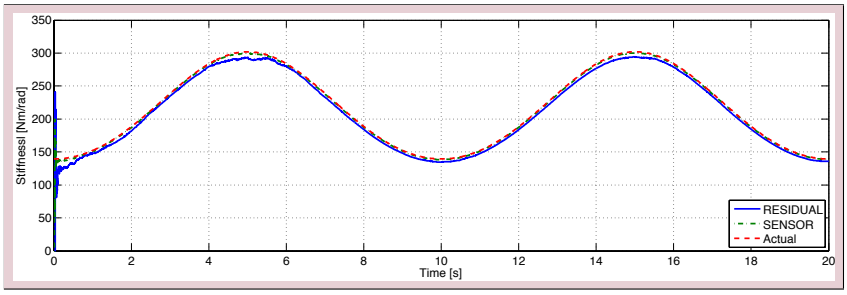

Figure 9.8: *Comparison of the device stiffness $\sigma(\theta_c, \phi)$ of the AwAS: Actual (dashed, red), SENSOR estimation (dot-dashed, green), and RESIDUAL estimation (solid, blue) —MODEL and SENSOR estimations practically overlap, so the former is not shown*

encoder quantization. The SENSOR estimation is also very accurate, confirming the benefit of using anyway a processing by the enhanced RLS algorithm. The RESIDUAL estimation has a higher MSE, due to the propagation of input noise through the two stages of the estimation process; however, its MSREP is still less than 1% which allows us to state that torque sensing seems not strictly needed.

Estimation	MSE	MSREP
MODEL	24.1365	0.12 %
SENSOR	24.3630	0.12 %
RESIDUAL	128.1614	0.58 %

Table 9.2: *Performance of estimations of the AwAS stiffness in simulation*

9.7 Choice of parameters and robustness

We provide in this section a short description of the role of the various parameters introduced for the estimator, and the guidelines for their selection.

The MKKF is characterized by four parameters: α, V_a, V_{max}, and V_{min}. The shape factor α changes the slope of the curve which represents the variance of the input noise; good filtered response has been obtained with values of α ranging from 4 to 6. The filter is not particularly sensitive to the variance V_a. However, this should be chosen so that the model covariance matrix $\boldsymbol{Q}$ does not have extremely small values. For the simulations, we considered $V_a = 10^{10}$. The parameters V_{max} and V_{min} are related instead to the encoder resolution. For a good estimation of the velocity, they need to be calibrated w.r.t. the actual encoder resolution. To simplify the choice of these two parameters, we have assumed the presence of low resolution encoders, thus with a large output noise variance R. Such a choice affects the convergence speed of the motor velocity estimation, but the stiffness estimator is still not very sensitive to this, thanks to the presence of a filtering effect in the residual and the RLS algorithm. For this reason, we considered $V_{max} = 10^5$ and $V_{min} = 10^4$. Note that, by considering an encoder with 40000 [counts/rev], these parameters would have been selected as $V_{max} = 10$ and $V_{min} = 0.1$.

The residual estimator is characterized by the single parameter K_I, which is the bandwidth of the low pass filter of the flexibility torque. In fact, when rewriting eq. (9.2) in the Laplace domain we obtain

$$\frac{r_e(s)}{\tau_e(s)} = \frac{K_I}{s + K_I}. \tag{9.34}$$

If the value of K_I is too small, the filtering action is too large and the signal may not be properly reconstructed. On the other hand, if it is too large external noises may be amplified. For both simulations and experiments, the value $K_I = 300$ resulted in a reasonable compromise.

The RLS algorithm depends on the parameters $\widehat{\boldsymbol{\alpha}}(0)$ (or $\widehat{\boldsymbol{\eta}}(0)$ for the AwAS), $\boldsymbol{P}(0)$, and c. During the tests, we assumed not to have an a priori knowledge of the transmission stiffness, and accordingly we have set $\widehat{\boldsymbol{\alpha}}(0) = \mathbf{0}$. The initialization of $\boldsymbol{P}(0)$ and c are strongly correlated, and they both act on the convergence rate of the estimator. With a large $\boldsymbol{P}(0)$ the RLS is more reactive and the convergence is faster; however, in case of poor excitation this fast reaction can produce an unstable behavior. On the other hand, when choosing c close to zero unstable behaviors are avoided, but the convergence is significantly slowed down. The ratio between $\boldsymbol{P}(0)$ and c^{-1} mostly affects the estimation convergence, and a good compromise is obtained when $\boldsymbol{P}(0)c = 1$. This relation can be used to obtain initial values for the two parameters; it is possible then to increase $\boldsymbol{P}(0)$ if the system is sufficiently excited (typically, for the VSA-II) in order to have faster convergence, or decrease c to improve the robustness of the estimator in case of a poorly excited system.

The importance of the stability factor $a(k)$ for the robustness is evaluated by considering the AwAS stiffness estimation obtained with the RESIDUAL method. The time evolution of this factor is shown on a semi-logarithmic scale in Fig. 9.9. By comparing this with Fig. 9.5, it is possible to note that the low peaks of $a(k)$ are associated to values of the transmission deformation close to

zero. In these cases, the Jacobian $\boldsymbol{F}$ contains very small values, which imply a poor excitation for the estimator. Note that, by using a constant and small stability factor the stiffness estimation is not affected by poor excitation but the convergence is very slow. On the other hand, with a constant and large stability factor, the convergence is faster but the estimation is very sensitive to poor excitation conditions. These behaviors are shown in Fig. 9.10, justifying the relevance of using the enhanced RLS algorithm with time-varying stability factor.

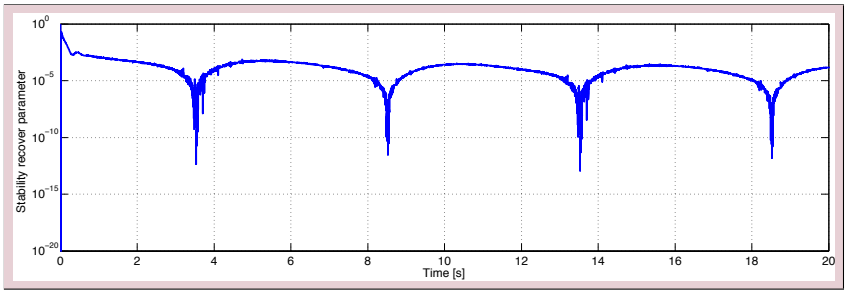

Figure 9.9: *Stability factor $a(k)$ in the RESIDUAL estimation method (semi-logarithmic scale)*

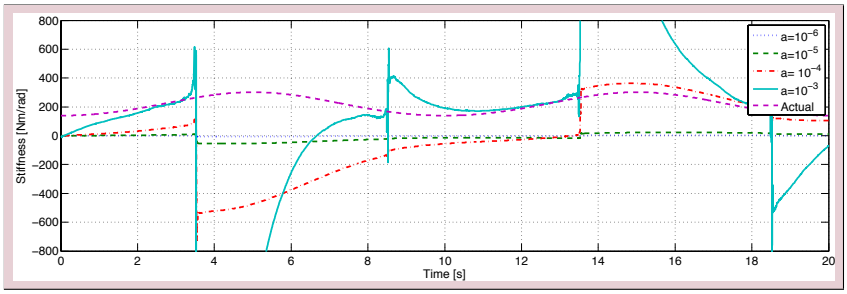

Figure 9.10: *Stiffness estimated by the RESIDUAL method and for different but constant stability factors*

To quantify the effects on the proposed estimator of the quality of encoder measurements, we simulated both systems with different encoder resolutions and verified the performance with the MSREP index. From Fig. 9.11 and Fig. 9.12 is evident that the RESIDUAL estimation has a greater MSREP in comparison with the SENSOR and MODEL estimations, especially at low resolutions. This is due to the fact that the RESIDUAL estimator uses the encoder signal both in the residual and in the RLS algorithm. Note that all estimators for both actuator typologies give a good estimation already with a resolution of 1024 [counts/rev]. This in turn implies that is possible to use an encoder with resolution of 256 [counts/rev], with quadrature detection. Comparing the results for the two typologies of VSA, the stiffness estimator for the AwAS has a higher MSREP due to a larger sensitivity to poor excitation conditions.

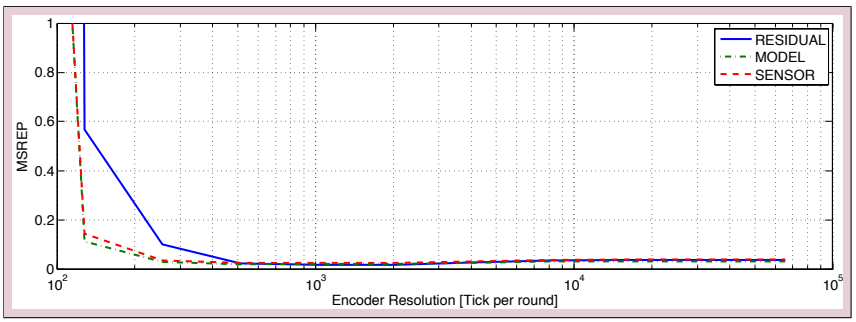

Figure 9.11: *MSREP obtained for the stiffness estimation of the VSA-II with different encoder quantization: RESIDUAL estimation (solid, blue), MODEL estimation (dot-dashed, green) and SENSOR estimation (dashed, red)*

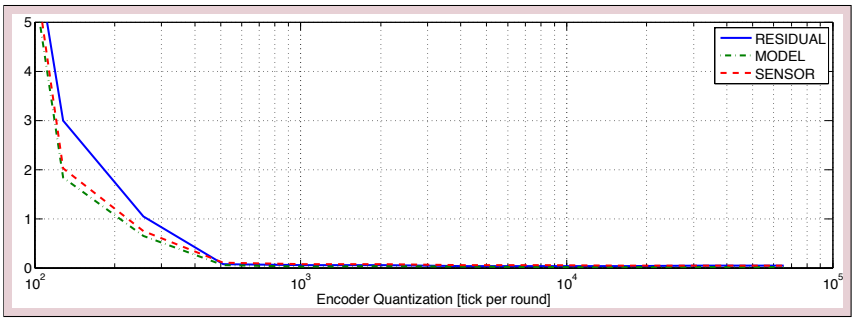

Figure 9.12: *MSREP obtained for the stiffness estimation of the AwAS with different encoder quantization: RESIDUAL estimation (solid, blue), MODEL estimation (dot-dashed, green) and SENSOR estimation (dashed, red)*

9.8 Experimental results

The stiffness estimation method has been tested through experiments using the Actuator with Adjustable Stiffness (AwAS) developed by the Italian Institute of Technology (IIT) and presented in Jafari et al. [2010]. The relative simplicity of the potential function associated to the transmission deformation of the AwAS and the presence of a sensor to measure the flexibility torque, which allows a validation of the results, makes this actuator a useful benchmark for testing our stiffness estimator. In the experiments, the principal and secondary motors drive the AwAS with sinusoidal torque signals. The obtained transmission deformation and the lever arm position are reported in Fig. 9.13 and Fig. 9.14, respectively.

To validate our estimation algorithm, we take advantage of the calibrated torque sensor available in the AwAS and we consider the flexibility torque measured by the torque sensor as the ground truth. The actual difference between the nominal flexibility torque and its measurement with the torque sensor is shown in Fig. 9.15.

Figure 9.16 shows the stiffness estimation results. As in the simulations of Sect. 9.6, we consider three different estimation modalities: MODEL, SENSOR, and RESIDUAL. It is worth noting that the nominal flexibility torque obtained

using eq. (4.8) and the nominal AwAS data given in Sect. 9.6 can be different from the real flexibility torque of the AwAS, due to unmodeled dynamics and uncertain knowledge of the model parameters. This will also be reflected in a difference between the real stiffness and the nominal one. In fact, the MODEL estimation method is very accurate in tracking the nominal stiffness (the two traces are practically superposed in Fig. 9.16). Indeed, the comparison of these two obtained results provides MSE = 9.36 and MSREP = 0.034% as performance indices. Stated differently, if the nominal stiffness had been the real one the MODEL estimation method would have worked properly. However, the results from the SENSOR estimation method, that we assume to provide the real ground truth stiffness, show a sensible difference with respect to the nominal stiffness and therefore the actual need for an independent stiffness estimator. On the other hand, the stiffness estimation by the RESIDUAL method is quite accurate in reproducing the SENSOR estimation results. Their relative comparison in terms of performance indices yields MSE = 63.02 and MSREP = 1.55%. However we have to consider that SENSOR and RESIDUAL are the result of the RLS, which has the same convergence behavior for both estimations.

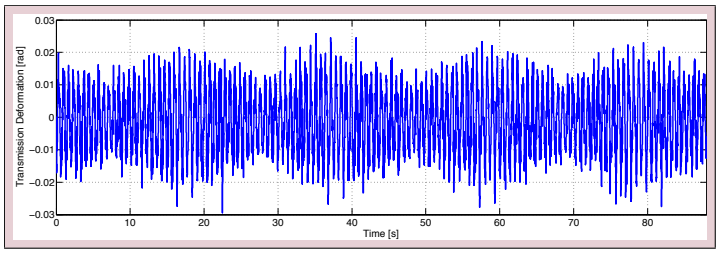

Figure 9.13: *Transmission deformation ϕ in AwAS experiment*

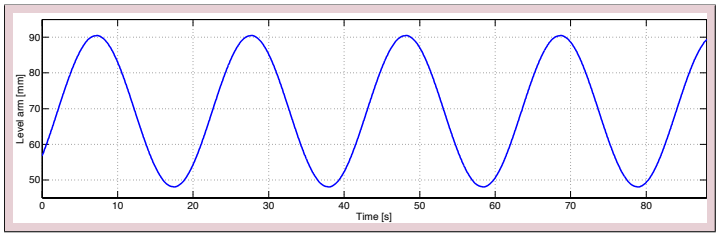

Figure 9.14: *Level arm position r in AwAS experiment*

9.9 Close the loop

In this section we would like to show how our stiffness estimator could be used in a real control loop as shown in Fig. 9.17. We take into account the feedback linearization control presented in Chapter 6.

Assuming now that that all robot dynamic parameters in eqs. (3.7–3.8) are known, except for those related to the transmission flexibility. The unknown components needed for implementing the feedback linearization law (6.9) are then the flexibility torques τ_{e_1} and τ_{1_2} and the transmissions stiffness σ_1 and

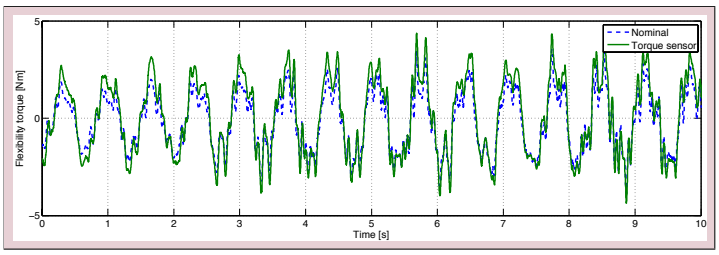

Figure 9.15: *Flexibility torque in AwAS experiment: nominal (dashed, blue), measured by the torque sensor (solid, green)*

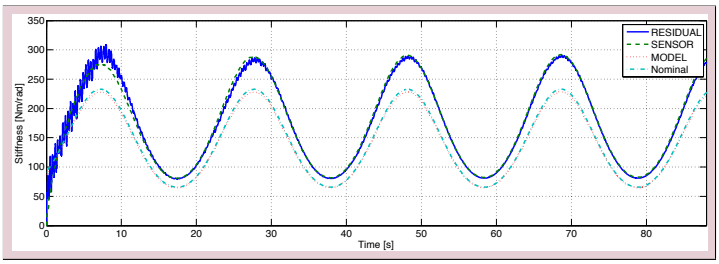

Figure 9.16: *Estimated stiffness in AwAS experiment: with nominal data (dot-dashed, green), with MODEL estimation method (dotted, red), with SENSOR estimation method (dashed, green), with RESIDUAL estimation method (solid, blue)*

σ_2, together with their first and second derivatives w.r.t. the deformations ϕ_1 and ϕ_2. More explicitly, we need $\frac{\partial \sigma_1}{\partial \phi_1}$, $\frac{\partial \sigma_2}{\partial \phi_2}$, $\frac{\partial^2 \sigma_1}{\partial \phi_1^2}$ and $\frac{\partial^2 \sigma_2}{\partial \phi_2^2}$. The last two quantities are used in the evaluation of $\boldsymbol{b}(\boldsymbol{x})$.

Using the proposed estimator we have for each trasmission

$$\widehat{\tau}_e(\phi) = f\left(\phi(k), \widehat{\boldsymbol{\alpha}}, n\right) = \sum_{h=1}^{n} \widehat{\alpha}_h \phi^{2h-1} \tag{9.35}$$

$$\widehat{\sigma}(\phi) = \sum_{h=1}^{n} \widehat{\alpha}_h (2h-1)\phi^{2h-2} \tag{9.36}$$

$$\frac{\partial \widehat{\sigma}(\phi)}{\partial \phi} = \sum_{h=2}^{n} \widehat{\alpha}_h (4h^4 - 6h + 2)\phi^{2h-3} \tag{9.37}$$

$$\frac{\partial^2 \widehat{\sigma}(\phi)}{\partial \phi^2} = \sum_{h=2}^{n} \widehat{\alpha}_h (8h^5 - 24h^2 + 22h - 6)\phi^{2h-4}, \tag{9.38}$$

therefore we can insert in the FBL loop the proposed estimator to estimate all unknown components.

In the follow simulation we have used the same reference signals and external control law used in Sect. 6.6. In order to avoid the non invertibility of the decoupling matrix the transmission must be pre-charged, thus we before to apply the FBL control the control $\tau_1 = 1.2Nm$ and $\tau_2 = -1.2Nm$ is applied for 0.1 seconds.

Figure 9.18 shows the point to point motion of the link (a) and the position error obtained (b). The stiffness trajectory is plotted in fig. 9.19, when the FBL

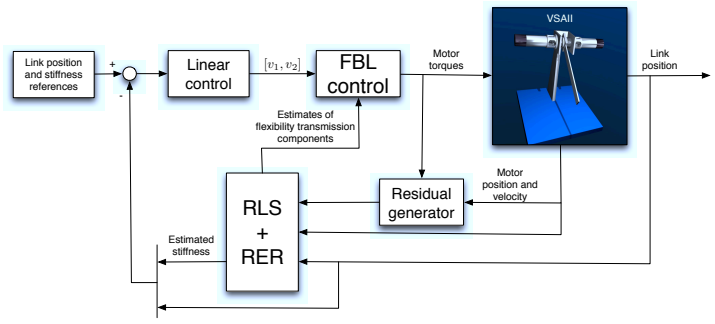

Figure 9.17: *Scheme of the stiffness estimation and of its use for feedback linearization control*

starts its control the error between the reference signal and the estimated is very small 9.19(b), moreover also the estimation error is relatively little 9.19(c).

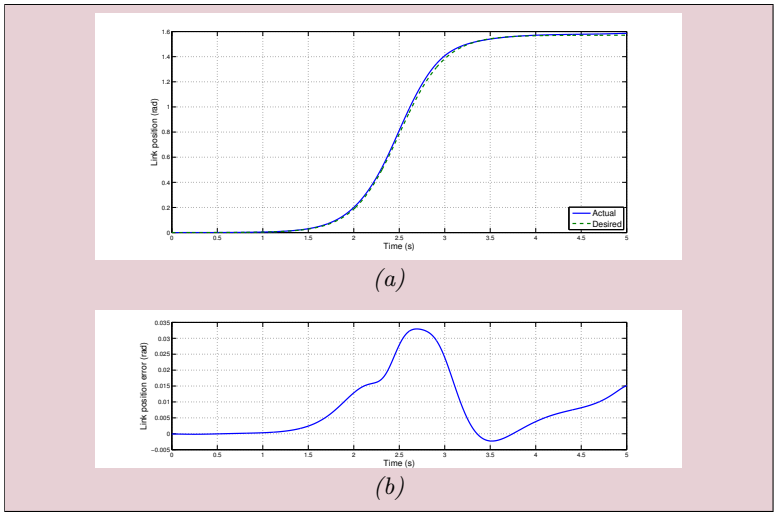

Figure 9.18: *Link position in the FBL simulation (a), the error between obtained trajectory and reference (b).*

9.10 Conclusions

We have presented a unified approach to the on-line estimation of the varying stiffness in SAFT or VSA devices having either an antagonistic configuration of the two motors and of the flexible transmissions or a serial configuration with a principal motor used for motion control and a secondary motor used to separately adjust stiffness.

Our approach builds up from the analysis of a single motor driving a nonlinear payload (e.g., a link under gravity) through a flexible transmission with nonlinear stiffness characteristic. The two-stage method initially estimates the flexibility torque of the transmission through a simple residual signal, using

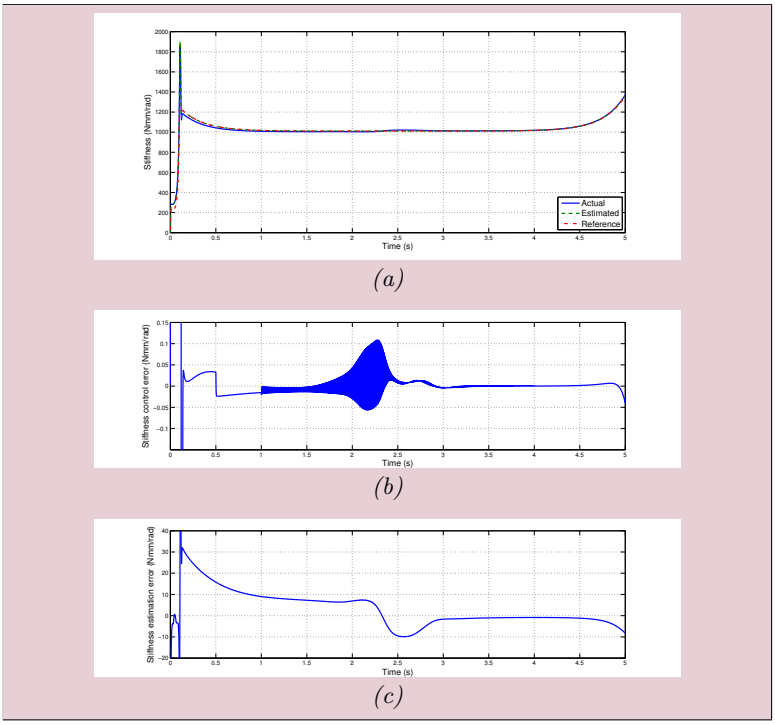

Figure 9.19: *Stiffness trajectory obtained with the FBL control (a), the control error (b) desired-estimated and the estimation error (c) desired-obtained.*

only the inertia and damping parameters of the motor and its position measurements, from where the motor velocity is obtained through a modified kinematic Kalman filter. Stiffness estimation is then completed using a RLS algorithm with a linearly parameterized generic model, chosen here as a polynomial in the deformation, taking as inputs the transmission deformation, obtained from the motor and payload/link positions, and the flexibility torque estimated in the first stage. The RLS algorithm has been enhanced so as to handle also poor excitation conditions (small deformations).

Being based only on position measurements local to the transmission, the proposed stiffness estimation method can be directly extended to the most common configurations of VSA. For a serial VSA, a double parameterization in the polynomial model of the flexibility torque of its main transmission is needed, since there is a separate functional dependence both on the deformation variable and on the position of the secondary motor. Furthermore, it is straightforward to address the multi-dof case of a VSA-driven robot since the stiffness estimation method can be applied in a decentralized way. Another merit of the proposed approach is that neither joint torque sensing, nor numerical differentiation of signals (in particular, to obtain acceleration) is needed, as opposed to other existing stiffness estimation methods. However , when a joint torque sensor is available the method is still valid; the estimator reduces to the second stage only and the measured transmission torque is taken as the input signal.

The extensive simulations conducted on representative devices of two VSA categories, the antagonistic VSA-II and the serial AwAS, have tested the dif-

ferent components of the estimator and the robustness of the method. The experimental results on the AwAS platform have shown the good performance of the stiffness estimation method, confirmed its necessity, as being able to compensate for uncertain parameters and unmodeled dynamics in the flexible transmission. In addition, they validated the full consistency of the approach (in particular, of the residual-based first stage) with the alternative resort to joint torque sensing.

The on-line nature of our method allows integrating the obtained time-varying estimate of the stiffness into a feedback control scheme which relies on an accurate value of this parameter. Moreover, the benefit of using estimated coefficients in a parametrized model of the stiffness is useful for obtaining the expression of stiffness derivatives in a closed analytic form, as needed by feedback linearization control laws. While the closed-loop stability of an estimation-based control law needs to be proven theoretically, which is not trivial in view of the nonlinearity of the problem and the lack of a separation principle, we present preliminary results with the nonlinear decoupling control of a VSA-II show the practical feasibility of this integration. An experimental validation of a feedback controller for the AwAS that uses the stiffness estimated on line with the proposed approach is part of our future work.

Conclusions

Compliant actuators represents a further step toward robots able to reach human motion capabilities. This is obtained by using new generation of joint actuators which permits to control the link motion together with the joint stiffness behavior, thanks to the presence of flexible elements opportunely arranged with motors inside the joint.

In the first part of this dissertation we presented an overview of the compliant joints developed in research centers and universities around the world, with a short description of their functionality. Considering the dynamic characteristic of these devices we presented a characterization in three typologies: Single Actuated Flexible Transmission (SAFT), Antagonistic Variable Stiffness Actuator (aVSA) and Serial Variable Stiffness Actuator (sVSA). For each typology we presented an equivalent arrangement of motors and flexible elements, together with the associated dynamic model which characterize it.

The second part of the Thesis was focused on the control of compliant actuators. we presented a feedback linearization low that permits to control the link position and the joint stiffness in a linearized and decoupled way. The effectiveness of this control law has been proved with simulations both for sVSA and aVSA. In the SAFT case only the link position can be controlled, since only motor is present. A simpler control solution is based on removing the gravity effects to the joint characteristic and then using a PD control law. Due to the non collocation of the gravity w.r.t. the control torque, its cancellation is not a trivial task. In this dissertation we presented the exact terms needed to cancel the gravity taking advantage of the feedback equivalence of the system in gravity and gravity free cases. Thanks to the control law we presented collision reaction strategies, which takes into account both link motion and joint stiffness, can be designed. For this goal we presented a collision detection approach, specially designed for compliant actuators, that does not need any extra sensor beyond the ones usually used for the control. The importance of the stiffness measure comes out from the control law we presented. Since does not exist a

sensor which is able to measure the stiffness of a compliant joint we presented a stiffness estimator based only on motors parameters and position measurements.

Using the stiffness estimator we presented the main problem is solved, nevertheless to control compliant joins the knowledge of joint and link dynamic parameters are needed. It is known that controls based on feedback equivalence are very sensible to perturbation of model parameters. To overcame this problem we are currently working on a robust version of our controller

Bibliography

A. Bicchi and G. Tonietti. Fast and soft arm tactics: Dealing with the safety-performance trade-off in robot armsdesign and control. *IEEE Robotics and Automation Mag.*, 11(2):22–33, 2004.

A. Bicchi, S. Lodi Rizzini, and G. Tonietti. Compliant design for intrinsic safety: General issue and preliminary design. In *Proc. IEEE/RSJ Int. Conf. on Intelligent Robots and Systems*, pages 1864–1869, 2001.

A. Bicchi, M. Bavaro, G. Boccadamo, D. De Carli, R. Filippini, G. Grioli, M. Piccigallo, A. Rosi, R. Schiavi, S. Sen, and G. Tonietti. Physical Human-Robot Interaction: Dependability, safety, and performance. In *Proc. 10th Int. Work. on Advanced Motion Control*, pages 9–14, 2008a.

A. Bicchi, M. A. Peshkin, and J. E. Colgate. Safety for physical human-robot interaction. In B. Siciliano and O. Khatib, editors, *Springer Handbook of Robotics*, pages 1335–1348. Springer, 2008b.

S. Bittanti, P. Bolzern, and M. Campi. Recursive least-squares identification algorithms wit incomplete excitation: Convergence analysis and application to adaptive control. *IEEE Trans. on Automatic Control*, 35(12):1371–1373, 1990.

G. Boccadamo, R. Schiavi, S. Sen, G. Tonietti, and A. Bicchi. Optimization and fail-safety analysis of antagonistic actuation for pHRI. In *European Robotics Symp.*, Springer Tracts in Advanced Robotics, pages 109–118. Springer Berlin, 2006.

M. G. Catalano, G. Grioli, F. Bonomo, R. Schiavi, and A. Bicchi. Vsa-hd: From the enumeration analysis to the prototypical implementation. In *IEEE/RSJ International Conference on Intelligent RObots and Systems*, pages 3676 – 3681, St. Louis MO USA, October 2010a.

M. G. Catalano, R. Schiavi, and A. Bicchi. Design of variable stiffness actuators mechanisms based on enumeration and analysis of performance. In *Proc. IEEE Int. Conf. on Robotics and Automation*, pages 3285–3291, 2010b.

J. Choi, S. Park, W. Lee, and S.-C. Kang. Design of a robot joint with variable stiffness. In *Proc. IEEE Int. Conf. on Robotics and Automation*, pages 1760–1765, 2008.

F. Coutinho and R. Cortesao. System stiffness estimation with the candidate observers algorithm. In *Proc. 18th Mediterranean Conf. on Control and Automation*, pages 796–801, 2010.

A. De Luca and W. Book. Robots with flexible elements. In B. Siciliano and O. Khatib, editors, *Springer Handbook of Robotics*, pages 287–319. Springer, 2008.

A. De Luca and F. Flacco. Dynamic gravity cancellation in robots with flexible transmissions. In *Proc. 49th IEEE Conf. on Decision and Control*, pages 288–295, 2010a.

A. De Luca and F. Flacco. Dynamic gravity cancellation and regulation control in robots with flexible transmissions: Constant, nonlinear, and variable stiffness. DIS Technical Report 11-2010, Università di Roma "La Sapienza", 2010b.

A. De Luca and F. Flacco. A pd-type regulator with exact gravity cancellation for robots with flexible joints. In *Proc. IEEE Int. Conf. on Robotics and Automation*, pages 317–323, 2011.

A. De Luca and P. Lucibello. A general algorithm for dynamic feedback linearization of robots with elastic joints. In *Proc. IEEE Int. Conf. on Robotics and Automation*, pages 504–510, 1998.

A. De Luca and R. Mattone. Actuator failure detection and isolation using generalized momenta. In *Proc. IEEE Int. Conf. on Robotics and Automation*, pages 634–639, 2003.

A. De Luca and R. Mattone. Sensorless robot collision detection and hybrid force/motion control. In *Proc. IEEE Int. Conf. on Robotics and Automation*, pages 1011–1016, 2005.

A. De Luca, B. Siciliano, and L. Zollo. PD control with on-line gravity compensation for robots with elastic joints: Theory and experiments. *Automatica*, 41(10):1809–1819, 2005.

A. De Luca, A. Albu-Schäffer, S. Haddadin, and G. Hirzinger. Collision detection and safe reaction with the DLR-III lightweight robot arm. In *Proc. IEEE/RSJ Int. Conf. on Intelligent Robots and Systems*, pages 1623–1630, 2006.

A. De Luca, F. Flacco, A. Bicchi, and R. Schiavi. Nonlinear decoupled motion-stiffness control and collision detection/reaction for the VSA-II variable stiffness device. In *Proc. IEEE/RSJ Int. Conf. on Intelligent Robots and Systems*, pages 5487–5494, 2009.

A. De Santis, B. Siciliano, A. De Luca, and A. Bicchi. An atlas of physical human-robot interaction. *Mechanism and Machine Theory*, 43(3):253–270, 2008.

N. Diolaiti, C. Melchiorri, and S. Stramigioli. Contact impedance estimation for robotic systems. *IEEE Trans. on Robotics*, 21(5):925–935, 2005.

O. Eiberger, S. Haddadin, M. Weis, A. Albu-Schäffer, and G. Hirzinger. On joint design with intrinsic variable compliance: Derivation of the dlr qa-joint. In *Proc. IEEE Int. Conf. on Robotics and Automation*, pages 1687–1694, 2010.

F. Flacco and A. De Luca. Residual-based stiffness estimation in robots with flexible transmissions. In *Proc. IEEE Int. Conf. on Robotics and Automation*, pages 5541–5547, 2011a.

F. Flacco and A. De Luca. Stiffness estimation and nonlinear control of robots with variable stiffness actuation. In *18th IFAC World Congr.*, pages 6872–6879, 2011b.

F. Flacco, A. De Luca, I. Sardellitti, and N. G. Tsagarakis. Robust estimation of variable stiffness in flexible joints. In *Proc. IEEE/RSJ Int. Conf. on Intelligent Robots and Systems*, pages 4026–4033, 2011.

G. Grioli and A. Bicchi. A non-invasive real-time method for measuring variable stiffness. In *Proc. Robotics Science and Systems (RSS 2010)*, Zaragoza, E, June 2010.

G. Grioli and A. Bicchi. A real-time parametric stiffness observer for vsa devices. In *Proc. IEEE Int. Conf. on Robotics and Automation*, Shanghai, PRC, May 2011.

S.S. Groothuis, G. Rusticelli, A. Zucchelli, S. Stramigioli, and R. Carloni. The vsaUT-II: a novel rotational variable stiffness actuator. In *[in preparation]*.

S. Haddadin, A. Albu-Schäffer, A. De Luca, and G. Hirzinger. Safety evaluation of physical human-robot interaction via crash-testing. In *Proc. Conf. on Robotics: Science and Systems (RSS 2007)*, Atlanta, GA, 2007.

S. Haddadin, A. Albu-Schäffer, A. De Luca, and G. Hirzinger. Collision detection and reaction: A contribution to safe physical human-robot interaction. In *Proc. IEEE/RSJ Int. Conf. on Intelligent Robots and Systems*, pages 3356–3363, 2008.

R. Ham, T. Sugar, B. Vanderborght, K. Hollander, and D. Lefeber. Compliant actuator designs. *IEEE Robotics and Automation Mag.*, 16(3):81–94, 2009.

R. Van Ham, B. Vanderborght, M. Van Damme, B. Verrelst, and D. Lefeber. MACCEPA, the mechanically adjustable compliance and controllable equilibrium position actuator: Design and implementation in a biped robot. *Robotics and Autonomous Systems*, 10:761–768, 2007.

J. Heinzmann and A. Zelinsky. Quantitative safety guarantees for physical human-robot interaction. *Int. J. of Robotics Research*, 22(7/8):479–504, 2003.

G. Hirzinger, A. Albu-Schäffer, M. Hähnle, I. Schaefer, and N. Sporer. On a new generation of torque controlled light-weight robots. In *Proc. IEEE Int. Conf. on Robotics and Automation*, pages 3356–3363, 2001.

J.W. Hurst, J.E. Chestnutt, and A.A. Rizzi. An actuator with mechanically adjustable series compliance. Technical Report CMU-RI-TR-04-24, Carnegie Mellon University, 2004.

Y. Ikegami, K. Nagai, R.C.V. Loureiro, and W.S. Harwin. Design of redundant drive joint with adjustable stiffness and damping mechanism to improve joint admittance. In *IEEE Int. Conf. on Rehabilitation Robotics (ICORR 2009)*, pages 202–210, June 2009. doi: 10.1109/ICORR.2009.5209474.

K. Ikuta, H. Ishii, and M. Nokata. Safety evaluation method of design and control for human-care robots. *Int. J. of Robotics Research*, 22(7/8):281–297, 2003.

A. Jafari, N.G. Tsagarakis, B. Vanderborght, and D.G. Caldwell. A novel actuator with adjustable stiffness (AwAS). In *Proc. IEEE/RSJ Int. Conf. on Intelligent Robots and Systems*, pages 4201–4206, 2010.

A. Jafari, N.G. Tsagarakis, and D.G. Caldwell. Awas-ii: A new actuator with adjustable stiffness based on the novel principle of adaptable pivot point and variable lever ratio. In *Proc. IEEE Int. Conf. on Robotics and Automation*, pages 3561–3569, 2011.

S. Jeon and M. Tomizuka. Benefits of acceleration measurements in velocity estimation and motion control. *IFAC Control Engineering Practice*, 15(3): 325–332, 2007.

B.-S. Kim and J.-B. Song. Hybrid dual actuator unit: A design of a variable stiffness actuator based on an adjustable moment arm mechanism,. In *Proc. IEEE Int. Conf. on Robotics and Automation*, pages 1655–1660, 2010.

B.-S. Kim, J.-B. Song, and J.-J. Park. A serial-type dual actuator unit with planetary gear train: Basic design and applications. *IEEE Trans. on Mechatronics,*, 15(1):108–116, 2010.

A. Kugi, C. Ott, A. Albu-Schäffer, and G. Hirzinger. On the passivity-based impedance control of flexible joint robots. *IEEE Trans. on Robotics*, 24(2): 416–429, 2008.

D. Ludvig and R. E. Kearney. Estimation of joint stiffness with a compliant load. In *Proc. 31st IEEE Int. Conf. on EMBS*, pages 2967–2970, 2009.

S.A. Migliore, E.A. Brown, and S.P. DeWeerth. Biologically inspired joint stiffness control. In *Proc. IEEE Int. Conf. on Robotics and Automation*, pages 4508–4513, 2005.

S. Morinaga and K. Kosuge. Collision detection system for manipulator based on adaptive impedance control law. In *Proc. IEEE Int. Conf. on Robotics and Automation*, pages 1080–1085, 2003.

T. Morita and S. Sugano. Development of one-dof robot arm equipped with mechanical impedance adjuster. In *IEEE/RSJ International Conference on Intelligent RObots and Systems*, pages 401 – 412, Pittsburgh, PA, USA, August 1995.

R. Ozawa and H. Kobayashi. Response characteristics of elastic joint robots driven by various types of controllers against external disturbances. In *Proc. 6th Int. Conf. on Motion and Vibration Control*, pages 420–425, 2002.

G. Palli, C. Melchiorri, T. Wimböck, M. Grebenstein, and G. Hirzinger. Feedback linearization and simultaneous stiffness-position control of robots with antagonistic actuated joints. In *Proc. IEEE Int. Conf. on Robotics and Automation*, pages 4367–4372, 2007.

G. Palli, C. Melchiorri, and A. De Luca. On the feedback linearization of robots with variable joint stiffness. In *Proc. IEEE Int. Conf. on Robotics and Automation*, pages 1753–1759, 2008.

J.-J. Park, Y.-J. Lee, J.-B. Song, and H.-S. Kim. Safe joint mechanism based on nonlinear stiffness for safe human-robot collision. In *Proc. IEEE Int. Conf. on Robotics and Automation*, pages 2177–2182, 2008.

F. Petit and A. Albu-Schäffer. Cartesian impedance control for a variable stiffness robot arm. In *Proc. IEEE/RSJ Int. Conf. on Intelligent Robots and Systems*, pages 4180–4186, 2011.

G. A. Pratt and M. M. Williamson. Series Elastic Actuators. In *Proc. IEEE/RSJ Int. Conf. on Intelligent Robots and Systems*, pages 399–406, 1995.

K. Salisbury, W. Townsend, B. Eberman, and D. DiPietro. Preliminary design of whole-arm manipulation systems (WAMS). In *Proc. IEEE Int. Conf. on Robotics and Automation*, pages 254–260, 1988.

R. Schiavi, G. Grioli, S. Sen, and A. Bicchi. VSA-II: A novel prototype of variable stiffness actuator for safe and performing robots interacting with humans. In *Proc. IEEE Int. Conf. on Robotics and Automation*, pages 2171–2176, 2008.

A. Serio, G. Grioli, I. Sardellitti, N. G. Tsagarakis, and A. Bicchi. A decoupled impedance observer for a variable stiffness robot. In *Proc. IEEE Int. Conf. on Robotics and Automation*, pages 5548–5553, 2011.

D. Shin, I. Sardellitti, Y.-L. Park, O. Khatib, and M. Cutkosky. Design and control of a bio-inspired human-friendly robot. *Int. J. of Robotics Research*, 29(5):571–584, 2010.

M. W. Spong. Modeling and control of elastic joint robots. *ASME J. of Dynamic Systems, Measurement, and Control*, 109(4):310–319, 1987.

K. Suita, Y. Yamada, N. Tsuchida, K. Imai, H. Ikeda, and N. Sugimoto. A failure-to-safety 'kyozon' system with simple contact detection and stop capabilities for safe human-autonomous robot coexistence. In *Proc. IEEE Int. Conf. on Robotics and Automation*, pages 3089–3096, 1995.

P. Tomei. A simple PD controller for robots with elastic joints. *IEEE Trans. on Automatic Control*, 36(10):1208–1213, 1991.

G. Tonietti, R. Schiavi, and A. Bicchi. Design and control of a variable stiffness actuator for safe and fast physical human/robot interaction. In *Proc. IEEE Int. Conf. on Robotics and Automation*, pages 528–533, 2005.

N.G. Tsagarakis, I. Sardellitti, and D.G. Caldwell. A new variable stiffness actuator (compact-vsa): Design and modelling. In *Proc. IEEE/RSJ Int. Conf. on Intelligent Robots and Systems*, pages 378 – 383, 2011.

B. Verrelst, R. Van Ham, B. Vanderborght, F. Daerden, and D. Lefeber. The pneumatic biped lucy actuated with pleated pneumatic artificial muscles. *Autonom. Robots*, 18(13):201–213, 2005.

D. Verscheure, I. Scharf, H. Bruyninckx, J. Swevers, and J. De Schutter. Identification of contact dynamics parameters for stiff robotic payloads. *IEEE Trans. on Robotics*, 25(2):240–252, 2009.

L. C. Visser, R. Carloni, and S. Stramigioli. Energy-efficient variable stiffness actuators. *IEEE Trans. on Robotics*, 27(5):865–875, 2011.

S. Wolf and G. Hirzinger. A new variable stiffness design: Matching requirements of the next robot generation. In *Proc. IEEE Int. Conf. on Robotics and Automation*, pages 1741–1746, 2008.

K. A. Wyrobek, E. H. Berger, H. F. M. Van der Loos, and J. K. Salisbury. Toward a personal robotics development platform: Rationale and design of an intrinsically safe personal robot. In *Proc. IEEE Int. Conf. on Robotics and Automation*, pages 2165–2170, 2008.

Y. Yamada, Y. Hirasawa, S. Huang, Y. Uematsu, and K. Suita. Human-robot contact in the safeguarding space. *IEEE/ASME Trans. on Mechatronics*, 2 (4):230–236, 1997.

M. Zinn, O. Khatib, B. Roth, and J. K. Salisbury. A new actuation approach for human-friendly robot design. *Int. J. of Robotics Research*, 23(4/5):379–398, 2005.